2015-03-01

Optimization of Nonadsorptive Polymerized Polyethylene Glycol Diacrylate as a Material for Microfluidics and Sensor Integration

Chad Rogers
Brigham Young University - Provo

Optimization of Nonadsorptive Polymerized Polyethylene Glycol Diacrylate as a Material for Microfluidics and Sensor Integration

Chad Isaac Rogers

A dissertation submitted to the faculty of
Brigham Young University
in partial fulfillment of the requirements for the degree of

Doctor of Philosophy

Adam T. Woolley, Chair
Gregory P. Nordin
Milton L. Lee
Steven R. Goates
Daniel E. Austin

Department of Chemistry and Biochemistry

Brigham Young University

February 2015

ABSTRACT

Optimization of Nonadsorptive Polymerized Polyethylene Glycol Diacrylate as a Material for Microfluidics and Sensor Integration

Chad I. Rogers
Department of Chemistry and Biochemistry, BYU
Doctor of Philosophy

Microfluidics is a continually growing field covering a wide range of applications, such as cellular analysis, biomarker quantification, and drug discovery; but in spite of this, the field of microfluidics remains predominately academic. New materials are pivotal in providing tailored properties to improve device integration and decrease prototype turnaround times. In biosensing, nonspecific adsorption in microfluidic systems can deplete target molecules in solution and prevent analytes, especially those at low concentrations, from reaching the detector. Polyethylene glycol diacrylate (PEGDA) mixed with photoinitiator forms, on exposure to ultraviolet (UV) radiation, a polymer with inherent resistance to nonspecific adsorption. Optimization of the polymerized PEGDA (poly-PEGDA) formula imbues this material with some of the same properties, including optical clarity, water stability, and low background fluorescence, that makes polydimethylsiloxane (PDMS) a widely used material for microfluidics. Poly-PEGDA demonstrates less nonspecific adsorption than PDMS over a range of concentrations of flowing fluorescently tagged bovine serum albumin solutions, and poly-PEGDA has greater resistance to permeation by small hydrophobic molecules than PDMS. Poly-PEGDA also exhibits long-term (hour scale) resistance to nonspecific adsorption compared to PDMS when exposed to a low (1 μg/mL) concentration of a model adsorptive protein. Electrophoretic separations of amino acids and proteins resulted in symmetrical peaks and theoretical plate counts as high as 4×10^5/m.

Pneumatically actuated, non-elastomeric membrane valves fabricated from poly-PEGDA have been characterized for temporal response, valve closure, and long-term durability. A ~100 ms valve opening time and a ~20 ms closure time offer valve operation as fast as 8 Hz with potential for further improvement. Comparison of circular and rectangular valve geometries indicates that the surface area for membrane interaction in the valve region is important for valve performance. After initial fabrication, the fluid pressure required to open a closed circular valve is ~50 kPa higher than the control pressure holding the valve closed. However, after ~1000 actuations to reconfigure polymer chains and increase elasticity in the membrane, the fluid pressure required to open a valve becomes the same as the control pressure holding the valve closed. After these initial conditioning actuations, poly-PEGDA valves show considerable robustness with no change in effective operation after 115,000 actuations.

Often, localized areas of surface functionalization are desired in biosensing, necessitating site-specific derivatization. Integration of poly-PEGDA with different substrates, such as glass,

silicon, or electrode-patterned materials, allows for broad application in biosensing and microfluidic devices. Deposition of 3-(trimethoxysilyl) propyl methacrylate or (3-acryloxypropyl) dimethylmethoxysilane onto these substrates makes bonding to poly-PEGDA possible under UV exposure. Primary deposition of (3-acryloxypropyl) dimethylmethoxysilane, followed by photolithographic patterning, allows for silane removal through HF surface etching in the exposed areas and subsequent deposition of 3-aminopropyldiisopropylethoxysilane on the etched regions. Fluorescent probes are used to evaluate surface attachment methods. Primary attachment via reaction of Alexa Fluor 488 TFP ester to the patterned aminosilane demonstrates excellent fluorescent signal. Initial results with glutaraldehyde were demonstrated but require more optimization before this method for secondary attachment is viable.

Fabrication of 3D printed microfluidic devices with integrated membrane-based valves is performed with a low-cost, commercially available stereolithographic 3D printer and a custom PEGDA resin formulation tailored for low non-specific protein adsorption. Horizontal microfluidic channels with designed rectangular cross sectional dimensions as small as 350 μm wide and 250 μm tall are printed with 100% yield, as are cylindrical vertical microfluidic channels with 350 μm designed (210 μm actual) diameters. Valves are fabricated with a membrane consisting of a single build layer. The fluid pressure required to open a closed valve is the same as the control pressure holding the valve closed. 3D printed valves are successfully demonstrated for up to 800 actuations.

Poly-PEGDA is a versatile material for microfluidic applications ranging from electrophoretic separations, valve implementation, and heterogeneous material integration. Further improvements in PEGDA resin formulation, in combination with a UV source 3D printer, will provide poly-PEGDA devices that are not only rapidly fabricated (<40 min per device), but that also include pumps and valves and are usable with a variety of detection methods, such as laser-induced fluorescence and immunoassays, for broad application in biosensing.

Keywords: Poly-PEGDA, Non-adsorptive polymer, Membrane valve, Valve characterization, 3D printed valve, Microchip electrophoresis, Bioanalytical

ACKNOWLEDGEMENTS

First and foremost, I would like to thank my wife and family for supporting me during this adventure. Without you I would not be who I am today. I am grateful for my advisor, Dr. Adam Woolley. Thanks for the gentle guidance and mentorship you have provided. I would also like to thank Dr. Greg Nordin for our collaboration. It has been enlightening and an honor. To my other committee members, Dr. Milton Lee, Dr. Steven Goates, and Dr. Daniel Austin, thank you for your assistance. Your guidance and thought provoking questions have helped shape me personally as well as my research. All five of you are wonderful mentors and great teachers.

To both previous and current group members of the ATW and Nordin labs, Thank You! It has been a pleasure to have you as my friends and comrades-in-arms. There are many of you, too many to list here, but particular thanks go out to Jayson Pagaduan, Mukul Sonker, Suresh Kumar, Dr. Vishal Sahore, Dr. Ryan Anderson, Dr. Stan Ness, Joseph Oxborrow, Ben Tsai, Kamran Qaderi, and Hua Gong. Thank you my friends. May your endeavors be blessed!

To my longtime friends, Dr. Dave Jensen and Dr. Landon Wiest, I have only one thing to say, Δ! It has been a long journey and now a new one begins!

TABLE OF CONTENTS

LIST OF TABLES

LIST OF FIGURES

1. BACKGROUND AND INTRODUCTION*

1.1. INTRODUCTION

Chemical analysis is a crucial part of science in understanding the world around us. Through probing a system of interest (e.g., via light, electricity, heat, mass, or mass-to-charge ratio) valuable information about relative quantities and chemical makeup is gained. For chemical analysis to work, energy added to the system must induce a change and be coupled with a way to detect that change.[1] Although a variety of ways have been developed to do this, the field of microfluidics, also known as lab-on-a-chip or micro total analysis systems (μTAS), will be the focus of this dissertation. The premise of lab-on-a-chip systems is taking larger, bulky analysis systems and shrinking them down so that a similar process can be done on a small chip. This results in reduced solvent and sample volumes, greater portability (as long as the supporting equipment is similarly shrunk down), and the ability to integrate multiple processes into one device. Due to smaller required sample volumes, one focus of microfluidics has been biochemical analysis, where only small sample amounts are available for testing (e.g., cerebrospinal fluid or antibodies, the latter due to cost).

Microfabricated structures between 1–500 μm for manipulation and handling of small liquid volumes (femtoliters to nanoliters) create the bulk of microfluidics. Although they utilize small volumes, capillary tubes connected with capillary fittings,[2] and millifluidics made by machine shop tools are not included in microfluidics in this chapter since they are not microfabricated and have larger channel dimensions (>500 μm).

Though microfluidics has been around since the 1970s,[3] the field did not gain much traction in academia until the 1990s.[4] Silicon and glass were the original materials used, but in the 1990s focus shifted to include polymer substrates, in particular, polydimethylsiloxane (PDMS). Since then the field has grown to include a wide variety of materials and applications. The successful demonstration and integration of electrophoresis in a microfluidic device provided a nonmechanical method for both fluid control and separation.[5] Laser induced fluorescence (LIF) provided for sensitive detection of fluorophores or fluorescently labeled molecules. The advent of high-resolution printing allowed for more rapid and cheaper mask fabrication for use in soft lithography.[6] A number of companies, including Abbott, Agilent, Caliper, Dolomite, Micralyne, Microfluidic Chip Shop, Micrux Technologies and Waters, have now developed microfluidic devices that are commercially available. For a more thorough review of the history of microfluidics, I refer you to reviews by Manz et al.[4, 7-11] or Whitesides et al.[12]

Microfluidics has many advantages compared to standard large scale systems. The first relates to a lesson taught to every first-year chemistry student. Simply stated, diffusion is slow! The equation for one dimensional diffusion is given by Eq. 1.1

$$x = \sqrt{4Dt} \qquad (1.1)$$

where x is distance, D is the diffusion coefficient, and t the time.[13] Rearranging this equation for t gives Eq. 1.2.

$$t = \frac{x^2}{4D} \qquad (1.2)$$

For a common protein, bovine serum albumin (BSA, $D = 6 \times 10^{-7}$ cm^2/s),[14] the time required to travel 1 mm is ~69 min. The smaller the distance required for interaction, the smaller the time needed for interaction (the diffusion time for BSA to travel 100 μm is ~42 s). Smaller channel

dimensions also can lead to smaller sample volumes (fL-nL) which can reduce the amount of sample and reagents required for testing and analysis. Reduced dimensions can also lead to more portable devices that can enable on-site testing (as long as the equipment to analyze the device and sample are similarly portable). Integration of different processes (like labeling, purification, separation, and detection) in a microfluidic device can contribute to broader applications.

Chip integration leads to a more complete analytical package. Microelectromechanical systems (MEMS) are small devices composed of electrical and mechanical parts to create an integrated sensor or system. Applications of MEMS devices are found in a range of areas including automobiles, phones, video games, and medical and biological sensors.[15] Lab-on-a-chip or μTAS are integrated microfluidic devices that are capable of multiple steps that can ideally provide minimal user involvement to sense molecules of interest. For example, a lab-on-a-chip system might selectively purify a complex mixture (through filtering, antibody immobilization, etc.), separate analytes, and detect those analytes.

Microfluidic devices consist of several similar components (Fig. 1.1). Negative features such as reservoirs (wells) and microchannels provide the standard starting point for most microfluidic devices. Positive features add increased functionality to the chip and can consist of membranes, monoliths, pneumatic controls and valves, and beams and pillars.

Initially, microfluidic materials consisted of silicon and glass substrates. As focus into microfluidics increased, other materials (e.g., polymers, ceramics, and paper) were characterized for utilization in microfluidics. These materials can be organized into three broad material categories: inorganic, polymeric, and paper. Inorganic materials have broadened beyond glass and silicon to include ceramics such as low temperature co-fired ceramics and vitoceramics.

Plastic or polymer based materials can be divided into elastomers and thermoplastics. Paper microfluidics is substantially different from polymer or inorganic materials and utilizes different methods for channel definition.

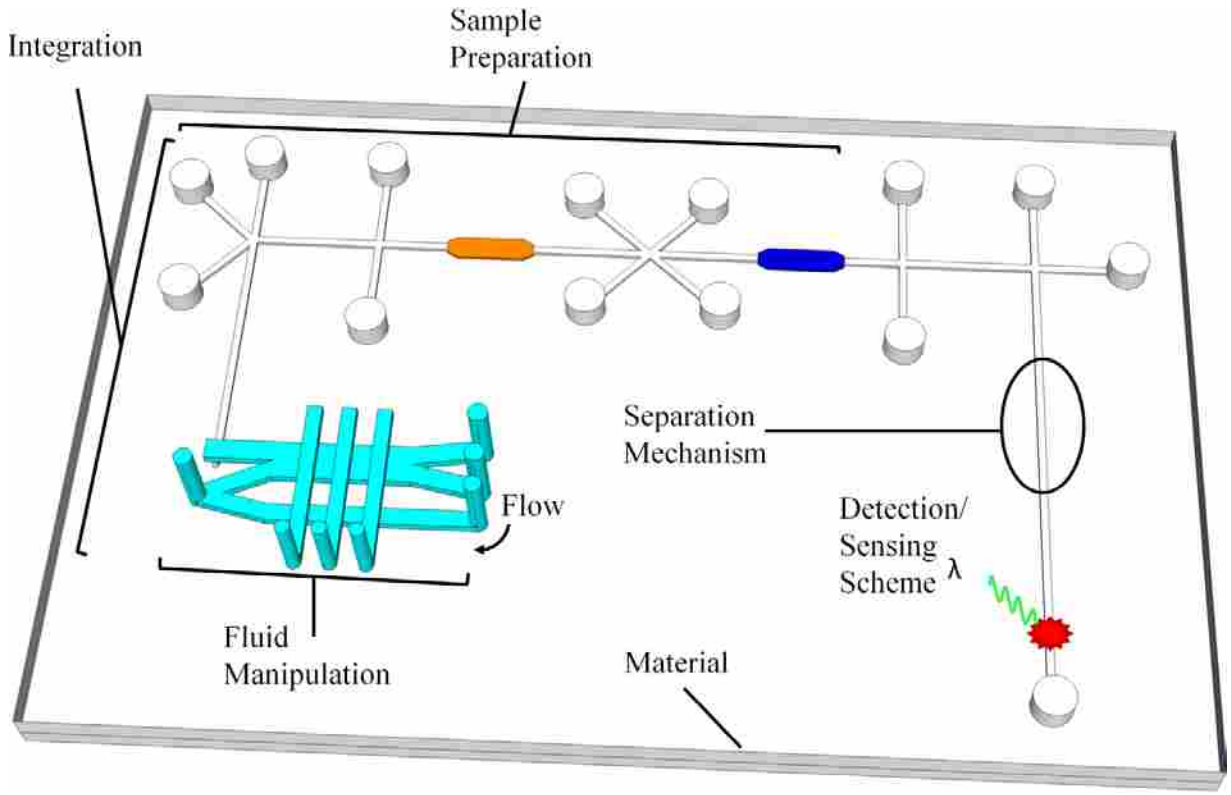

Figure 1.1. Schematic of common microfluidic components in an integrated device, demonstrating different components such as fluid manipulation (channels, valves, and pumps), sample preparation (purification, labeling, etc.), separation mechanism, and detection scheme.

Smaller channel sizes increase the surface-to-volume ratio and lead to differing fluid properties from what is commonly found in larger volumes. Interactions with a material surface provide for interesting chemistries that can be used to manipulate fluid movement (such as electrophoresis). A larger surface-to-volume ratio can also lead to problems such as nonspecific adsorption and

surface fouling. Flow in these devices is normally nonturbulent due to a low Reynolds number. Since flow is nonturbulent, mixing is normally diffusion limited.

Surface charge on the exposed material surface exerts a greater influence on the fluid in the channel as channel size decreases. Water, an amphoteric molecule, can be drawn through small channels through capillary action because of attraction between polar water molecules and partial or full charges present on the channel surface. In the presence of a salt solution, this interaction creates an electrical double layer of charge (Fig. 1.2) as buffer ions interact with surface charge. This double layer is the basis for electroosmosis as an applied voltage causes the loosely bound secondary layer to move towards an electrode and drag the bulk channel solution along with it to create electroosmotic flow. Hydrophobic channel surfaces are harder to fill with aqueous solutions (only van der Waals interactions) and can cause proteins in solution to denature and stick to the channel surface.

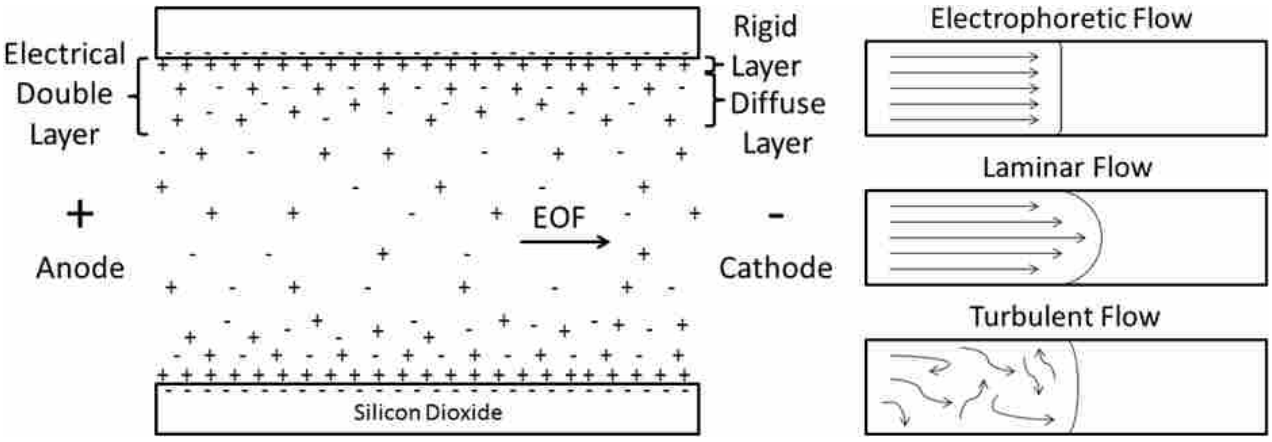

Figure 1.2. Overview of electroosmotic flow (EOF) and flow profile comparison. (Left) Ions concentrated at the surface create an electrical double layer which consists of two parts: a tightly bound rigid layer and loosely bound diffuse layer. Applied voltage causes the diffuse layer to move, pulling the bulk solution along with it, creating flow. (Right) Flow profile differs based on driving mechanism: EOF is relatively flat, laminar flow is parabolic, and turbulent flow is flattened in comparison to laminar flow.

This chapter will discuss properties and applications of commonly used materials followed by a brief overview of lab-on-a-chip functions. Finally, a summary of my research on the development of polymerized polyethylene glycol diacrylate as a microfluidic substrate will be given.

1.2. MATERIALS FOR MICROFLUIDICS

There are three main factors to choosing a design or material to use in a microfluidic system: required function, degree of integration, and application. Closely related, these three factors require consideration of material properties and fabrication processes. Flexibility, air permeability, nonspecific adsorption, cellular compatibility, solvent compatibility, and optical transmission are all physical characteristics that must be considered when choosing a material. Integration of fluid movement and control, detection mechanism, and chip automation can introduce a higher level of complexity in the fabrication process. The most important question, however, is what are you trying to accomplish with this device? Aqueous solutions are compatible with a broad range of materials, and limiting choices could be more of personal preference. Many organic solutions cause polymer substrates to swell and crack, or dissolve. Paper microfluidic devices are limited to capillary action as fluid wicks through the paper. Active components made from glass and silicon are more difficult to fabricate and fragile. Interfacing these materials with a more flexible material such as PDMS can enable integration of pneumatic pumps and valves.[16, 17] These characterizations are only a few of the considerations needing to be made when choosing a material for an application.

1.2.1 Inorganic Materials

Silicon was the first material used for microfluidics,[3] but current focus is on hybrid devices (glass or polymer bonded to silicon).[18, 19] Silicon is transparent to infrared wavelengths but not

ultraviolet-visible wavelengths, making fluorescence detection or debugging impossible in this range for an embedded channel in silicon. This is overcome by having a UV-VIS transparent material (polymer or glass) bound to silicon. Silicon chemistry focuses on the silanol group (–Si-OH) and is well-developed so surface modification is easily accomplished. Silicon has a high elastic modulus (130-180 GPa) and is not easily made into active fluidic components. Applications of silicon microfabricated devices have ranged from PCR[20] and nanowires[21] to cellular culture.[22] Nonspecific adsorption can be reduced and cellular growth improved through chemical modification of the surface.[23, 24] Fabrication for silicon (and consequently glass devices) utilizes either subtractive methods (chemical wet or dry etching) or additive methods, such as metal or chemical deposition, to create channels.[25]

Glass has low background fluorescence and like silicon, modification chemistries are silanol based. Since glass has a large elastic modulus (varies by composition), hybrid devices are required for active components such as valves and pumps.[16, 17] It is possible to deposit electrodes onto glass but the raised area of the electrodes creates problems when trying to bond to a glass top-layer. Glass is compatible with biological samples, has relatively low nonspecific adsorption, and is not gas permeable. Microfluidic channels are created by etching into the glass through wet or dry etch methods.[25] Applications focus on both all-glass and hybrid microchips.

1.2.2 Polymers

Polymers are organic-based, long-chain materials that have gained significant traction in microfluidics in the past 15 years. Polymers are advantageous for microfluidic device fabrication because they are relatively inexpensive, amenable to mass production processes (e.g., hot embossing, injection molding, etc.), and adaptable through formulation changes and chemical modification.

1.2.2.1 Elastomers

PDMS was first introduced as a microfluidic substrate in the late 1990s.[26, 27] Now it is one of the most common microfluidic substrates in use due to its rapid fabrication time, good bond strength, and ease of implementation. Device molds are formed utilizing soft lithography methods and multiple layers can be used to create complex fluidic designs.[28] Low elastic modulus (300-500 kPa) makes PDMS popular for use in valves and pumps.[29-31] PDMS is gas permeable, but low-molecular-weight oligomers in the polymer can drift to the surface causing hydrophobic recovery after plasma exposure.[32] Oligomers can also leach out into the sample solution, negatively impacting cellular studies, for example.[33] A hydrophobic material, PDMS is susceptible to nonspecific adsorption and permeation by hydrophobic molecules.[34] Chemical modification is needed to correct for these shortcomings. Plasma exposure will hydrophilize the exposed polymer surface, but only for a short time.[32, 35] Silanol reaction usually follows plasma activation to prevent this change in surface properties.[36, 37]

The inertness of perfluorinated compounds (e.g., Teflon-coated cookware) makes this class of materials attractive for microfluidics; such surfaces are both oleophobic and hydrophobic. Although there are several formula variations, most fluoroelastomers are perfluoropolyethers (PFPE), sometimes described as “liquid Teflon”. Rolland et al.[38] demonstrated that PFPE diol methacrylate (DMA) could be utilized to make valves similar to ones in PDMS. PFPE DMA showed reduced swelling in the presence of organic solvents compared to PDMS and had a Young’s modulus of 3.9 MPa. Rolland et al.[39] further demonstrated that PFPE-DMA could form sub-micron resolution molds down to 50 nm. De Marco et al.[40] showed that UV-cured PFPE could be bound to PDMS and determined a 1.52 MPa delamination pressure between bonded

PFPE layers. Since fluorinated surfaces are both hydrophobic and oleophobic, bonding to glass and similar substrates tends to be very weak.[41]

1.2.2.2 Thermoplastics

Thermoplastics are densely crosslinked polymers that are moldable when heated to their glass transition temperature but retain their shape when cooled. These materials are generally durable, amenable to micromachining processes, optically clear, resistant to permeation of small molecules and stiffer than elastomers. Thermoplastics require pedestal-valve geometries[16] for valves since the material is unable to collapse on itself to form a seal. Thermoplastic raw materials are available commercially through companies such as Topas, Zeonex, Aline Components and Optical Polymers Lab Corp.

Polystyrene (PS) is preferred by biologists over PDMS for cell culture, and most focus in microfluidics for this material is on cell culture and analysis.[33] PS microdevices are formed by melting polymer beads onto a mold to form channels.[42] PS having predominately styrene on the surface requires plasma oxidation or chemical modification to make PS hydrophilic.[42, 43] Adaptation of "Shrinky Dinks", a childrens' toy made from PS, resulted in well-sealed devices and higher channel aspect ratios due to polymer shrinkage.[44] Young et al.[43] optimized, using an epoxy mold, the formation of PS channels by hot embossing to create a more rapid fabrication process. Subsequent thermal bonding resulted in very strong adhesion between two PS layers.

Polycarbonate (PC) is a durable material created by polymerization of bisphenol A and phosgene, resulting in repeating carbonate groups. Predominately used for DNA analysis due to its high softening temperature (~145°C), PC channels are fabricated by hot embossing a silicon

mold into a thin layer of PC and subsequently laminating two layers together using thermal bonding.[45, 46] PC has an elastic modulus of 2.3-2.4 GPa.[47]

Poly(methyl methacrylate) (PMMA), formed through the polymerization of methyl methacrylate, is widely known under the commercial names of Plexiglas and Lucite. PMMA has an elastic modulus of 3.3 GPa and good optical clarity.[48] Channels are formed in PMMA through hot embossing.[49] Several different methods for bonding have been demonstrated to avoid collapsed channels.[50] Brown et al.[51] evaluated bonding strength with different chemical surface modifications. Yang et al.[52] demonstrated separation of α-fetoprotein (AFP) from blood serum using immunoaffinity extraction followed by electrophoretic separation and compared results to ELISA. Yang et al.[53] further demonstrated that multiple proteins could be selectively extracted from human serum and then quantified in a multiplexed device.

Chemical modification of acrylic polymers through direct incorporation of polyethylene glycol (PEG) helps to reduce nonspecific adsorption of proteins and cells.[54] Kim et al. [54] demonstrated that channels could be made down to 50 nm using UV exposure to bond PEG diacrylate (PEGDA) or PEG dimethacrylate (PEGDMA) layers. Kim et al.[55] further evaluated formation of nanochannels and nanostructures over an entire wafer using PEGDA reversibly attached to a gold or silicon substrate as mold for nanostructures made from a mercapto-ester adhesive, NOA 71. Plasma oxidized gold was shown to aid in the release of PEGDA from the mold. Extended UV exposure was used to avoid liquid residue on the PEGDA-silicon interface. Liu et al.[56] (and later Sun et al.[57]) demonstrated electrophoretic separations of amino acids, peptides and proteins in a PEG-based copolymer containing PEGDA, PEG methyl ether methacrylate (PEGMEMA), and methyl methacrylate (MMA). Sun et al.[58] showed that this PEG functionalized copolymer could be used in electric field gradient focusing. Klasner et al.[59]

demonstrated a PDMS-co-poly(ethylene oxide) material which had decreased optical clarity compared to PDMS but incorporated the non-adsorptive poly(ethylene oxide) moiety directly within the PDMS without requiring surface modification. Amino acid separations were also demonstrated within devices made from this polymer.

Cyclic-olefin copolymer (COC) is a commercially available, optically transparent material[60] that is suitable for use with most solvents and aqueous solutions,[61, 62] has good moldability, and low background fluorescence. Steigert et al.[63] demonstrated COC device formation through utilization of an epoxy mold master. The epoxy mold was used to emboss macro and micro features into the COC through embossing. Roy et al.[64] investigated the effect of plasma exposure on COC using oxygen, argon, and nitrogen. Each treatment was compared for bonding strength and platelet adhesion. They further determined that nitrogen plasma treatment of COC provided the best combination of hydrophilicity, EOF strength, and biocompatibility. Since COC is a hydrophobic polymer, chemical modification is necessary to be able to separate proteins using COC devices.[60] Dynamic coating with 2-hydroxylethyl cellulose reduces nonspecific protein adsorption noticeably as has been demonstrated by Zhang et al.[60]

SU8 is an epoxy-based polymer that is most commonly used in microfluidics to form a mold to create channels in another polymer. Multiple SU8 layers are easily fabricated,[65] and high aspect ratio features are readily made using soft lithography techniques. SU8 is transparent in the visible spectrum but not the UV and has an orange-brown coloration. SU8 has an elastic modulus of 2.0 GPa and has been used to create flexible check valves.[66] Protein detection was demonstrated showing low nonspecific adsorption and protein compatibility.[67] SU8/Pyrex devices are now being sold commercially through Micrux Technologies.

1.2.3 Paper

Paper is a flexible material predominantly made of cellulose and is beneficial as a microfluidic substrate for several reasons: (1) paper is cheap and readily available around the world; (2) the material burns easily and safely and will naturally degrade; (3) inkjet and solid wax printing enable easy channel or pattern definition and functionalization; (4) its porous structure allows for a combination of flow, filtering, and separation; (5) paper is biologically compatible; (6) paper can be chemically modified through composition/formulation changes or through attachment chemistries; (7) and the normally white background provides great contrast for color-based detection methods.[68, 69] Paper-based microfluidics relies on the passive mechanism of capillary action to pull solutions through the device. Electrochemical micro-paper-based analytical devices have been demonstrated to detect glucose, cholesterol, and lactose in blood serum.[70] Colorimetric detection was utilized to quantify nitrites in saliva and ketones in urine using a paper-based microfluidic device.[71]

1.2.4 Opportunities for Future Development

Numerous materials for microfluidics have been introduced over the past 25 years. Each material comes with a set of inherent strengths and weaknesses. Many materials (e.g., PDMS) have remained firmly planted in the academic world but have failed to gain traction commercially. How can the field break this barrier? The key lies in both the fabrication and evaluation of materials that are not only readily mass producible and inexpensive, but also an integral part of a compelling application. Hybrid devices, which reap the benefits of each material's strengths, have shown promise in achieving this goal. In biological applications, development of a material with inherent resistance to nonspecific adsorption is desirable, as long as the material still has other desirable properties for microfluidic applications (e.g., good optical clarity, water stability,

high bond strength, low background fluorescence, resistance to small molecule permeation, and the ability to create valves and pumps). The ideal material also needs to be capable of short design and turnaround times for rapid prototyping and integration with different substrates.

1.3 FUNCTIONS IN LAB-ON-A-CHIP SYSTEMS

Microfluidic functions are the basic operations in a microchip system, which combined lead to the desired analysis capability. Key functions include sample preparation, separation, detection, and liquid transport. Device functions and the overall objective of the analysis dictate the design and hardware required for each platform. A brief overview is included here.

1.3.1 Sample Preparation

Though the integration of sample preparation in microfluidics devices can be challenging, significant progress has been made in this area.[72] Advantages include reduction in analysis time and improved throughput.[73]

1.3.1.1 Extraction and Purification

Solid-phase extraction (SPE) is a popular preparation method wherein analytes are retained on a solid support and are subsequently eluted in a concentrated form.[74, 75] This method is easily integrated with other processes like PCR, separation, and detection in a microfluidic platform.[76] The most common SPE modes in microfluidics are reversed-phase, for non-polar to moderately polar compounds, and affinity. Affinity extraction techniques which are based on the strong affinity between an analyte and a compound bonded to the column are highly specific.

1.3.1.2 Preconcentration

Various on-line sample preconcentration techniques, utilizing analyte characteristics such as charge, affinity, mobility, and size, have been applied to overcome the low concentration

sensitivity resulting from the short optical path lengths in microfluidic channels.[77] An additional benefit of concentrating samples prior to analysis is improved detection of low concentration analytes typically encountered in real world samples.[78]

1.3.1.3 On-chip Labeling

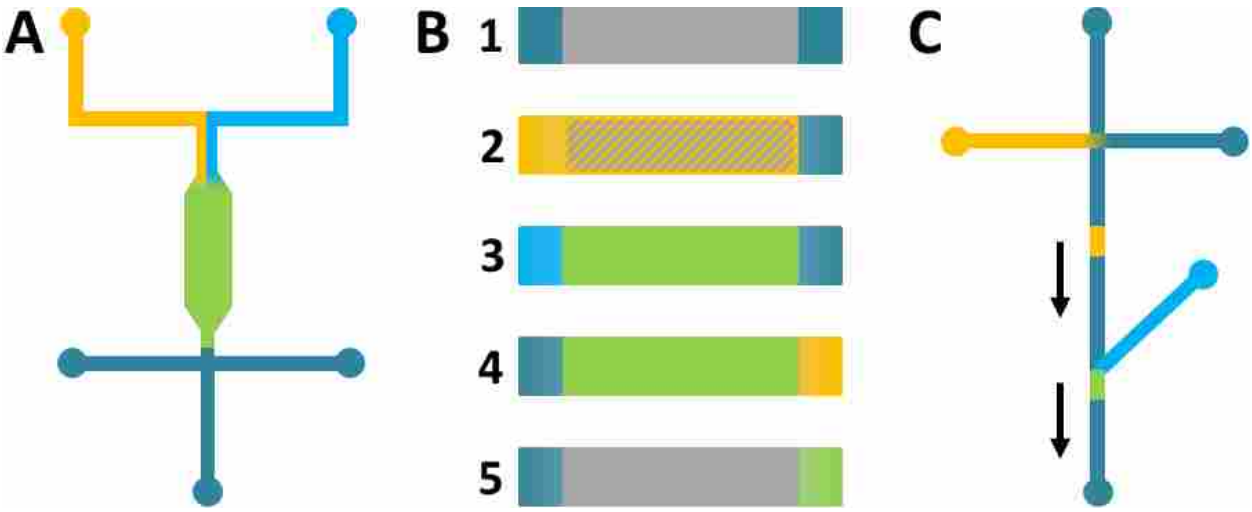

Figure 1.3. On-chip labeling overview. (A) Analyte (yellow) and reactive fluorophore (blue) solutions flow into a reaction chamber (green) for pre-separation labeling. (B) A solid phase extraction monolith (1) can be utilized for labeling. (2) Sample is flowed through the monolith and adsorbed nonspecifically. (3) A reactive fluorescent probe is then introduced into the monolith, allowed to incubate, and (4) the unreacted probe is then flushed. (5) Fluorescently labeled analyte is then eluted from the column. (C) In post-column labeling, a sample is separated and then reacted with a fluorescent label before detection.

Many samples do not fluoresce naturally and have to be derivatized to benefit from the low limits of detection of LIF. Although off-chip sample labeling is the most common, both off-chip and on-chip labeling have been performed. On-chip labeling can be divided into pre-column and post-column arrangements. Initial demonstration of pre-column labeling (see Fig. 1.3A) used an expanded channel geometry to allow an amino acid to react with *o*-phthaldialdehyde before

microchip capillary electrophoresis separation and subsequent fluorescent detection.[79] Yu et al.[80] adapted this approach for parallel multichannel analysis for up to eight unlabeled samples. A monolith for solid phase extraction (see Figure 1.3B) was used to augment the reaction of fluorescent dye with nonspecifically adsorbed analytes and improve automation and integration utilizing voltage control.[81] Post-column derivatization (see Fig. 1.3C) utilizes a secondary channel following the separation channel to label the analytes before detection.[82, 83] Other labeling methods have been demonstrated including using a series of monoliths as a micromixer for better mixing and more efficient labeling[84] and droplet microfluidics to control and merge sample and fluorescent label before microchannel introduction and separation.[85]

1.3.2 Separation Methods

Common separation techniques including chromatography, electrophoresis and fractionation have been demonstrated in microdevices. Although miniaturized electrophoretic systems received more initial attention than chromatographic ones, important progress has been made in both areas, as covered in greater detail in recent review articles on microfluidic chromatography[86, 87] and electrophoretic methods.[88, 89] Chromatography and fractionation methods will not be discussed further here due to limited overlap with the content of this dissertation.

1.3.2.1 Electrophoresis

Electrophoresis is one of the most powerful liquid-phase separation techniques, and can be used to separate a diverse range of analytes. Microchip capillary electrophoresis (μCE), first proposed and demonstrated in the early 1990s, is one of the best miniaturized separation techniques because it requires no moving parts, and provides fast, high-resolution separations.[90, 91] It is a highly useful separation technique for the analysis of biological, forensic, environmental,

pharmaceutical, and food samples.[92] Unlike in traditional CE instrumentation, which consists of a single capillary, many different capillaries and fluidic channels can be patterned on a microfluidic device to improve throughput.[91] Advantages of electrophoretic methods include high efficiency, speed, and low sample consumption.[92] Importantly, μCE's usefulness is increased by the integration of processes such as PCR, enzymatic digestion, and SPE.[91] However, μCE's applicability is limited because it has lower concentration sensitivities than liquid chromatography, due to the injection of small volumes in addition to a short optical path length as a result of the small height of the microchannel.[92]

A schematic of a typical μCE device is shown in Figure 1.4. In this design, sample is placed in the left reservoir and buffer in the rest of the device. Applied voltages move the sample through the device due to electroosmotic flow (see Fig. 1.2) or electrophoresis. For injection, the voltage applied to the right reservoir pulls the sample through the channel cross-section. For separation, an intermediate voltage is applied to the left and right reservoirs while a larger voltage is applied to the bottom reservoir, which causes a small plug of sample to move through the separation channel. As the sample plug travels down the channel, the components are separated due to differences in electrophoretic mobility; they are detected at the end of the channel.

1.3.3 Sensing and Detection

1.3.3.1 Optical Detection

Optical detection methods have several advantages. They have high sensitivity, do not require contact with fluid and can be adapted to a wide variety of compounds.[93] Several classes of optical detection are currently being implemented in microfluidic devices. These can be label based such as fluorescence and chemiluminescence or label free.

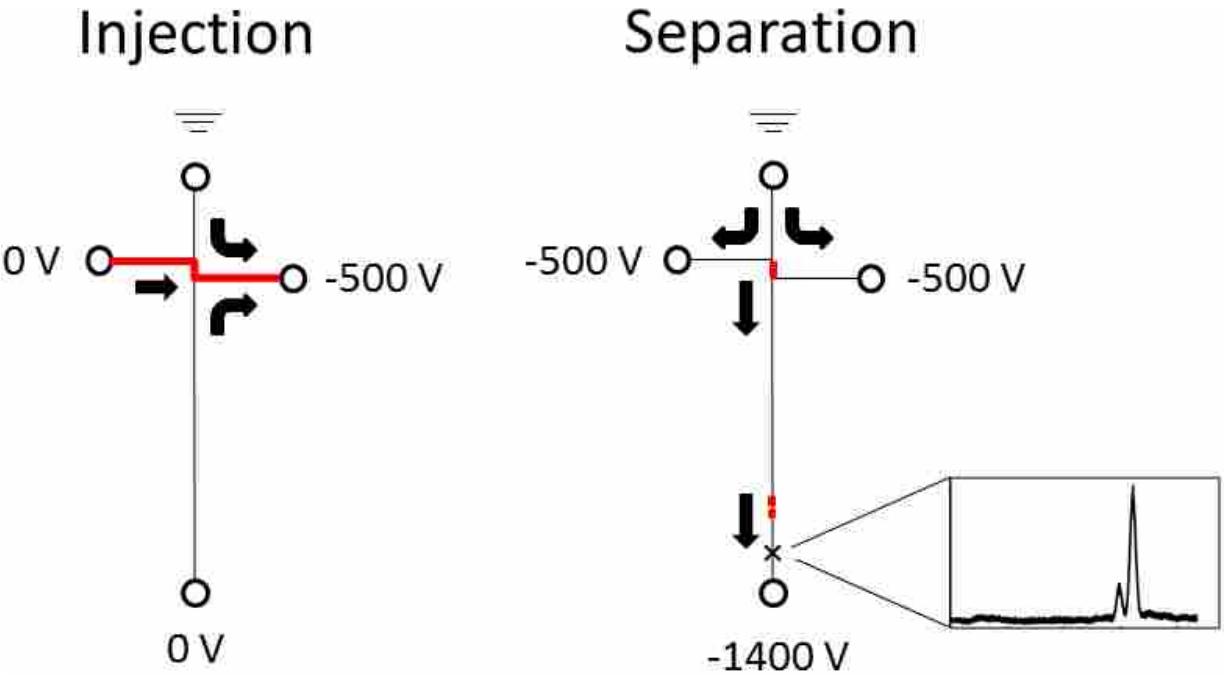

Figure 1.4. Overview of "pinched" injection and separation in μCE. (Left) Injection: voltage is applied in one reservoir to move the sample (red line) through the cross-section. Flow direction is shown by the black arrows. (Right) Separation: components of the sample move down the channel, are separated, and then are detected toward the end of the channel (X).

Laser-induced fluorescence (LIF) is the most widely used optical method in μCE because of its high sensitivity.[94] However, samples that do not fluoresce naturally need to be derivatized, often with variants of either fluorescein or rhodamine, which fluoresce in the green and red regions of the spectrum, respectively.[94] In most cases the actual optics used for detection in microfluidics are not integrated in the chip. For LIF detection, a laser is used for excitation, and a photomultiplier or CCD is used for detection (see Fig. 1.5).[95, 96] While label-based methods require time consuming sample derivatization, their detection limits are typically better than for label-free methods.

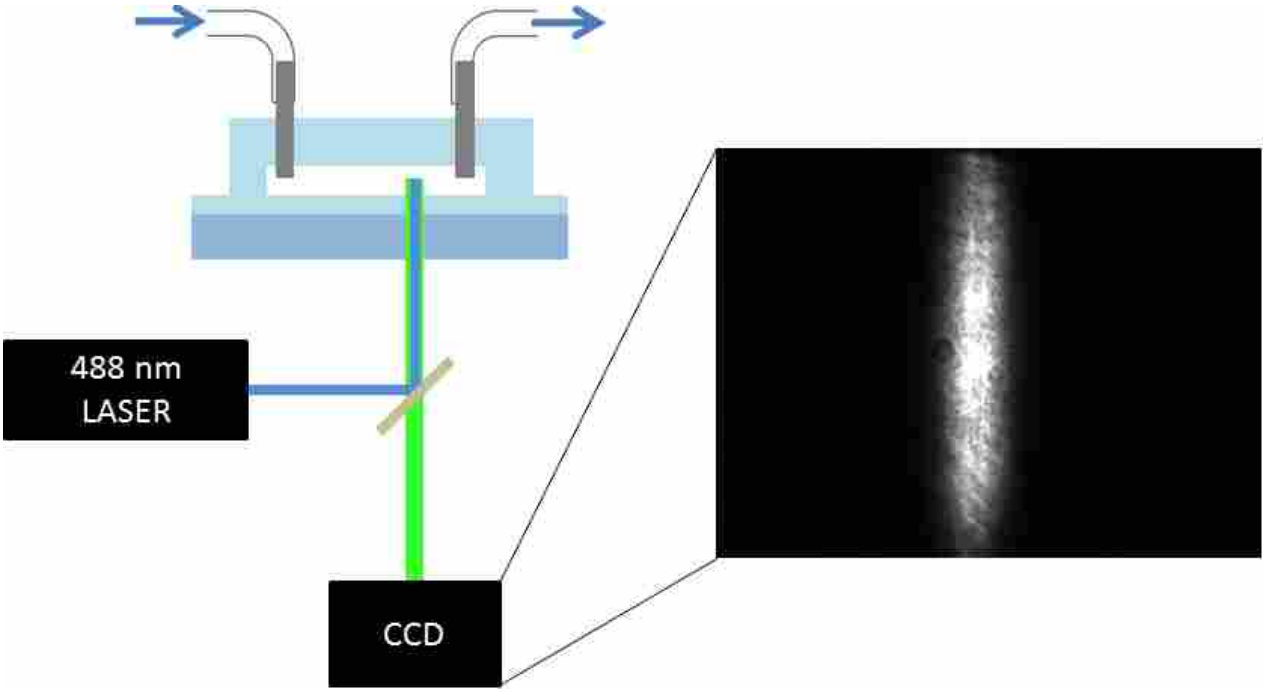

Figure 1.5. Overview of LIF setup.

Chemiluminescence detection, which has the advantage of not requiring excitation instrumentation that produces background interference, but instead requires very sensitive detectors, has also been demonstrated in both off-chip and on-chip formats. The technique is based on the production of electromagnetic radiation when the product of a chemical reaction luminesces or donates its energy to another molecule that luminesces.[97] Microchip electrophoresis and chemiluminescence detection were developed for the determination of intracellular sulphydryl compounds using the luminol–$Na_2S_2O_8$ reaction.[98]

UV absorbance is a label-free detection method commonly used in chromatography and electrophoresis systems because of its ability to directly detect a wide range of analytes without a derivatization step. However, in microfluidic systems, the sensitivity is limited by the short

optical path length across the separation channel.[99] This detection method has been described in both off-chip and on-chip formats in microdevices. For example, a simple cross geometry fused-silica microchip was used for the electrophoretic separation of four toxic alkaloids followed by UV-absorbance detection.[100]

1.3.3.2 Biosensors

A biosensor consists of a transducer that converts a chemical or biochemical signal into an electrical signal, and a molecular recognition component that establishes a sensor response.[101, 102] The biosensor component can be formed by immobilization of a biorecognition element on the transducer surface. This method offers label-free detection. Various biosensors have been studied utilizing hybrid microfluidic devices incorporating different materials and relying on surface chemistry modification. Microcantilever based sensors, which transduce changes in mass into a resonant frequency shift, have been optimized and used to perform real-time detection of proteins.[103] Affinity biosensors rely on highly selective affinity receptors to recognize target biomolecules. A PDMS microfluidic platform with a microchamber packed with aptamer-functionalized microbeads was used to purify, enrich, and detect trace amounts of fluorescently labeled arginine vasopressin.[104]

1.3.4 Fluid Manipulation

1.3.4.1 Pumps

Fluid pumping is an essential function of microfluidic systems and can be categorized as passive or active. Passive pumps such as surface tension-based pumping and evaporation/capillary force pumping do not require any external energy sources. The surface energy present in a tiny drop of liquid can be used to pump liquids through a microchannel. This has been demonstrated with a PDMS device having a reservoir port with a large drop of liquid and a pumping port with a

smaller drop of liquid. The pressure gradient due to uneven reservoir fluid levels caused the fluid to flow through the microchannel towards the reservoir with the lower level.[105] The combination of evaporation and capillary force has been exploited to produce a continuous transport process for liquids in microchannels.[106]

Active pumping methods require an external source of energy. Electroosmotic pumps (EOPs) which use EOF to drive liquids around within fluidic conduits have several advantages. They are bi-directional (i.e., EOF direction can be reversed by changing the polarity of the electric field), have no moving parts and are capable of generating constant and pulse-free flows. Importantly, EOPs can be easily integrated into microfluidic devices.[107] When the electrodes are located inside a microfluidic channel in the direct current voltage mode, electrolysis produces bubbles at the electrodes. To avoid this bubble formation, alternating current (AC) EOPs have been developed since application of an AC voltage does not result in any net electrolysis.[108] An AC electroosmotic pump was made of an interdigitated array of unequal width electrodes located at the bottom of a channel, with an AC voltage applied between the small and the large electrodes.[109] To avoid the evolution of gas bubbles that adhere and block parts of the electrodes and the membrane, platinum electrodes were replaced by Ag/Ag_2O electrodes. The pumps, which operated at voltages below the thermodynamic threshold for electrolysis of water so that neither H_2 nor O_2 were produced, generated sufficient flow for the delivery of drugs.[110] An integrated AC microfluidic pump consisting of a long serpentine microchannel was used to perform DNA hybridization.[111]

Electrochemical pumps based on the electrochemical generation of gas bubbles by the electrolysis of water have very low power consumption and generate almost no heat.[112, 113] For the implementation of an electrolysis based pump in a microchip, gold electrodes were arranged

on the COC surface to serve as anode and cathode for electrolysis. The electrode arrangement reduced the bulk resistance across the electrodes resulting in reduced power consumption.[114] Low-power electrochemical microfluidic pumps have also been integrated in PDMS microfluidic devices.[115, 116]

Pneumatically actuated valves and pumps have fast response times. The driving force comes from the actuation of a thin membrane by pressurized air in a control layer that is positioned over microchannels embedded in a fluid layer.[117] In a pneumatic valve usually made of a thin membrane that separates a layer containing the fluid channel and a layer that contains the control channel, application of pressure in the control channel deflects the membrane into the fluid channel and stops the flow. Peristaltic pumping is achieved by sequential actuation of the pneumatic valves and produces unidirectional motion of fluid in the fluid channel.[117] Such a pump has been integrated in a PDMS-glass device and used to perform labeling, dilution, and separation of amino acids with minimal operator intervention.[118] Cole et al.[117] reported a method for multiplexing pneumatic valves in such a manner that a large number of peristaltic pumps could be controlled by few external pneumatic connections. They demonstrated that four sets of pumping valves could be connected to a single pneumatic inlet.

1.3.4.2 Valves

Passive valves include check and burst valves. Check valves (Fig. 1.6A) allow fluid to flow in only one direction. A simple check valve was constructed via an in situ fabrication method inside a PDMS platform.[119] A check valve designed for low Reynolds number flow rates typical of lab-on-a-chip devices has also been demonstrated.[120] Burst valves (Fig. 1.6B) are single-use, passive microvalves that "burst" open irreversibly when the driving pressure exceeds the flow resistance of the valve.[121] Capillary-burst valves were integrated in microchannels of different dimensions

and used to study the critical burst pressure or rotational speed needed to overcome the capillary valve.[122]

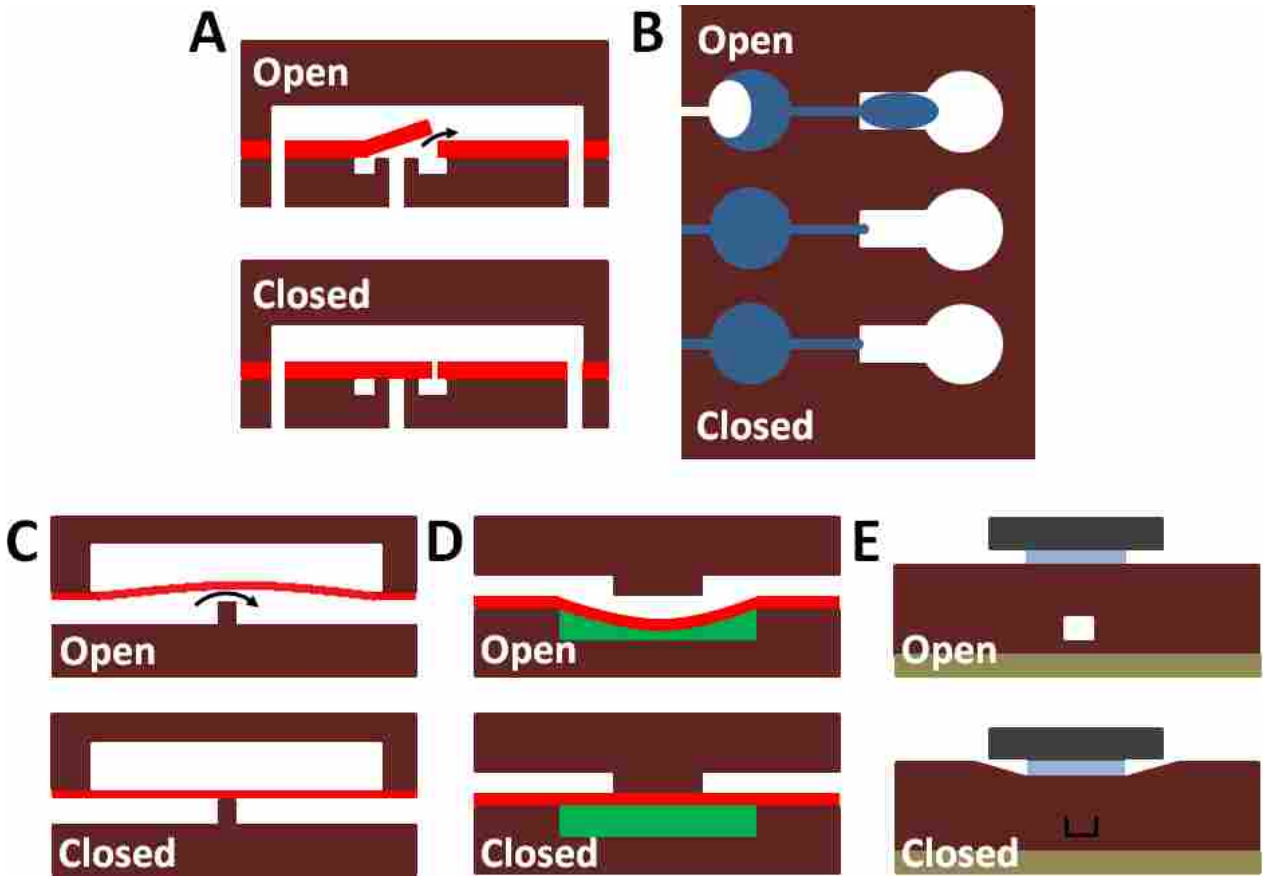

Figure 1.6. Overview of passive and active valves. Passive valves: (A) Check valves are mechanical valves that open with unidirectional flow under differential pressure. (B) Capillary burst valves are non-mechanical valves that utilize changes in channel geometry where the valve remains closed as long as the surface tension retains the solution in the channel. Active valves: (C) Pneumatic valves utilize deflection of a membrane via application of external pressure. (D) Phase-change valves employ materials with a volume difference in a phase change; here, the valve closes as the solution is heated and the volume increases. (E) External or integrated magnets can be used for moving magnetic materials to open and close channels.

Active valves, like active pumps, require an external energy source with rapid response time.[123] Pneumatic valves are actuated by applied pressure (Fig. 1.6C).[124] A pneumatic valve positioned at the intersection of the sample introduction and separation channels was used to control hydrodynamic injection in a PDMS-based microchip.[125] Screws embedded in the PMMA frame of a PDMS-PMMA valve assembly have been shown to actuate pneumatic valves.[126] Pneumatically actuated "lifting gate" microvalves and pumps were made by fabricating a fluidic layer containing the gate structure and a pneumatic layer in PDMS. The microvalve structures were then bonded to glass or plastic substrates to form microchannel structures.[127] Pneumatically actuated monolithic membrane valves have also been described.[16, 17]

Other active valves are phase-change (Fig. 1.6D), pinch and magnetic (Fig. 1.6E) microvalves. Paraffin, which changes phase with temperature, was used as valving material for thermal actuation.[128] A microvalve that was actuated by the volumetric change between the solid and liquid phases of PEG was used to couple genetic amplification and μCE.[129] Pinch microvalving is achieved by physically deforming PDMS using mechanical pressure. A variation known as TWIST valves was used for storing and pumping fluids in PDMS devices.[130] A magnetically controlled valve was fabricated by placing a permanent magnet above the device and iron plate beneath the device. The attractive force between the magnet and iron plate pressed a spacer against the deformable PDMS. Valving was controlled by manually placing or removing the permanent magnet.[123]

1.4 DISSERTATION OVERVIEW

Development and optimization of new materials are needed for microfluidics to gain a greater foothold in chemical analysis outside of academia. As biological and medical applications are the

focus for much current research, in this dissertation I focus on the development of a material inherently resistant to nonspecific protein adsorption. Since the material I have chosen is a thermoplastic, formula optimization is needed to adapt this material for use with valves while maintaining other desirable properties listed in Section 1.2.4. For greater utilization in microfluidics, this material should be amenable to electrophoresis, capable of incorporating valves, able to be integrated with different substrates (such as glass with electrodes for biosensor applications), and have reduced turnaround times for rapid prototyping. This dissertation covers my research in optimization and development of polymerized polyethylene glycol diacrylate (poly-PEGDA) having these desirable properties for broad utilization in microfluidics.

Chapter 2 discusses my initial characterization and development of poly-PEGDA. Repeating polyethylene glycol subunits within the polymer itself, imbue this material with reduced nonspecific adsorption, especially compared to PDMS, whose wide use in microfluidics makes it ideal to compare against. Resistance to protein nonspecific adsorption is demonstrated over time and concentration for PEGDA compared to PDMS. Poly-PEGDA demonstrates resistance to small molecule permeation and shows compatibility for use in electrophoretic separations of peptides and proteins, the latter showing well-resolved, symmetrical peaks. Although the elastic modulus >0.1 GPa[55] for PEGDA is too high to use in self-collapsing valves, it has potential for use in latch-valve designs.[131]

Since poly-PEGDA is a thermoplastic and has a Young's modulus of ~0.13 GPa, a different type of valve design is required compared to elastomeric polymers, such as PDMS. Chapter 3 shows the characterization results for the fabrication of three-layer monolithic membrane valves having both circular and square geometries. Valve performance is measured by comparing the valve closure pressure, the input pressure in the fluidic line required to open the valve, and tracking the

meniscus movement over a range of applied pressures (0-30 PSI). Initially, the valve opening pressure is ~48 kPa greater than the applied pressure to close the valve, but after an initial ~1000 actuations, this pressure difference drops to zero. Valves can be actuated at a rate of 8 Hz with a ~100 ms valve opening time and a ~20 ms closure time. The valves demonstrate good repeatability for over 115,000 actuations.

The ability to bond poly-PEGDA to different substrates, such as silicon, glass, or other polymers, allows for integration with a variety of different sensing mechanisms (e.g., attachment to glass with electrodes for potentiometry or MEMS devices for biosensing). Chapter 4 introduces a method for dual silane deposition on glass for site specific functionalization. Deposition of an acrylate containing silane allows poly-PEGDA to bind to the glass surface, while a secondary deposition of an aminosilane in lithographically patterned areas provides a way to attach desired surface functionalities, such as amine-linked DNA or proteins through glutaraldehyde crosslinking.

The fifth chapter focuses on the optimization of 3D printed poly-PEGDA microfluidic devices having integrated valves and the adaptation of a poly-PEGDA prepolymer resin for use in 3D printing for improved turnaround times. 3D printed devices are made utilizing a B9 Creator 3D printer and a photosensitive resin containing poly-PEGDA in a layer-by-layer process while changing the projected image to create different microfluidic features. 3D printing a complete device drastically reduces total fabrication time (devices take less than 45 min to create) and allows for rapid prototyping, where designs change frequently. Channel dimensions down to 350 μm wide by 250 μm tall were printed with a 100% success rate. Chapter 5 also contains the first demonstration of 3D printed microfluidic valves.

In Chapter 6, I will discuss my conclusions about the characterization and optimization of poly-PEGDA. The adaptation of this material for use in valves enables its broader application as a microfluidic substrate. Heterogeneous material integration coupled with dual silane deposition allows integration with silicon and quartz devices while providing site-specific functionalization for further surface modification. Utilization of 3D printing in creation of poly-PEGDA devices with integrated valves improves turnaround times for device rapid prototyping. Future directions for the continued development of optically transparent, 3D-printed poly-PEGDA devices to increase its allure in microfluidic applications, and one-step surface attachment to improve the site-specific chemistry of surface functionalization will also be discussed.

1.5 REFERENCES

(1) Skoog, D. A.; Holler, F. J.; Crouch, S. R. *Principles of Instrumental Analysis*, 6th ed.; Thomson Brooks Cole: Belmont, CA, 2007.
(2) Guzman, N. A.; Phillips, T. M. *Electrophoresis* **2011**, *32*, 1565-1578.
(3) Terry, S. C.; Jerman, J. H.; Angell, J. B. *IEEE Trans. Electron Devices* **1979**, *26*, 1880-1886.
(4) Reyes, D. R.; Iossifidis, D.; Auroux, P.-A.; Manz, A. *Anal. Chem.* **2002**, *74*, 2623-2636.
(5) Harrison, D. J.; Manz, A.; Fan, Z.; Luedi, H.; Widmer, H. M. *Anal. Chem.* **1992**, *64*, 1926-1932.
(6) Martinez, A. W.; Phillips, S. T.; Wiley, B. J.; Gupta, M.; Whitesides, G. M. *Lab Chip* **2008**, *8*, 2146-2150.
(7) Auroux, P.-A.; Iossifidis, D.; Reyes, D. R.; Manz, A. *Anal. Chem.* **2002**, *74*, 2637-2652.
(8) Vilkner, T.; Janasek, D.; Manz, A. *Anal. Chem.* **2004**, *76*, 3373-3386.
(9) Dittrich, P. S.; Tachikawa, K.; Manz, A. *Anal. Chem.* **2006**, *78*, 3887-3908.
(10) West, J.; Becker, M.; Tombrink, S.; Manz, A. *Anal. Chem.* **2008**, *80*, 4403-4419.
(11) Arora, A.; Simone, G.; Salieb-Beugelaar, G. B.; Kim, J. T.; Manz, A. *Anal. Chem.* **2010**, *82*, 4830-4847.
(12) Whitesides, G. M. *Nature* **2006**, *442*, 368-373.
(13) Berthier, J.; Silberzan, P. *Microfluidics for Biotechnology*; Artech House: Norwood, MA, 2006, 95.
(14) Placidi, M.; Cannistraro, S. *Europhysics Letters* **1998**, *43*, 476-481.
(15) Madou, M. J. *Fundamentals of Microfabrication: The Science of Miniaturization*, 2nd ed.; CRC Press: Boca Raton, 2002.
(16) Grover, W. H.; Skelley, A. M.; Liu, C. N.; Lagally, E. T.; Mathies, R. A. *Sensor Actuat B-Chem* **2003**, *89*, 315-323.
(17) Grover, W. H.; Ivester, R. H. C.; Jensen, E. C.; Mathies, R. A. *Lab Chip* **2006**, *6*, 623-631.

(18) Washburn, A. L.; Gunn, L. C.; Bailey, R. C. *Anal. Chem.* **2009**, *81*, 9499-9506.
(19) Anderson, R. R.; Hu, W.; Noh, J. W.; Dahlquist, W. C.; Ness, S. J.; Gustafson, T. M.; Richards, D. C.; Kim, S.; Mazzeo, B. A.; Woolley, A. T.; Nordin, G. P. *Lab Chip* **2011**, *11*, 2088-2096.
(20) Wang, F.; Burns, M. A. *Biomed. Microdevices* **2009**, *11*, 1071-1080.
(21) Chua, J. H.; Chee, R.-E.; Agarwal, A.; Wong, S. M.; Zhang, G.-J. *Anal. Chem.* **2009**, *81*, 6266-6271.
(22) Sung, J. H.; Shuler, M. L. *Lab Chip* **2009**, *9*, 1385-1394.
(23) Sharma, S.; Popat, K. C.; Desai, T. A. *Langmuir* **2002**, *18*, 8728-8731.
(24) Zhang, M.; Desai, T.; Ferrari, M. *Biomaterials* **1998**, *19*, 953-960.
(25) Iliescu, C.; Taylor, H.; Avram, M.; Miao, J. M.; Franssila, S. *Biomicrofluidics* **2012**, *6*.
(26) Effenhauser, C. S.; Bruin, G. J. M.; Paulus, A.; Ehrat, M. *Anal. Chem.* **1997**, *69*, 3451-3457.
(27) Duffy, D. C.; McDonald, J. C.; Schueller, O. J. A.; Whitesides, G. M. *Anal. Chem.* **1998**, *70*, 4974-4984.
(28) Ng, J. M. K.; Gitlin, I.; Stroock, A. D.; Whitesides, G. M. *Electrophoresis* **2002**, *23*, 3461-3473.
(29) Li, N.; Hsu, C.-H.; Folch, A. *Electrophoresis* **2005**, *26*, 3758-3764.
(30) Araci, I. E.; Quake, S. R. *Lab Chip* **2012**, *12*, 2803-2806.
(31) Cellar, N. A.; Burns, S. T.; Meiners, J.-C.; Chen, H.; Kennedy, R. T. *Anal. Chem.* **2005**, *77*, 7067-7073.
(32) Hillborg, H.; Tomczak, N.; Olàh, A.; Schönherr, H.; Vancso, G. J. *Langmuir* **2004**, *20*, 785-794.
(33) Berthier, E.; Young, E. W. K.; Beebe, D. *Lab Chip* **2012**, *12*, 1224-1237.
(34) Roman, G. T.; Hlaus, T.; Bass, K. J.; Seelhammer, T. G.; Culbertson, C. T. *Anal. Chem.* **2005**, *77*, 1414-1422.
(35) Bodas, D.; Khan-Malek, C. *Microelectron. Eng.* **2006**, *83*, 1277-1279.
(36) Wang, D.; Oleschuk, R. D.; Horton, J. H. *Langmuir* **2008**, *24*, 1080-1086.
(37) Sui, G.; Wang, J.; Lee, C.-C.; Lu, W.; Lee, S. P.; Leyton, J. V.; Wu, A. M.; Tseng, H.-R. *Anal. Chem.* **2006**, *78*, 5543-5551.
(38) Rolland, J. P.; Van Dam, R. M.; Schorzman, D. A.; Quake, S. R.; DeSimone, J. M. *J. Am. Chem. Soc.* **2004**, *126*, 2322-2323.
(39) Rolland, J. P.; Hagberg, E. C.; Denison, G. M.; Carter, K. R.; De Simone, J. M. *Angew. Chem.* **2004**, *116*, 5920-5923.
(40) De Marco, C.; Girardo, S.; Mele, E.; Cingolani, R.; Pisignano, D. *Lab Chip* **2008**, *8*, 1394-1397.
(41) Devaraju, N. S. G. K.; Unger, M. A. *Lab Chip* **2011**, *11*, 1962-1967.
(42) Dusseiller, M. R.; Schlaepfer, D.; Koch, M.; Kroschewski, R.; Textor, M. *Biomaterials* **2005**, *26*, 5917-5925.
(43) Young, E. W. K.; Berthier, E.; Guckenberger, D. J.; Sackmann, E.; Lamers, C.; Meyvantsson, I.; Huttenlocher, A.; Beebe, D. J. *Anal. Chem.* **2011**, *83*, 1408-1417.
(44) Chen, C.-S.; Breslauer, D. N.; Luna, J. I.; Grimes, A.; Chin, W.-c.; Lee, L. P.; Khine, M. *Lab Chip* **2008**, *8*, 622-624.
(45) Wang, Y.; Chen, H.; He, Q.; Soper, S. A. *Electrophoresis* **2008**, *29*, 1881-1888.
(46) Chen, P.-C.; Park, D. S.; You, B.-H.; Kim, N.; Park, T.; Soper, S. A.; Nikitopoulos, D. E.; Murphy, M. C. *Sens. Actuators, B* **2010**, *149*, 291-300.

(47) Qi, H.; Chen, T.; Yao, L.; Zuo, T. *Opt. Laser Eng.* **2009**, *47*, 594-598.
(48) Tsao, C. W.; Hromada, L.; Liu, J.; Kumar, P.; DeVoe, D. L. *Lab Chip* **2007**, *7*, 499-505.
(49) Kelly, R. T.; Woolley, A. T. *Anal. Chem.* **2003**, *75*, 1941-1945.
(50) Tsao, C.-W.; DeVoe, D. *Microfluid. Nanofluid.* **2009**, *6*, 1-16.
(51) Brown, L.; Koerner, T.; Horton, J. H.; Oleschuk, R. D. *Lab Chip* **2006**, *6*, 66-73.
(52) Yang, W.; Sun, X.; Wang, H.-Y.; Woolley, A. T. *Anal. Chem.* **2009**, *81*, 8230-8235.
(53) Yang, W.; Yu, M.; Sun, X.; Woolley, A. T. *Lab Chip* **2010**, *10*, 2527-2533.
(54) Kim, P.; Jeong, H. E.; Khademhosseini, A.; Suh, K. Y. *Lab Chip* **2006**, *6*, 1432-1437.
(55) Kim, P.; Suh, K. Y. *Langmuir* **2007**, *23*, 4549-4553.
(56) Liu, J. K.; Sun, X. F.; Lee, M. L. *Anal. Chem.* **2007**, *79*, 1926-1931.
(57) Sun, X. F.; Li, D.; Lee, M. L. *Anal. Chem.* **2009**, *81*, 6278-6284.
(58) Sun, X.; Farnsworth, P. B.; Woolley, A. T.; Tolley, H. D.; Warnick, K. F.; Lee, M. L. *Anal. Chem.* **2007**, *80*, 451-460.
(59) Klasner, S. A.; Metto, E. C.; Roman, G. T.; Culbertson, C. T. *Langmuir* **2009**, *25*, 10390-10396.
(60) Zhang, J.; Das, C.; Fan, Z. *Microfluid. Nanofluid.* **2008**, *5*, 327-335.
(61) Liu, J.; Chen, C.-F.; Tsao, C.-W.; Chang, C.-C.; Chu, C.-C.; DeVoe, D. L. *Anal. Chem.* **2009**, *81*, 2545-2554.
(62) Faure, K.; Albert, M.; Dugas, V.; Crétier, G.; Ferrigno, R.; Morin, P.; Rocca, J.-L. *Electrophoresis* **2008**, *29*, 4948-4955.
(63) Steigert, J.; Haeberle, S.; Brenner, T.; Müller, C.; Steinert, C. P.; Koltay, P.; Gottschlich, N.; Reinecke, H.; Rühe, J.; Zengerle, R.; Ducrée, J. *J. Micromech. Microeng.* **2007**, *17*, 333.
(64) Roy, S.; Yue, C. Y. *Plasma Processes Polym.* **2011**, *8*, 432-443.
(65) Carlier, J.; Arscott, S.; Thomy, V.; Fourrier, J. C.; Caron, F.; Camart, J. C.; Druon, C.; Tabourier, P. *J. Micromech. Microeng.* **2004**, *14*, 619.
(66) Ezkerra, A.; Fernandez, L. J.; Mayora, K.; Ruano-Lopez, J. M. *Lab on a chip* **2011**, *11*, 3320-3325.
(67) Heyries, K. A.; Loughran, M. G.; Hoffmann, D.; Homsy, A.; Blum, L. J.; Marquette, C. A. *Biosens. Bioelectron.* **2008**, *23*, 1812-1818.
(68) Martinez, A. W.; Phillips, S. T.; Whitesides, G. M.; Carrilho, E. *Anal. Chem.* **2009**, *82*, 3-10.
(69) Pelton, R. *TrAC, Trends Anal. Chem.* **2009**, *28*, 925-942.
(70) Nie, Z.; Deiss, F.; Liu, X.; Akbulut, O.; Whitesides, G. M. *Lab Chip* **2010**, *10*, 3163-3169.
(71) Klasner, S.; Price, A.; Hoeman, K.; Wilson, R.; Bell, K.; Culbertson, C. *Anal. Bioanal. Chem.* **2010**, *397*, 1821-1829.
(72) Kovarik, M. L.; Gach, P. C.; Ornoff, D. M.; Wang, Y.; Balowski, J.; Farrag, L.; Allbritton, N. L. *Anal. Chem.* **2011**, *84*, 516-540.
(73) Zhang, J. Y.; Do, J.; Premasiri, W. R.; Ziegler, L. D.; Klapperich, C. M. *Lab Chip* **2010**, *10*, 3265-3270.
(74) Geiser, L.; Eeltink, S.; Svec, F.; Fréchet, J. M. J. *J. Chromatogr. A* **2007**, *1140*, 140-146.
(75) Kang, Q.-S.; Li, Y.; Xu, J.-Q.; Su, L.-J.; Li, Y.-T.; Huang, W.-H. *Electrophoresis* **2010**, *31*, 3028-3034.
(76) Reedy, C. R.; Hagan, K. A.; Strachan, B. C.; Higginson, J. J.; Bienvenue, J. M.; Greenspoon, S. A.; Ferrance, J. P.; Landers, J. P. *Anal. Chem.* **2010**, *82*, 5669-5678.

(77) Sueyoshi, K.; Kitagawa, F.; Otsuka, K. *Anal. Chem.* **2008**, *80*, 1255-1262.
(78) Chun, H.; Chung, T. D.; Ramsey, J. M. *Anal. Chem.* **2010**, *82*, 6287-6292.
(79) Jacobson, S. C.; Hergenröder, R.; Moore, A. W., Jr.; Ramsey, J. M. *Anal. Chem.* **1994**, *66*, 4127-4132.
(80) Yu, M.; Wang, Q.; Patterson, J. E.; Woolley, A. T. *Anal. Chem.* **2011**, *83*, 3541-3547.
(81) Nge, P. N.; Pagaduan, J. V.; Yu, M.; Woolley, A. T. *J. Chromatogr. A* **2012**, *1261*, 129-135.
(82) Jacobson, S. C.; Koutny, L. B.; Hergenröder, R.; Moore, A. W., Jr.; Ramsey, J. M. *Anal. Chem.* **1994**, *66*, 3472-3476.
(83) Li, M. W.; Martin, R. S. *Analyst* **2008**, *133*, 1358-1366.
(84) Mair, D. A.; Schwei, T. R.; Dinio, T. S.; Svec, F.; Fréchet, J. M. J. *Lab Chip* **2009**, *9*, 877-883.
(85) Abdelgawad, M.; Watson, M. W. L.; Wheeler, A. R. *Lab Chip* **2009**, *9*, 1046-1051.
(86) Lavrik, N. V.; Taylor, L. T.; Sepaniak, M. J. *Anal. Chim. Acta* **2011**, *694*, 6-20.
(87) Kutter, J. P. *J. Chromatogr. A* **2012**, *1221*, 72-82.
(88) Breadmore, M. C. *J. Chromatogr. A* **2012**, *1221*, 42-55.
(89) Kenyon, S. M.; Meighan, M. M.; Hayes, M. A. *Electrophoresis* **2011**, *32*, 482-493.
(90) Felhofer, J. L.; Blanes, L.; Garcia, C. D. *Electrophoresis* **2010**, *31*, 2469-2486.
(91) Henry, C. S.; Henry, C. S., Ed.; Humana Press, 2006; Vol. 339, 1-9.
(92) Ramautar, R.; de Jong, G. J.; Somsen, G. W. *Electrophoresis* **2012**, *33*, 243-250.
(93) Angelescu, D. E. *Highly Integrated Microfluidic Design*; Artech House: Norwood, MA, 2011, 115-120.
(94) Myers, F. B.; Lee, L. P. *Lab Chip* **2008**, *8*, 2015-2031.
(95) Mitra, I.; Zhuang, Z.; Zhang, Y.; Yu, C.-Y.; Hammoud, Z. T.; Tang, H.; Mechref, Y.; Jacobson, S. C. *Anal. Chem.* **2012**, *84*, 3621-3627.
(96) Mainz, E. R.; Gunasekara, D. B.; Caruso, G.; Jensen, D. T.; Hulvey, M. K.; Fracassi da Silva, J. A.; Metto, E. C.; Culbertson, A. H.; Culbertson, C. T.; Lunte, S. M. *Anal. Methods* **2012**, *4*, 414-420.
(97) García-Campaña, A. M.; Lara, F. J.; Gámiz-Gracia, L.; Huertas-Pérez, J. F. *TrAC, Trends Anal. Chem.* **2009**, *28*, 973-986.
(98) Zhao, S.; Huang, Y.; Ye, F.; Shi, M.; Liu, Y.-M. *J. Chromatogr. A* **2010**, *1217*, 5732-5736.
(99) Ohlsson, P. D.; Ordeig, O.; Mogensen, K. B.; Kutter, J. P. *Electrophoresis* **2009**, *30*, 4172-4178.
(100) Newman, C. I. D.; Giordano, B. C.; Copper, C. L.; Collins, G. E. *Electrophoresis* **2008**, *29*, 803-810.
(101) Anderson, H.; Jönsson, M.; Vestling, L.; Lindberg, U.; Aastrup, T. *Sens. Actuators, B* **2007**, *123*, 27-34.
(102) Rapp, B. E.; Gruhl, F. J.; Länge, K. *Anal. Bioanal. Chem.* **2010**, *398*, 2403-2412.
(103) Ricciardi, C.; Canavese, G.; Castagna, R.; Ferrante, I.; Ricci, A.; Marasso, S. L.; Napione, L.; Bussolino, F. *Biosens. Bioelectron.* **2010**, *26*, 1565-1570.
(104) Nguyen, T.; Pei, R.; Landry, D. W.; Stojanovic, M. N.; Lin, Q. *Sens. Actuators, B* **2011**, *154*, 59-66.
(105) Walker, G. M.; Beebe, D. J. *Lab Chip* **2002**, *2*, 131-134.
(106) Goedecke, N.; Eijkel, J.; Manz, A. *Lab Chip* **2002**, *2*, 219-223.

(107) Wang, X.; Wang, S.; Gendhar, B.; Cheng, C.; Byun, C. K.; Li, G.; Zhao, M.; Liu, S. *TrAC, Trends Anal. Chem.* **2009**, *28*, 64-74.
(108) Wang, X.; Cheng, C.; Wang, S.; Liu, S. *Microfluid. Nanofluid.* **2009**, *6*, 145-162.
(109) Debesset, S.; Hayden, C. J.; Dalton, C.; Eijkel, J. C. T.; Manz, A. *Lab Chip* **2004**, *4*, 396-400.
(110) Shin, W.; Lee, J. M.; Nagarale, R. K.; Shin, S. J.; Heller, A. *J. Am. Chem. Soc.* **2011**, *133*, 2374-2377.
(111) Huang, C.-C.; Bazant, M. Z.; Thorsen, T. *Lab Chip* **2010**, *10*, 80-85.
(112) Nestler, J.; Morschhauser, A.; Hiller, K.; Otto, T.; Bigot, S.; Auerswald, J.; Knapp, H.; Gavillet, J.; Gessner, T. *Int. J. Adv. Manuf. Technol.* **2010**, *47*, 137-145.
(113) Chiu, S.-H.; Liu, C.-H. *Lab Chip* **2009**, *9*, 1524-1533.
(114) Park, S.-m.; Lee, K.; Craighead, H. *Biomed. Microdevices* **2008**, *10*, 891-897.
(115) Lui, C.; Stelick, S.; Cady, N.; Batt, C. *Lab Chip* **2010**, *10*, 74-79.
(116) Blanco-Gomez, G.; Glidle, A.; Flendrig, L. M.; Cooper, J. M. *Anal. Chem.* **2009**, *81*, 1365-1370.
(117) Cole, M. C.; Desai, A. V.; Kenis, P. J. A. *Sens. Actuators, B* **2011**, *151*, 384-393.
(118) Mora, M. F.; Greer, F.; Stockton, A. M.; Bryant, S.; Willis, P. A. *Anal. Chem.* **2011**, *83*, 8636-8641.
(119) Kim, J.; Baek, J.; Lee, K.; Park, Y.; Sun, K.; Lee, T.; Lee, S. *Lab Chip* **2006**, *6*, 1091-1094.
(120) Loverich, J.; Kanno, I.; Kotera, H. *Microfluid. Nanofluid.* **2007**, *3*, 427-435.
(121) Au, A. K.; Lai, H.; Utela, B. R.; Folch, A. *Micromachines* **2011**, *2*, 179-220.
(122) Chen, J.; Huang, P.-C.; Lin, M.-G. *Microfluid. Nanofluid.* **2008**, *4*, 427-437.
(123) Chen, C.-Y.; Chen, C.-H.; Tu, T.-Y.; Lin, C.-M.; Wo, A. M. *Lab Chip* **2011**, *11*, 733-737.
(124) Ogilvie, I. R. G.; Sieben, V. J.; Cortese, B.; Mowlem, M. C.; Morgan, H. *Lab Chip* **2011**, *11*, 2455-2459.
(125) Sun, X.; Kelly, R. T.; Danielson, W. F.; Agrawal, N.; Tang, K.; Smith, R. D. *Electrophoresis* **2011**, *32*, 1610-1618.
(126) Zheng, Y.; Dai, W.; Wu, H. *Lab Chip* **2009**, *9*, 469-472.
(127) Kim, J.; Kang, M.; Jensen, E. C.; Mathies, R. A. *Anal. Chem.* **2012**, *84*, 2067-2071.
(128) Liu, R. H.; Bonanno, J.; Yang, J.; Lenigk, R.; Grodzinski, P. *Sens. Actuators, B* **2004**, *98*, 328-336.
(129) Kaigala, G. V.; Hoang, V. N.; Backhouse, C. J. *Lab Chip* **2008**, *8*, 1071-1078.
(130) Weibel, D. B.; Siegel, A. C.; Lee, A.; George, A. H.; Whitesides, G. M. *Lab Chip* **2007**, *7*, 1832-1836.
(131) Rogers, C. I.; Oxborrow, J. B.; Anderson, R. R.; Tsai, L. F.; Nordin, G. P.; Woolley, A. T. *Sens. Actuators, B* **2014**, *191*, 438-444.

2. SINGLE-MONOMER FORMULATION OF POLYMERIZED POLYETHYLENE GLYCOL DIACRYLATE AS A NONADSORPTIVE MATERIAL FOR MICROFLUIDICS*

2.1 INTRODUCTION

The field of microfluidics has gained increasing research focus for small volume analysis over the last 20 years.[1-4] Ideally, microfluidic devices must be small and inexpensive, have rapid analysis times, and not require extensive training to use. As specimen sizes get smaller, microfluidics provide a means for reagent control and delivery, improved mass transport, and more efficient sample use in small spaces. Recent examples of the power of microfluidic systems can be found in cell-based assays,[5, 6] droplet microfluidics,[7-10] and chemical analysis.[11-13] Goral et al.[14] used polydimethylsiloxane (PDMS) in a perfusion-based microsystem to mimic *in vivo* conditions for hepatocytes without the need for special matrices or coagulants. Shi et al.[15] utilized a droplet microfluidic system made from PDMS to immobilize an array of nematodes and test the effects of varying doses of neurotoxins. Yang et al.[16, 17] recently showed that poly(methyl methacrylate) devices having photopolymerized affinity columns could be used to selectively purify and quantitate cancer-related biomarkers from a complex sample such as blood serum. These examples demonstrate the great potential of microfluidics in biomedical research and point-of-care clinical analysis.

Biological samples pose a particular problem of interest for microfluidic systems. However, PDMS, which is a popular material in these microfluidic systems, is prone to nonspecific adsorption and fouling.[18, 19] Because biological samples may be limited to very small quantities, some or all of the analytes of interest could be lost to an adsorptive surface, instead of being

detected. Although many methods have attempted to address this important issue by modifying the PDMS itself,[20-24] an increasingly attractive alternative is to find a replacement material for PDMS, which retains the ability to be patterned and formed easily, but does not suffer from severe surface fouling.

Most current research in microfluidics uses static or dynamic surface changes to reduce adsorption to the device material. In PDMS, plasma oxidation has been shown to increase the hydrophilicity of the surface, but the effect is only temporary (lasting hours), because of low-molecular-weight oligomers that are present in the bulk of the PDMS and return slowly to the surface;[25, 26] this process can be slowed if the oxidized PDMS is rapidly transferred to water.[27] Solution-phase reactions can be used to functionalize oxidized PDMS surfaces with perfluorosilanes[28] or polyethylene glycol silanes.[29] Dynamic surface modification methods are by definition temporary coatings that must be replenished frequently.

Alternative materials to PDMS have been developed in the last 10 years, but they have yet to gain significant traction. Perfluoropolymers like perfluoropolyether (PFPE)[30, 31] provide inherent resistance to nonspecific adsorption and have been used instead of PDMS as microfluidic supports, but bonding separate layers can be problematic. Thermoset polyester microfluidic devices[32] use similar soft photolithography methods to PDMS for fabrication; however, atom-transfer radical polymerization was needed to passivate surfaces before protein separations.[33] A mildly hydrophilic polymer, polyethylene glycol (PEG), is known for its resistance to nonspecific binding.[34] Integrating PEG directly into PDMS has been attempted, but the optical clarity of the resulting polymer is greatly reduced.[35] Incorporating PEG into an acrylate plastic creates an optically clear, UV curable polymer that can be formed using soft lithography techniques.[36] Repeating PEG subunits in the bulk of the polymer provide an inherent way to

reduce nonspecific binding in fluidic pathways without further chemical modification or replenishment. Kim et al.[37] demonstrated that either PEG diacrylate (PEGDA) or PEG dimethacrylate (PEGDMA), when mixed with a photoinitiator, could be cured quickly via UV exposure and form stable channel features as small as 50 nm. Undercured individual layers were bonded after they were placed together and fully cured. Poly-PEGDMA was shown to offer lower nonspecific protein and cell adhesion than either PDMS or PEG-silanized PDMS, but no adsorption studies on poly-PEGDA were done. Furthermore, analytical separations were not demonstrated in either poly-PEGDMA or poly-PEGDA devices. Liu et al.[36] polymerized a multicomponent mixture of acrylate monomers, some of which included PEG groups, and demonstrated this material's potential as a microfluidic substrate for capillary electrophoresis. PEG methyl ether methacrylate (PEGMEMA) was included in the formulation to extend the UV exposure time, but methyl methacrylate (MMA), which is a more hydrophobic monomer that lacks a PEG moiety and raises nonspecific adsorption concerns, was required to regain rigidity in the resulting polymer.

This chapter describes the development of polymerized PEGDA (poly-PEGDA) as a nonadsorptive alternative microfluidics material to PDMS. I demonstrated that varying the composition of monomer and changing the photoinitiator concentration in poly-PEGDA formulas can affect the water stability, bond strength (burst pressure), and optical clarity of the resulting polymer. Poly-PEGDA made with a low photoinitiator concentration and three ethylene glycol repeats (258 Da monomer) had the best combination of these properties, and was further optimized to have background fluorescence comparable to PDMS. Importantly, poly-PEGDA demonstrated better resistance than PDMS to permeation of small hydrophobic molecules. Innate resistance to protein adsorption in uncoated and unmodified poly-PEGDA was demonstrated by

flowing increasing protein concentrations through PDMS and poly-PEGDA microchannels to compare nonspecific adsorption over a six order-of-magnitude concentration range. Furthermore, a low concentration (1 μg/mL) of fluorescently labeled bovine serum albumin flowed through microchannels was utilized to illustrate the difference in nonspecific adsorption between PDMS and poly-PEGDA over time. Poly-PEGDA exhibited a stable fluorescence signal while the PDMS fluorescence signal increased by over 3-fold in an hour's time. Finally, microchip electrophoresis experiments demonstrated that poly-PEGDA sustains stable electroosmotic flow and enables quality separations.

2.2 EXPERIMENTAL

2.2.1 Materials

Fluorescein isothiocyanate labeled bovine serum albumin (FITC-BSA), PEGDA (molecular weight (MW) of 258), PEGMEMA (MW = 1100), MMA (99%), 2,2'-dimethoxy-2-phenylacetophenone (DMPA), rhodamine B base (97%), DL-tryptophan (99%), dimethyl sulfoxide (DMSO, 99.7%), porcine thyroglobulin, and β-lactoglobulin A were purchased from Sigma-Aldrich (Milwaukee, WI). L-lysine HCl was obtained from United States Biochemical Corporation (Cleveland, OH) and FITC was acquired from Invitrogen (Carlsbad, CA). Anhydrous granular sodium sulfate (99.2%) and dichloromethane (99.5%) were purchased from Mallinckrodt (Phillipsburg, NJ). Omnipur 10x phosphate buffer solution was purchased from EMD Chemicals (Gibbstown, NJ) and diluted with deionized (DI) water (18.2 MΩ). An aqueous saturated solution of sodium carbonate was made from powdered anhydrous sodium carbonate (99.5%, EMD Chemicals) and DI water. Boric acid (99.5%) obtained from EM Science (Darmstadt, Germany), sodium tetraborate decahydrate (99.5%) acquired from Sigma-Aldrich, and DI water were used to make 25 mM borate buffer (pH 9.3). Rhodamine B base was diluted

in borate buffer to create a 10 μM solution. A mixture of sodium carbonate (99.5%) purchased from EMD Chemicals, sodium bicarbonate (99.7%) obtained from EM Science, and DI water was used to make carbonate buffers at pH 9.3 and pH 10.0. SU8-2025, SU8-2015 and SU8 developer were purchased from Microchem (Newton, MA). PDMS Sylgard 184 base and curing agent were obtained from Dow Corning (Midland, MI).

2.2.2 PDMS Fabrication Summary

PDMS microfabrication is well known in the literature[38-40] and is only summarized briefly here. A two-layer flow channel is made, starting with fabrication of the upper PDMS layer by plasma cleaning of a silicon wafer at 250 W for 3 min using a Planar Etch II system (Technics, San Jose, CA). SU8-2025 was spun onto the cleaned wafer at 900 rpm to the desired thickness of 60–80 μm. A patterned chrome-coated glass mask was used to define the desired design into the photoresist. After UV exposure for 50 s, the resist was developed in SU8 developer, leaving raised rectangular-shaped features. The SU8 pattern formed a negative mold for the PDMS. A 4:1 ratio of PDMS to curing agent was mixed, degassed, poured over the SU8 mold and allowed to cure at 80°C for 45 min. The ~2-mm-thick cured PDMS was removed, cut to size using a razor, and input and output holes were punched using a 21 gauge needle. A 3.5 in. diameter glass wafer was plasma-cleaned as described previously. A 3:1 ratio of PDMS to curing agent was mixed, degassed, and spun onto the wafer using a Laurell Spinner (WS-400A-6NPP-LITE, North Wales, PA) at 2000 rpm for 60 s. This thin PDMS was allowed to cure at 80°C for 45 min. The molded upper layer was stamped in curing agent and placed onto the lower layer, and the combined structure was heated to 80°C for 1 h to bond the two layers together.

2.2.3 Poly-PEGDA Fabrication Summary

The fabrication process of a poly-PEGDA flow channel is shown in Figure 2.1. PEGDA is a liquid that requires a mold to form structures via polymerization; the chemical structures of the PEGDA monomer and poly-PEGDA are depicted in Figure 2.2. The flow channel mold was made by patterning SU8-2025 on a surface (Fig. 2.1A, features "1" and "2"). A PDMS-coated glass piece and poly-PEGDA spacers were used to define the polymerization region for the upper layer (Fig. 2.1A, feature "3"). PDMS was coated onto the glass wafer to facilitate the removal of the cover plate. A Karl Suss Aligner was used to expose the wafer to 10 mW/cm^2 UV light. The exposure time varied depending on the polymer thickness and formula. Once polymerized, the poly-PEGDA was easily removed from the mold (Fig. 2.1A, feature "4"), cut into individual dies, and holes were formed into the poly-PEGDA using a CO_2 laser cutter (VersaLASER VLS 2.30, Scottsdale, AZ). Although other methods, such as using PDMS cylinders in the polymer cast, can be used to form reservoir holes,[36] laser cutting provides reproducibility and patterning flexibility for different designs. The poly-PEGDA substrates were cleaned with isopropyl alcohol to remove any residue or debris left on the surface. A second, unpatterned poly-PEGDA layer was created with a similar setup to Figure 2.1A, feature "3", but glass slides and poly-PEGDA spacers were used to form the mold (Figs. 2.1A, features "6" and "7"). Excess liquid at the surface of the bottom layer was removed. The poly-PEGDA layers were intentionally undercured to help bind the two layers together subsequently; if either layer was significantly overcured, success in irreversible bonding of the two decreased. The top layer was placed onto the bottom layer and any bubbles that formed at the interface were extruded by gently applying pressure. A second exposure to UV light completed the curing and bonding process (Fig. 2.1A, feature "8"). Nanoports (Upchurch Scientific, Oak Harbor, WA) were attached to the finished poly-PEGDA

device to allow interfacing with tubing and a syringe pump (Fig. 2.1B). The completed device was then taped onto a glass slide (Fig. 2.1A, feature "9").

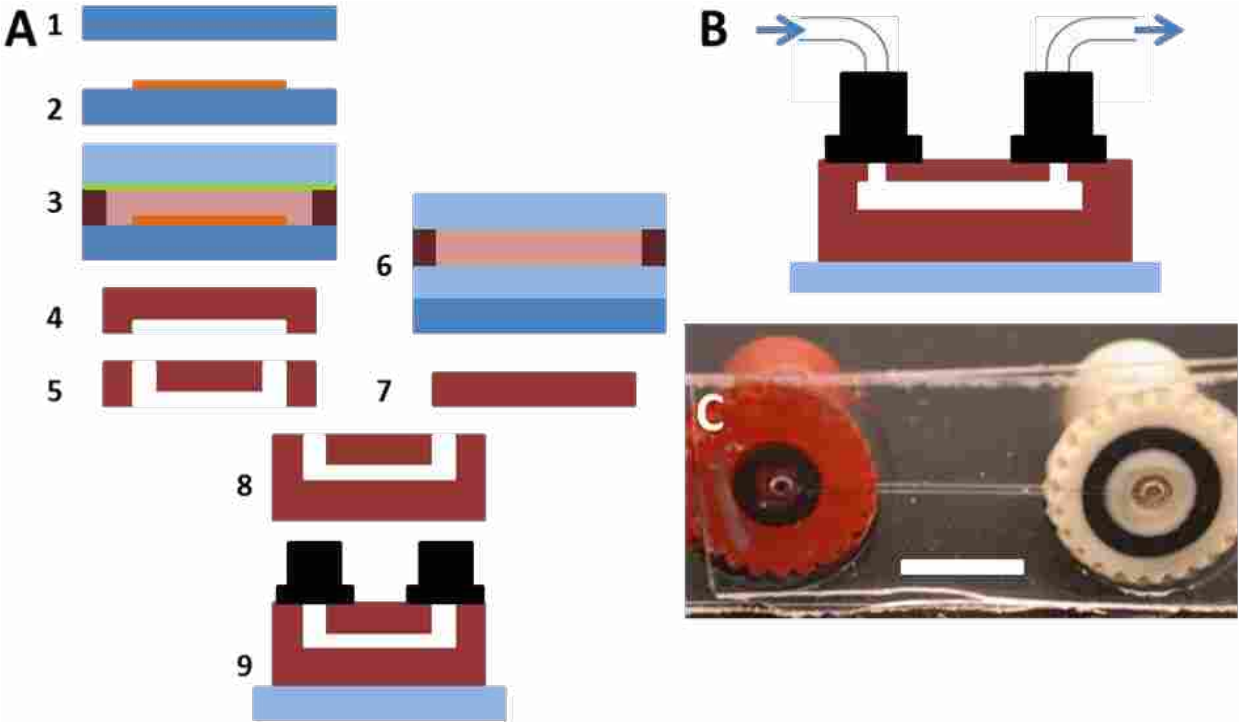

Figure 2.1. Poly-PEGDA flow channel device used to evaluate nonspecific adsorption. (A) Fabrication process for making a flow channel in poly-PEGDA. Polymerized PEGDA layers and spacers are shown in red, unpolymerized PEGDA in pink, SU8 in orange, PDMS in green, silicon wafer in dark blue, and glass wafer in light blue. [Legend: (1, 2) patterning of the SU8 photoresist; (3) PEGDA is polymerized; (4) polymerized PEGDA is removed; (5) holes are cut in poly-PEGDA, using a CO_2 laser; (6) an unpatterned layer of PEGDA is polymerized with a silicon wafer underneath to provide a flat, reflective surface during UV exposure; (7) poly-PEGDA is removed; (8) poly-PEGDA layers are bonded; (9) nanoport connectors are attached and the complete device is affixed to a glass slide. See text for further details.] (B) Side-view schematic of a poly-PEGDA device (the channel is 1.5–2.5 cm long, 60–80 μm high, and 300 μm wide; the top and bottom layers are ~350 μm thick). (C) Bottom-view photograph of a finished poly-PEGDA device; white bar is 0.5 cm.

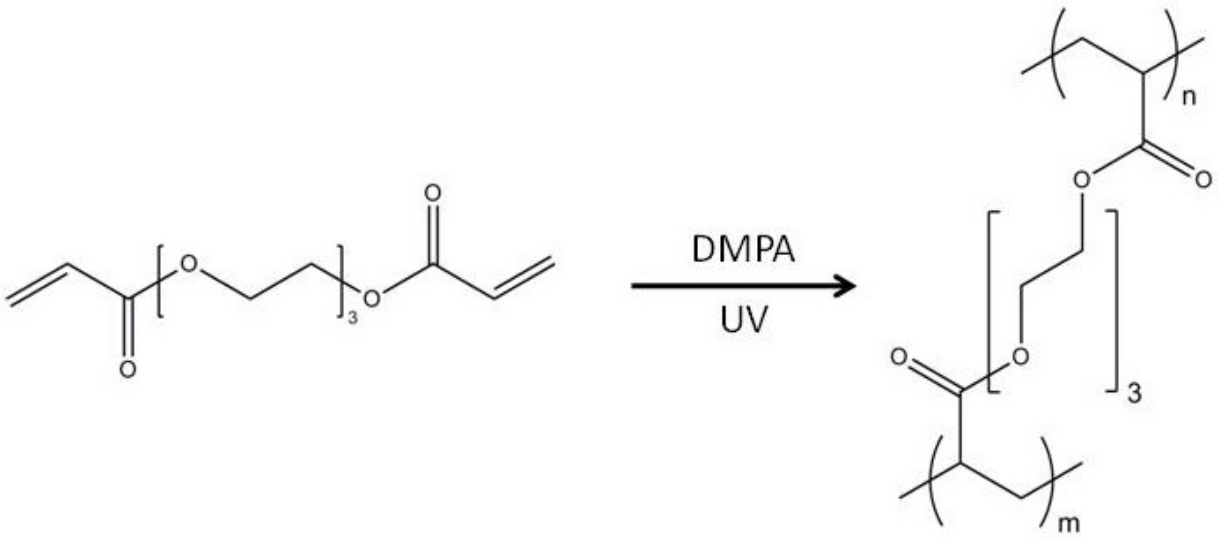

Figure 2.2. Polymerization of PEGDA to form poly-PEGDA.

2.2.4 Formula Optimization

A series of different poly-PEGDA formulations was tested for optical clarity, water stability, and polymerization. The variations evaluated were as follows: molecular weight of PEGDA (258 vs. 575 Da), 0.05% vs 3% DMPA photoinitiator, PEGDA with different amounts of additives (PEGMEMA and MMA) versus PEGDA-only, and polymerization for 10 s vs. 25 s (see Table 2.1). Each variant was rated for clarity on a 0–2 scale and polymerization on a 0–5 scale. The polymer samples were then completely immersed in water for 16 h to test for stability in an aqueous environment.

To remove any impurities from PEGDA that might contribute to background fluorescence, I used a purification method reported previously by Liu et al.[36] Briefly, 50 mL of PEGDA monomer was rinsed with three 30 mL aliquots of a saturated solution of Na_2CO_3. The PEGDA was then

rinsed with three 50 mL aliquots of dichloromethane. Residual water was removed with granular sodium sulfate, and a rotovap was used to remove the dichloromethane.

Table 2.1. Formulas for PEG Optimization for Water Stability.

Sample ID	% DMPA	% PEGMEMA	% PEGDA 258	% MMA	Ratio PEGDA/ PEGMEMA
A	0.05	16.3	81.6	2.0	**5.0**
B	0.30	16.1	81.5	2.1	**5.1**
C	0.05	15.8	79.1	5.0	**5.0**
D	0.30	15.8	78.8	5.0	**5.0**
E	0.05	8.9	88.9	2.2	**10.0**
F	0.31	8.9	88.7	2.1	**10.0**
G	0.05	8.7	86.2	5.1	**9.9**
H	0.31	8.6	86.1	5.0	**10.0**
Sample ID	**% DMPA**	**% PEGMEMA**	**% PEGDA 575**	**% MMA**	**Ratio PEGDA/ PEGMEMA**
I	0.06	16.2	81.2	2.5	**5.0**
J	0.32	16.3	81.3	2.1	**5.0**
K	0.05	15.8	79.1	5.0	**5.0**
L	0.31	15.6	78.9	5.2	**5.1**
M	0.05	8.9	89.0	2.0	**10.0**
N	0.30	8.9	88.8	2.0	**10.0**
O	0.05	8.6	86.3	5.0	**10.0**
P	0.31	8.6	86.0	5.1	**10.0**
Sample ID	**% DMPA**	**% PEGMEMA**	**% PEGDA 258**	**% MMA**	**Ratio PEGDA/ PEGMEMA**
Q	0.10	-	99.9	-	**-**

2.2.5 Burst Pressure Testing

A completed poly-PEGDA device was attached to tubing and a syringe pump. DI water was pumped through the channel to displace the air. Once the channel was clear of bubbles, a piece of PDMS was placed over the exit and held in place using a clamp (see Fig. 2.3A). A Honeywell pressure sensor (24PCFFA6G) was attached in-line, using the same setup as that used by Satyanarayana et al.[41] As fluid was pumped into the channel, pressure sensor data were recorded, as a function of time using LabView.

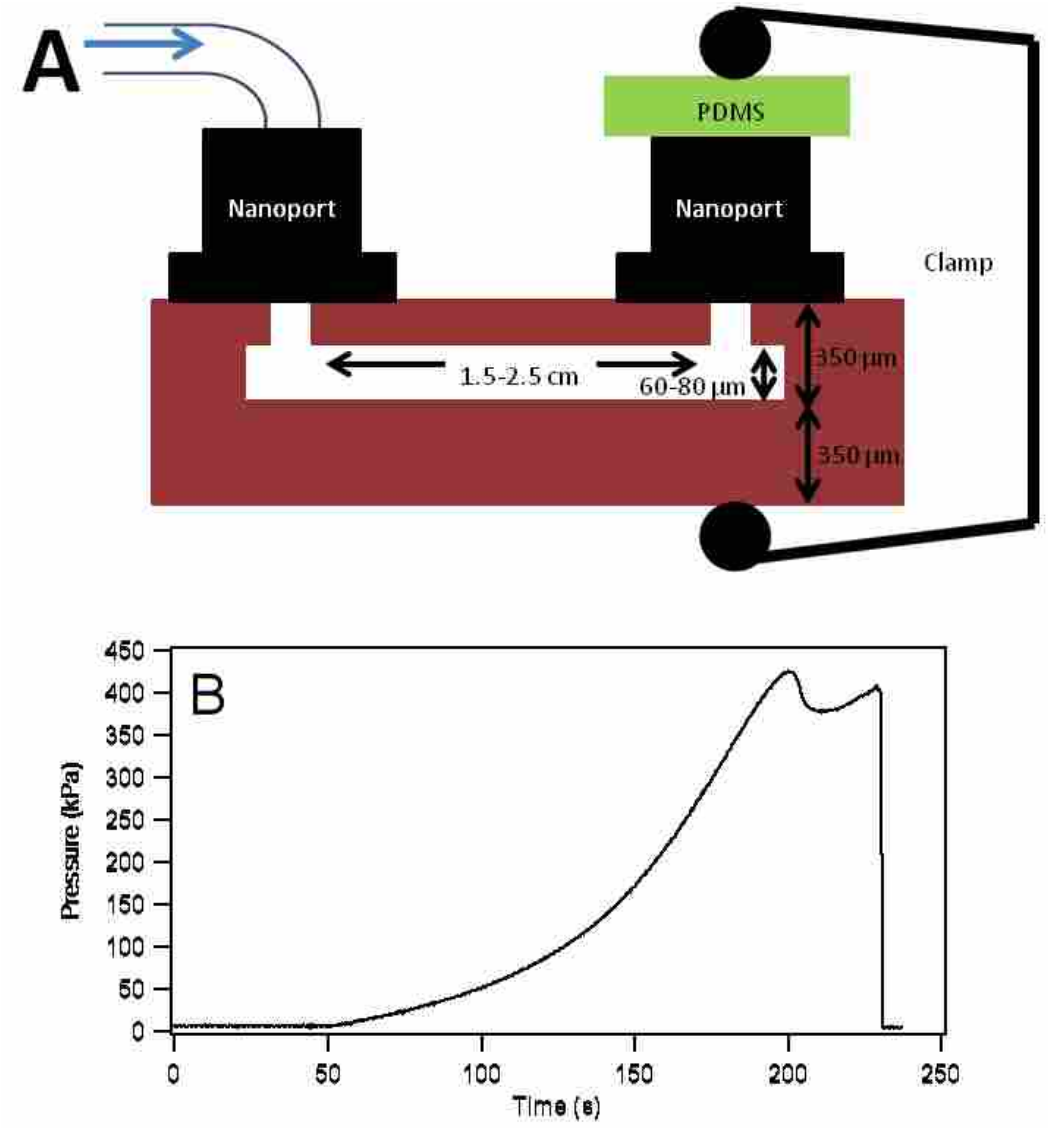

Figure 2.3. Burst pressure testing of bond strength between poly-PEGDA layers. (A) Side-view schematic of the poly-PEGDA device setup for burst pressure tests; water is introduced into the channel and the channel is sealed using a piece of PDMS held in place with a clamp while pressure is applied. (B) Graph of pressure buildup in a poly-PEGDA flow channel made using 0.0015% DMPA photoinitiator. Pressure release due to failure of some attachment point (in this case, the pressure gauge connection) is seen as the sudden drop at ~230 s. Since the poly-PEGDA did not delaminate, the burst pressure was at least 420 kPa.

2.2.6 Bulk Fluorescence Comparison

To test bulk fluorescence properties, 700-μm-thick layers were formed of PDMS, poly-PEGDA made with 1% DMPA, and poly-PEGDA made with purified monomer and 1% DMPA. Regions illuminated by a Reliant 150 M 488 nm laser (Laser Physics, West Jordan, UT) expanded to a ~1.4-mm-diameter diffuse beam were imaged using a CoolSNAPHQ CCD (Photometrics, Tucson, AZ). The power of the laser at the detection point was 1 mW. After initial images, the devices were exposed to ~3.5 mW at the detection point for 30 min to survey for any photobleaching once the power was returned to 1 mW and additional fluorescence images were taken.

2.2.7 Rhodamine B Comparison

Roman et al.[42] demonstrated that hydrophobic molecules such as rhodamine B can readily diffuse into PDMS. I used a similar method to compare the diffusion of rhodamine B into poly-PEGDA and PDMS. A 50-μm-wide, ~20-μm-tall, and 3.0-cm-long feature made from patterned SU8-2015 was used to cast channels in both materials. Fluorescence images using the same laser/CCD setup as above were obtained for the channels under flow (0.2 μL/min) of borate buffer (0 min) and 10 μM rhodamine B at several time intervals up to 4 h. The laser was blocked between measurements to avoid photobleaching.

2.2.8 Fluorescence Comparison

PDMS and poly-PEGDA two-layer devices, each having a flow channel, were used to compare nonspecific binding on channel surfaces. Laser-induced fluorescence (LIF) at 488 nm, as described in Section 2.2.6, was used to detect nonspecific adsorption of FITC-BSA. Background signal for the polymer in each device was photobleached by raising the laser power from 1 mW to 3.5 mW at the detection point for 15 min.

A series of exposures to increasing concentrations of FITC-BSA followed by buffer rinses was used to compare nonspecific binding for PDMS and poly-PEGDA. Initially, 1x PBS solution was rinsed through the flow channel at a rate of 110 μL/min for 3 min. The flow was reduced to 10 μL/min and allowed to flow for 1 min before a fluorescence image was taken. A sample of 1 ng/mL FITC-BSA was introduced in the same fashion and allowed to sit in the channel with no flow for 5 min. An image was taken after resuming flow for 1 min at 10 μL/min. The laser was blocked except during fluorescence measurement to avoid photobleaching of surface-adsorbed molecules. PBS was then used to rinse the channel as described previously, and another image was taken with buffer only in the channel. These steps were repeated for FITC-BSA concentrations increasing from 3 ng/mL to 1 mg/mL. The fluorescence images from the CCD were analyzed using ImageJ 1.43u. In all cases, background images were captured with buffer flowing in the channel at 10 μL/min, and the resulting background signal was subtracted from the sample fluorescent images.

2.2.9 Time Comparison

A low concentration of a model adsorptive species (FITC-BSA), flowed slowly through a microchannel, enables the determination of the time dependence of nonspecific binding for a substrate. The flow rate was set such that diffusional transport would allow FITC-BSA throughout the channel to interact with the surface prior to the detection location. The equation for diffusion in one dimension is given by Eq. 1.1 in Section 1.1 where x is distance, D is the diffusion coefficient, and t the time.[43] A value of $D = 6 \times 10^{-7}$ cm^2/s was used for FITC-BSA.[44] Rearranging Eq. 1.1 to solve for t gives the time for a molecule to diffuse across a distance x. In this channel geometry, ~27 s are required for a FITC-BSA molecule to diffuse 80 μm (top to bottom surface), and just ~7 s are needed to travel 40 μm (midchannel to wall). FITC-BSA in

solution flowing at 0.2 μL/min to the shortest distance to detection (0.2 cm) would take ~14 s to arrive, thus allowing adequate time for any given FITC-BSA molecule to come into contact with the channel surface prior to the detection point.

The flow channel and detection setup were the same as that described in Sections 2.2.6 and 2.2.8. The channel was rinsed with PBS for 10 min at 100 μL/min to remove any bubbles or debris. After rinsing, an air bubble was introduced into the channel before a 1 μg/mL solution of FITC-BSA (to signal when the sample had entered the channel). Data acquisition started when the bubble was visible in the channel but before the fluorescent sample had entered the detection zone. Images were taken every minute for poly-PEGDA, and every minute for PDMS for the first 35 min, with images taken every 5 or 10 min thereafter.

2.2.10 Microchip Electrophoresis

Lysine and tryptophan at 1 mg/mL in carbonate buffer (pH 9.3) were labeled with 4 mg/mL FITC in DMSO by mixing 25 μL of FITC solution with 75 μL of amino acid solution and reacting at room temperature for 24 h.[16] β-lactoglobulin A (2 mg/mL) was labeled with FITC by mixing 5 μL of FITC solution with 100 μL of protein solution, while thyroglobulin was labeled by mixing 10 μL of FITC solution with 100 μL of 2 mg/mL thyroglobulin. Protein solutions were then filtered to remove excess FITC using a 3 kDa Amicon Ultra filter (Billerica, MA). Protein concentrations were quantified using a Nanodrop ND-1000 spectrophotometer (Wilmington, DE).

The offset-T design electrophoresis microchip[45] was fabricated in poly-PEGDA, as described in Section 2.2.7 for the rhodamine B test devices. The injection arms were 0.5 cm long, and the separation channel was 3.0 cm from the intersection to the end reservoir. The channels were 50

μm wide and 18 μm tall. Pinched injection times of 20 s for amino acids and 30 s for proteins were used to introduce the analytes into the separation channel. The amino acid separation used -850 V across the injection pathway, -2000 V along the separation channel, and pH 9.3 carbonate buffer. Protein analysis was done using -900 V for injection and -2000 V for separation with pH 10.0 carbonate buffer. Fluorescence was collected at a separation distance of 2.5 cm using a point detection system described previously.[45]

2.3 RESULTS AND DISCUSSION

2.3.1 Formula Optimization

The polymer formulation is critical to achieving the desired device properties. If a higher molecular weight of PEGDA (i.e., 575 or 700 Da) is used (see Tables 2.2 and 2.3), the resulting polymer is susceptible to swelling, and eventual buckling and cracking when exposed to water, typically within as little as 10 min of submersion (similar to results from Kim et al.[37]). The concentration of DMPA affected the rate of polymerization: higher concentrations required shorter UV exposure times but generated heat which resulted in cracking of the polymer material. The addition of PEGMEMA increased the UV exposure time but required the use of MMA in higher concentrations for structural stability. By comparing a series of formulations including PEGDA-only, I determined an optimal formula for making thin (~350 μm) layers while maintaining optical clarity and water stability. Scanning electron microscopy (SEM) images detail channel features in poly-PEGDA (see Fig. 2.4).

Poly-PEGDA made from a low-molecular-weight PEGDA (258 Da) and having 0.0015%–1.0% DMPA photoinitiator was found to be the most stable in water while still having good optical clarity (see Fig. 2.5). Although three other polymer formulations that also contained PEGMEMA and MMA in addition to PEGDA survived submersion for more than 16 h, the

PEGDA-only formulas were simpler to prepare and had some mechanical flexibility (see Fig. 2.6), making poly-PEGDA the most desirable formulation for subsequent testing.

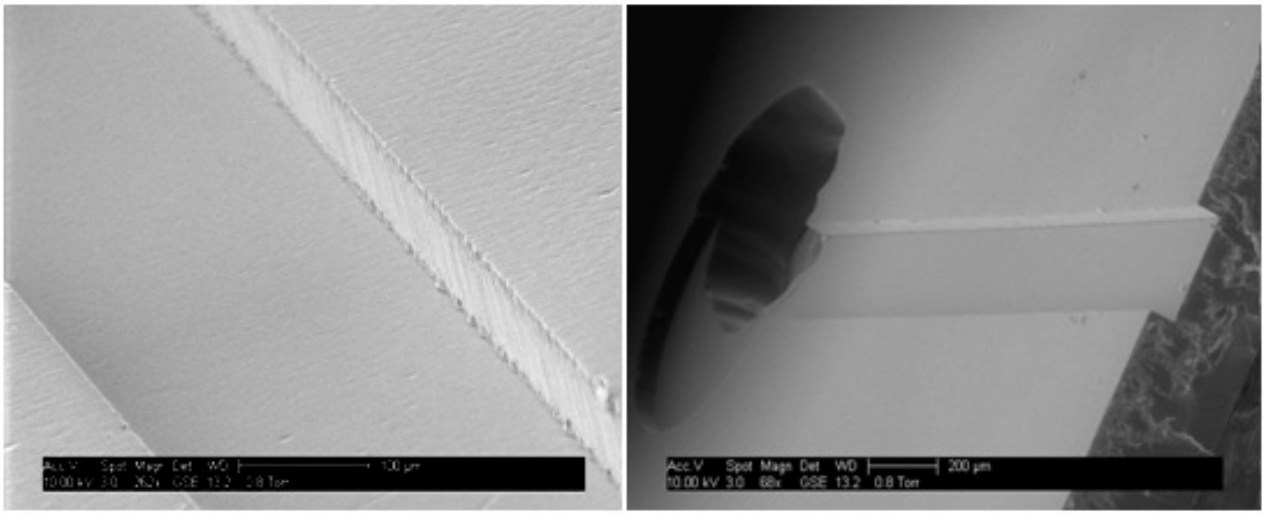

Figure 2.4. SEM images of poly-PEGDA channels. The left image details channel surface features in poly-PEGDA created using patterned SU8 as a mold. The right image shows a straight channel feature as well as the fluidic input hole created using a CO_2 laser cutter. Channel dimensions are 300 µm wide and ~70 µm tall.

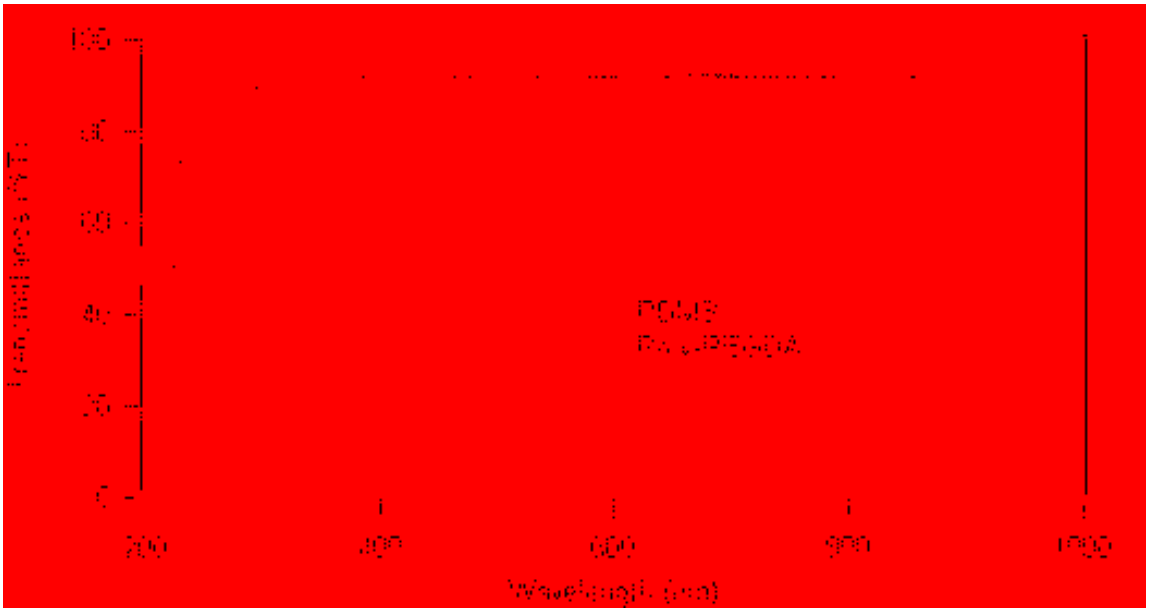

Figure 2.5. Transmission spectra of 200-µm-thick layers of PDMS and poly-PEGDA.

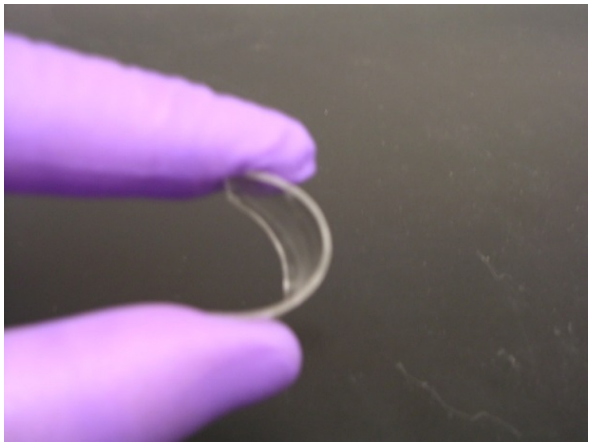

Figure 2.6. Mechanical flexibility. Flexibility of poly-PEGDA is demonstrated as pressure is applied to a 350 µm thick layer.

Table 2.2. Results for PEG Optimization for Water Stability with 10 s Exposure Time.

Sample ID	Polymerization	Clarity	Water Immersion Test	Comments
A	1	0	<0.5 min	Became white
B	5	1	>10 min	Survived
C	1	0	<0.5 min	Became white
D	5	0	>10 min	Survived
E	0	0	<0.5 min	Became white
F	5	1	>10 min	Survived
G	0	0	<0.5 min	Became white
H	5	0	<0.5 min	Became white
I	1	0	>10 min	Survived but not completely polymerized
J	4	0	1:10 min	Buckled
K	1	0	4 min	Buckled
L	3	0	<1 min	Buckled
M	2	2	>10 min	Really soft
N	4	1	4:30 min	Buckled
O	2	0	4 min	Buckled
P	4	0	1 min	Buckled
Q	5	0	>10 min	Survived

Table 2.3. Results for PEG Optimization for Water Stability with 25 s Exposure Time.

Sample ID	Polymerization	Clarity	Water Immersion Test	Comments
A	5	1	>10 min	Survived
B	5	2	>10 min	Survived
C	3	0	>10 min	Survived but really soft when removed from wafer
D	5	1	>10 min	Survived
E	5	1	>10 min	Survived
F	5	2	>10 min	Survived
G	3	1	<0.5 min	Turned white
H	5	1	>10 min	Survived
I	3	0	1:30 min	Buckled
J	5	0	7 min	Buckled
K	3	0	6:30 min	Buckled
L	4	0	2:18 min	Buckled
M	5	1	4 min	Buckled
N	5	0	>10 min	Survived
O	3	0	3 min	Buckled
P	5	0	>10 min	Some separation from silicon but no buckling
Q	5	0	>10 min	Survived

2.3.2 Burst Pressure Tests

Burst pressure measurement provided a way to evaluate the bond strength between two layers by pressurizing a liquid into the interface between them. Recent work by Tsai et al.[46] showed that burst pressure—and, therefore bond strength—of PDMS is largely dependent on the method used to bind two layers. The burst pressure for silicon with PDMS cured without heat or adhesive is relatively weak at ~50 kPa. When PDMS curing agent is used as an adhesive and cured at room temperature for 16 h, the silicon-PDMS burst pressure increases to ~430 kPa. Heat curing at 90 ºC for 30 min can raise the silicon-PDMS burst pressure even further to 770 kPa, but heat curing techniques are not compatible with protein functionalized surfaces. Pressures in the poly-PEGDA flow channel reached up to 420 kPa (Fig. 2.3B) before the pressure sensor became disconnected from the tubing. It should be noted that, since the pressure

sensor connection failed before the bonded poly-PEGDA layers, the actual burst pressure of these devices could be much higher. More accurate burst pressures for these devices could be recorded using a more robust attachment of the pressure sensor, as well as a pressure sensor with a higher pressure range. Importantly, microchannel stability to at least 420 kPa is sufficient for most applications in microfluidics.

2.3.3 Bulk Fluorescence Comparison

Polymers provide a simpler alternative for the fabrication of microfluidics compared to glass, but generally have higher background fluorescence. One of the reasons PDMS is popular is because its fluorescent background is relatively low and closer to that of glass.[47] Here, I compared the fluorescence background of PDMS and poly-PEGDA. The dark-current-subtracted background fluorescence signal for PDMS was ~36 CCD units. This signal was not reduced by photobleaching with 30 min of 2.3 mW/mm^2 488 nm laser exposure. As-received poly-PEGDA started at a signal of 75, which dropped to ~50 after photobleaching. It is possible to further reduce the background fluorescence of poly-PEGDA by removing impurities such as inhibitors from the monomer. Poly-PEGDA made from purified monomer had a lower initial signal of ~50 CCD units, which reduced to ~35 CCD units, the same level as PDMS, after photobleaching in the same manner as the PDMS. Thus, purifying the monomer and photobleaching can make a poly-PEGDA material that offers comparable bulk background fluorescence to PDMS.

2.3.4 Rhodamine B Comparison

Hydrophobic molecules such as rhodamine B readily diffuse into unmodified PDMS.[42] A comparison of the diffusion of rhodamine B in poly-PEGDA and plasma-bonded PDMS is given in Figure 2.7. PDMS showed a significant fluorescence signal and spatial distribution increase over 4 h as rhodamine B diffused into the bulk PDMS surrounding the channel. In contrast, the

fluorescence signal for poly-PEGDA remained confined and at levels characteristic of analyte within the channel even after 4 h. Resistance to permeation by small hydrophobic molecules without chemical modification demonstrates the innately superior performance of poly-PEGDA relative to PDMS.

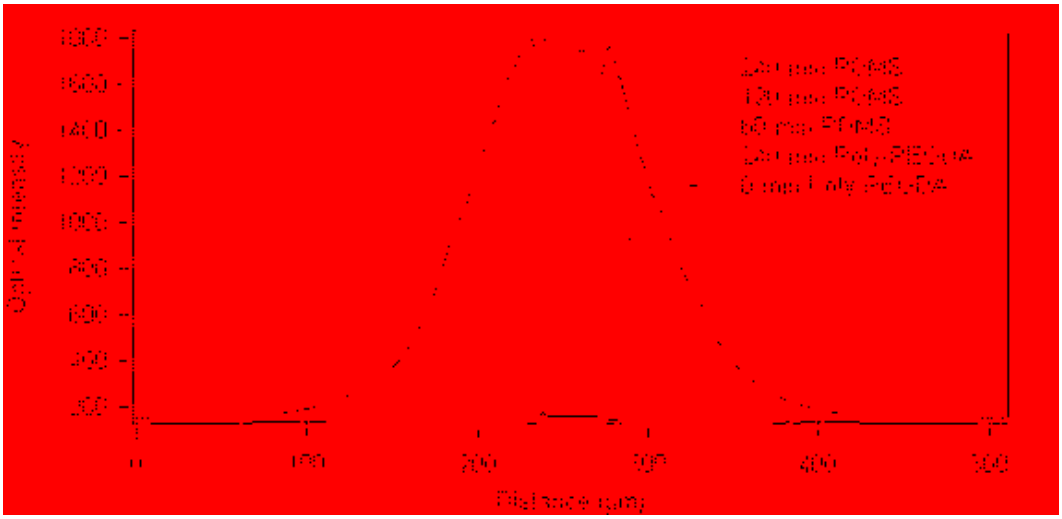

Figure 2.7. Plot of fluorescence signal cross sections at different times during flow of 10 µM rhodamine B at 0.2 µL/min in 50 µm wide channels in poly-PEGDA and plasma-bonded PDMS. Fluorescence in PDMS increases as rhodamine B diffuses into the polymer over 4 h, indicating susceptibility to permeation by hydrophobic molecules. After 4 h of exposure to rhodamine B, fluorescence signal in poly-PEGDA remains confined to the channel. Initial background buffer signal (0 min) before analyte flow was comparable for PDMS and poly-PEGDA, so only the result for poly-PEGDA is shown.

2.3.5 Fluorescence Comparison

I compared nonspecific adsorption in PDMS and poly-PEGDA channels over a six order-of-magnitude range of increasing FITC-BSA concentrations (Fig. 2.8). In this experiment, fluorescence signal can be broken down into two components: fluorescence due to FITC-BSA molecules nonspecifically bound to the surfaces of the channel (F_s) and fluorescence from molecules in the bulk liquid in the channel (F_v). Fluorescence signals obtained from flowing

FITC-BSA sample solutions contain both F_s and F_v, while signals from the PBS rinse consist of only F_s. Theoretically F_v should provide a linear increase in fluorescence with concentration resulting in a slope of 1 as long as $F_s = 0$. After only a 5-min exposure to the lowest FITC-BSA concentration (1 ng/mL) and flowing at 10 μL/min for 1 min, the background-subtracted fluorescence signal for PDMS was already higher than the detector noise level (the standard deviation of the signal prior to background subtraction). In contrast, poly-PEGDA exposed to FITC-BSA concentrations under 100 ng/mL exhibited background subtracted fluorescence below the level of detector noise. Only at FITC-BSA concentrations above ~50 μg/mL was the signal due to protein in the PDMS channel greater than the signal due to FITC-BSA nonspecifically bound to the walls ($F_v > F_s$). In contrast, the protein solution signal is distinct from F_s above ~10 μg/mL FITC-BSA in poly-PEGDA, indicating lower levels of nonspecific adsorption. The slope of signal as a function of FITC-BSA concentration is well below 1 in PDMS, because of significant nonspecific adsorption at lower concentrations ($F_s \neq 0$), leading to much higher signals observed than would be expected from the channel contents alone (F_v). For just the highest two FITC-BSA concentrations (≥500 μg/mL), the signal versus concentration plot has the slope of 0.94 (~1) for PDMS. For poly-PEGDA exposed to FITC-BSA, the signal versus concentration slope from 50 μg/mL to 1 mg/mL was 0.91 (~1), offering an order-of-magnitude larger linear range than in PDMS. This result clearly demonstrates less nonspecific adsorption in poly-PEGDA, making this material better suited for quantitative measurements on adsorptive proteins.

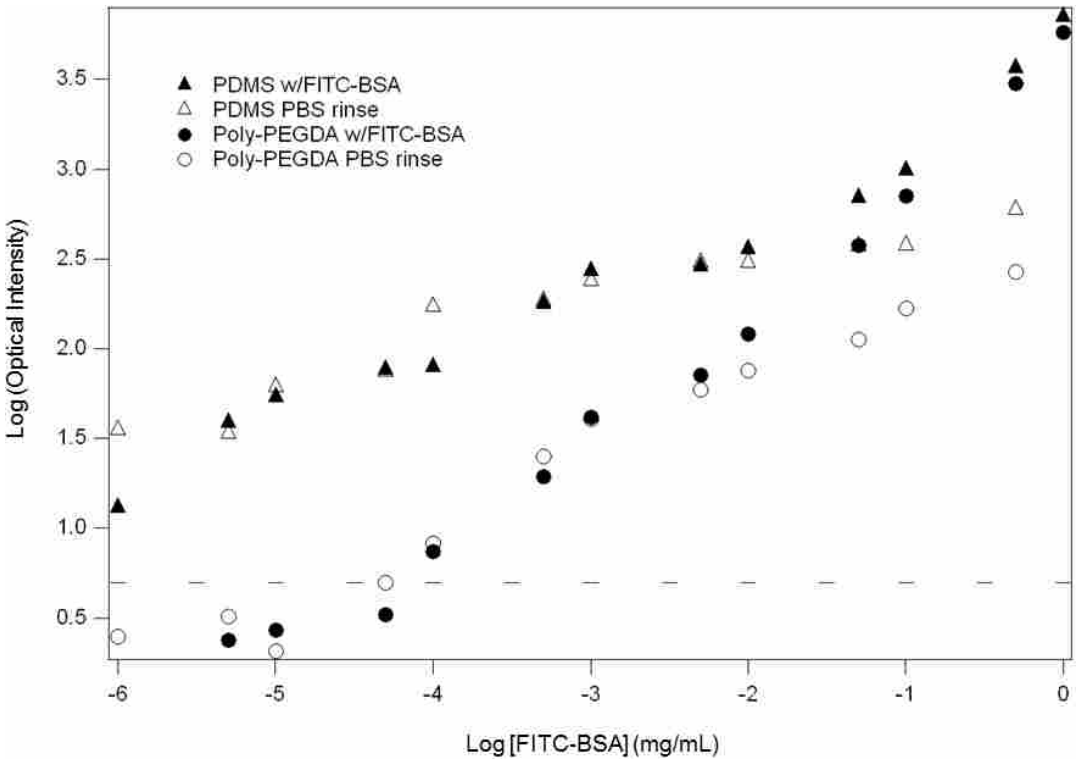

Figure 2.8. Background-subtracted fluorescence signal in PDMS and poly-PEGDA microdevices for increasing FITC-BSA concentrations. The standard deviation of signal before background subtraction is shown as a dashed line. In poly-PEGDA, the signal for 1 ng/mL FITC-BSA was at the level of dark current and was not plotted.

2.3.6 Time Comparison

PDMS and poly-PEGDA behaved differently when exposed to flow of a low concentration of FITC-BSA over time (Fig. 2.9). This experiment thus expands over a prior publication,[37] where only the end results of nonspecific adsorption were reported. The steady increase in fluorescence signal in the PDMS device was due to nonspecific adsorption of FITC-BSA to the channel surface in the detection window ($F_s \neq 0$). The fluorescence signal for FITC-BSA in the PDMS channel was initially less than in the poly-PEGDA channel but it slowly increased to three times the poly-PEGDA amount within 100 min. The initially lower signal in PDMS during the first ~20 min was most likely due to depletion of FITC-BSA flowing in the channel, through surface adsorption prior to the detection point. The PDMS signal was detected 2 mm from the sample

inlet, which at the flow rate of 0.2 µL/min gave a flow time of 14 s for FITC-BSA to reach the detection point. Since only 7 s were needed for a molecule to diffuse the 40 µm from the center of the channel to the surface, on average, the introduced FITC-BSA molecules should come into contact with the wall multiple times and have an opportunity to nonspecifically bind to the surface. In contrast, the FITC-BSA signal in poly-PEGDA was detected 0.7 cm from the sample inlet, leaving ~50 s to reach the detection point. Even though significantly more opportunity was allowed for FITC-BSA to interact with the poly-PEGDA surface, no initial depletion zone was observed. Furthermore, the signal was essentially constant over the time of the experiment, indicating that $F_s << F_v$ in the detection region over time, again unlike with PDMS. Thus, it is clear that poly-PEGDA is more resistant than PDMS to surface fouling over time.

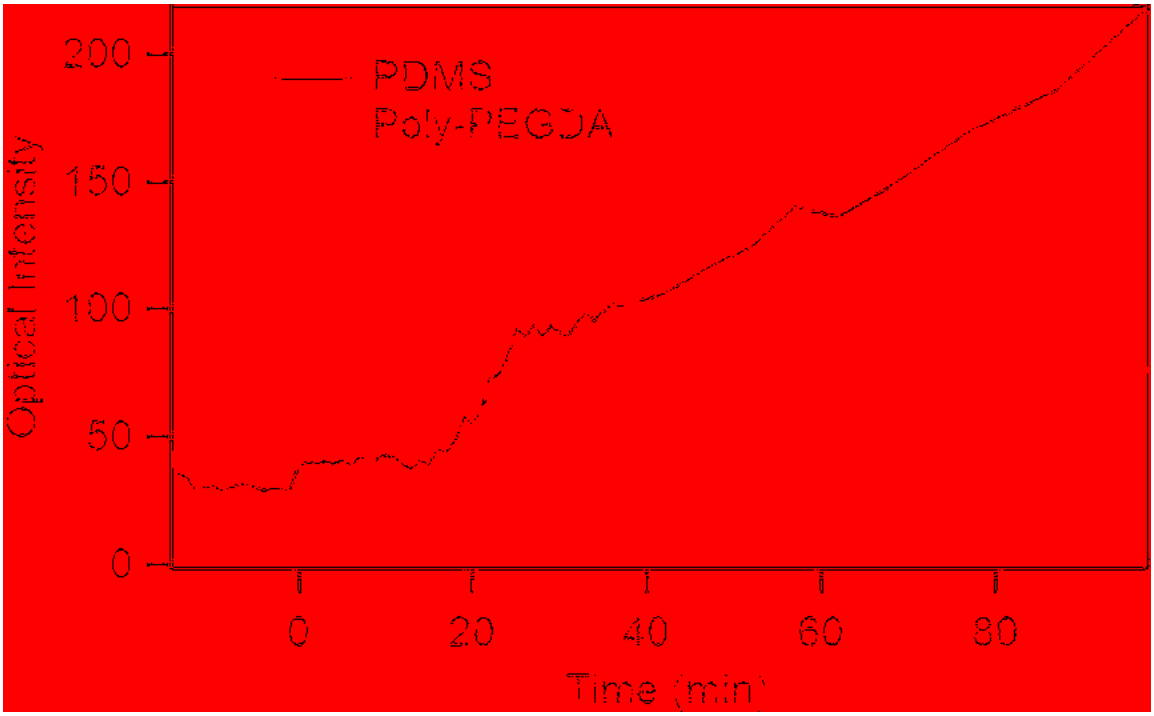

Figure 2.9. Fluorescence comparison of PDMS and poly-PEGDA over time during flow of a dilute FITC-BSA solution. A 1 µg/mL solution of FITC-BSA was flowed at 0.2 µL/min. The signal in PDMS increased substantially, while that in poly-PEGDA remained stable. Signal is dark-current-subtracted. The laser was shuttered between each fluorescence image to avoid photobleaching in the detection zone.

2.3.7 Microchip Electrophoresis

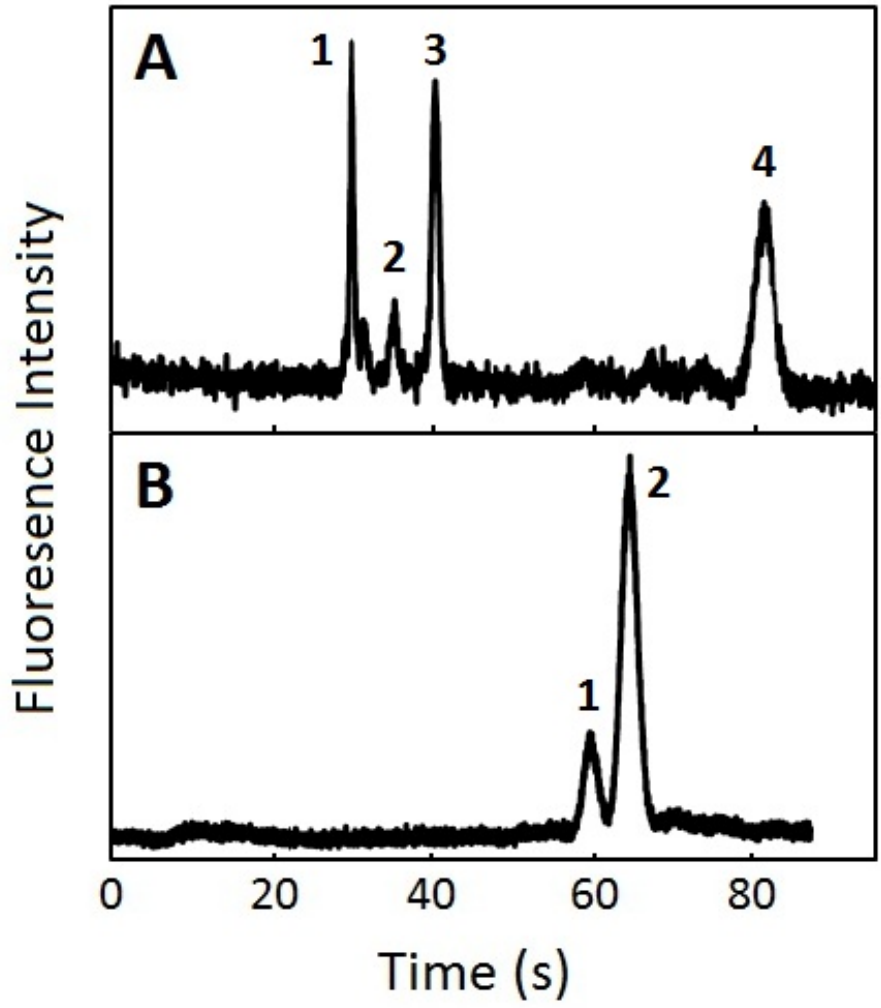

Figure 2.10. Electrophoretic separation of amino acids and proteins using a poly-PEGDA microchip. (A) Separation of 1 μM FITC-Lys (peak "1") and 1 μM FITC-Trp (peak "4"). Peaks "2" and "3" due to free FITC are well-separated from the labeled amino acids. (B) Separation of 1 μg/mL FITC-thyroglobulin (peak "1") and 10 μg/mL FITC-β-lactoglobulin A (peak "2").

Electrophoretic separations of amino acids and proteins are shown in Figure 2.10. In the amino acid separation (Fig. 2.10A), FITC-lysine eluted at 30 s and FITC-tryptophan eluted at 81 s; theoretical plate counts of 10,000 (4.0×10^5 N/m) for FITC-Lys and 4500 (1.8×10^5 N/m) for FITC-Trp were achieved. In the protein separation (Fig. 2.10B), FITC-thyroglobulin eluted at

59 s and FITC-β-lactoglobulin A eluted at 64 s, with a resolution of 1.4. Theoretical plate numbers were 4900 (2.0 x 10^5 N/m) for FITC-thyroglobulin and 4400 (1.8 x 10^5 N/m) for FITC-β-lactoglobulin A. In comparison, Wang et al.[48] demonstrated that unmodified PDMS gave poor resolution for both amino acids and proteins. They further showed that modifying PDMS surfaces with chitosan improved the resolution, but their best theoretical plate counts were much smaller at 6.2 x 10^4 N/m for an amino acid and 2.2 x 10^4 N/m for a protein. The theoretical plate counts for unmodified poly-PEGDA indicate great promise for use of this material in high-performance separations.

2.4 CONCLUSIONS

A material formed from photopolymerization of poly(ethylene glycol) diacrylate (poly-PEGDA) was made using a similar fabrication process to polydimethylsiloxane (PDMS). Poly-PEGDA was shown to be stable in water, have a high burst pressure (bond strength), and have optical clarity similar to PDMS. Poly-PEGDA also demonstrated excellent resistance to diffusion of small hydrophobic molecules into the bulk material, lower nonspecific binding than PDMS over a range of increasing adsorptive protein concentrations, and greater resistance over time to surface fouling during exposure to low protein concentrations. Poly-PEGDA shares with PDMS the favorable characteristic of low intrinsic fluorescent background. Finally, symmetric peaks and theoretical plate counts in electrophoretic separations of amino acids and proteins demonstrate the value of poly-PEGDA for biological sample analysis.

Low nonspecific adsorption, coupled with low background fluorescence for poly-PEGDA, makes this polymer worthy of consideration as an alternative to PDMS for microfluidic devices. An important feature of PDMS is its elasticity, which allows for the implementation of valves and pumps into microsystems. These poly-PEGDA layers similarly have some elasticity, as

demonstrated by the ability to flex or bend without breaking. Further optimization of poly-PEGDA formulations is ongoing to provide comparable mechanical properties to PDMS. Creating flexible valves and pumps entirely from poly-PEGDA would allow fewer areas for analyte adsorption and contribute to lower detection limits. The integration of nonadsorptive microfluidic materials, such as poly-PEGDA, with analyte sensing mechanisms such as microcantilevers or nanowires should provide broader application and further enable the evaluation of new detection modalities in biomedical research.

2.5 REFERENCES

(1) Reyes, D. R.; Iossifidis, D.; Auroux, P.-A.; Manz, A. *Anal. Chem.* **2002**, *74*, 2623-2636.
(2) Arora, A.; Simone, G.; Salieb-Beugelaar, G. B.; Kim, J. T.; Manz, A. *Anal. Chem.* **2010**, *82*, 4830-4847.
(3) Wang, J.; Ren, L.; Li, L.; Liu, W.; Zhou, J.; Yu, W.; Tong, D.; Chen, S. *Lab Chip* **2009**, *9*, 644-652.
(4) Lindström, S.; Andersson-Svahn, H. *Lab Chip* **2010**, *10*, 3363-3372.
(5) Anglin, E. J.; Salisbury, C.; Bailey, S.; Hor, M.; Macardle, P.; Fenech, M.; Thissen, H.; Voelcker, N. H. *Lab Chip* **2010**, *10*, 3413-3421.
(6) Dudek, M. M.; Kent, N.; Gustafsson, K. M.; Lindahl, T. L.; Killard, A. J. *Anal. Chem.* **2010**, *83*, 319-328.
(7) Teh, S.-Y.; Lin, R.; Hung, L.-H.; Lee, A. P. *Lab Chip* **2008**, *8*, 198-220.
(8) Pei, J.; Nie, J.; Kennedy, R. T. *Anal. Chem.* **2010**, *82*, 9261-9267.
(9) Huebner, A.; Bratton, D.; Whyte, G.; Yang, M.; deMello, A. J.; Abell, C.; Hollfelder, F. *Lab Chip* **2009**, *9*, 692-698.
(10) Jeffries, G. D. M.; Lorenz, R. M.; Chiu, D. T. *Anal. Chem.* **2010**, *82*, 9948-9954.
(11) Benhabib, M.; Chiesl, T. N.; Stockton, A. M.; Scherer, J. R.; Mathies, R. A. *Anal. Chem.* **2010**, *82*, 2372-2379.
(12) Bruzewicz, D. A.; Reches, M.; Whitesides, G. M. *Anal. Chem.* **2008**, *80*, 3387-3392.
(13) Mellors, J. S.; Jorabchi, K.; Smith, L. M.; Ramsey, J. M. *Anal. Chem.* **2010**, *82*, 967-973.
(14) Goral, V. N.; Hsieh, Y.-C.; Petzold, O. N.; Clark, J. S.; Yuen, P. K.; Faris, R. A. *Lab Chip* **2010**, *10*, 3380-3386.
(15) Shi, W.; Wen, H.; Lu, Y.; Shi, Y.; Lin, B.; Qin, J. *Lab Chip* **2010**, *10*, 2855-2863.
(16) Yang, W.; Sun, X.; Wang, H.-Y.; Woolley, A. T. *Anal. Chem.* **2009**, *81*, 8230-8235.
(17) Yang, W.; Yu, M.; Sun, X.; Woolley, A. T. *Lab Chip* **2010**, *10*, 2527-2533.
(18) Sia, S. K.; Whitesides, G. M. *Electrophoresis* **2003**, *24*, 3563-3576.
(19) Huang, B.; Wu, H.; Kim, S.; Zare, R. N. *Lab Chip* **2005**, *5*, 1005-1007.
(20) Phillips, K. S.; Kang, K. M.; Licata, L.; Allbritton, N. L. *Lab Chip* **2010**, *10*, 864-870.
(21) Roman, G. T.; Culbertson, C. T. *Langmuir* **2006**, *22*, 4445-4451.
(22) Séguin, C.; McLachlan, J. M.; Norton, P. R.; Lagugné-Labarthet, F. *Appl. Surf. Sci.* **2010**, *256*, 2524-2531.

(23) Barbier, V.; Tatoulian, M.; Li, H.; Arefi-Khonsari, F.; Ajdari, A.; Tabeling, P. *Langmuir* **2006**, *22*, 5230-5232.
(24) Kim, B.-Y.; Hong, L.-Y.; Chung, Y.-M.; Kim, D.-P.; Lee, C.-S. *Adv. Funct. Mater.* **2009**, *19*, 3796-3803.
(25) Bodas, D.; Khan-Malek, C. *Microelectron. Eng.* **2006**, *83*, 1277-1279.
(26) Hillborg, H.; Tomczak, N.; Olàh, A.; Schönherr, H.; Vancso, G. J. *Langmuir* **2004**, *20*, 785-794.
(27) Bausch, G. G.; Stasser, J. L.; Tonge, J. S.; Owen, M. J. *Plasmas and Polymers* **1998**, *3*, 23-34.
(28) Wang, D.; Oleschuk, R. D.; Horton, J. H. *Langmuir* **2008**, *24*, 1080-1086.
(29) Sui, G.; Wang, J.; Lee, C.-C.; Lu, W.; Lee, S. P.; Leyton, J. V.; Wu, A. M.; Tseng, H.-R. *Anal. Chem.* **2006**, *78*, 5543-5551.
(30) Truong, T. T.; Lin, R.; Jeon, S.; Lee, H. H.; Maria, J.; Gaur, A.; Hua, F.; Meinel, I.; Rogers, J. A. *Langmuir* **2007**, *23*, 2898-2905.
(31) Willis, P. A.; Greer, F.; Lee, M. C.; Smith, J. A.; White, V. E.; Grunthaner, F. J.; Sprague, J. J.; Rolland, J. P. *Lab Chip* **2008**, *8*, 1024-1026.
(32) Fiorini, G. S.; Lorenz, R. M.; Kuo, J. S.; Chiu, D. T. *Anal. Chem.* **2004**, *76*, 4697-4704.
(33) Pan, T.; Fiorini, G. S.; Chiu, D. T.; Woolley, A. T. *Electrophoresis* **2007**, *28*, 2904-2911.
(34) Schlapak, R.; Pammer, P.; Armitage, D.; Zhu, R.; Hinterdorfer, P.; Vaupel, M.; Frühwirth, T.; Howorka, S. *Langmuir* **2006**, *22*, 277-285.
(35) Klasner, S. A.; Metto, E. C.; Roman, G. T.; Culbertson, C. T. *Langmuir* **2009**, *25*, 10390-10396.
(36) Liu, J. K.; Sun, X. F.; Lee, M. L. *Anal. Chem.* **2007**, *79*, 1926-1931.
(37) Kim, P.; Jeong, H. E.; Khademhosseini, A.; Suh, K. Y. *Lab Chip* **2006**, *6*, 1432-1437.
(38) Duffy, D. C.; McDonald, J. C.; Schueller, O. J. A.; Whitesides, G. M. *Anal. Chem.* **1998**, *70*, 4974-4984.
(39) Cooksey, G. A.; Elliott, J. T.; Plant, A. L. *Anal. Chem.* **2011**, *83*, 3890-3896.
(40) Afshar, R.; Moser, Y.; Lehnert, T.; Gijs, M. A. M. *Anal. Chem.* **2011**, *83*, 1022-1029.
(41) Satyanarayana, S.; Karnik, R. N.; Majumdar, A. *J. Microelectromech. Syst.* **2005**, *14*, 392-399.
(42) Roman, G. T.; Hlaus, T.; Bass, K. J.; Seelhammer, T. G.; Culbertson, C. T. *Anal. Chem.* **2005**, *77*, 1414-1422.
(43) Berthier, J.; Silberzan, P. *Microfluidics for Biotechnology*; Artech House: Norwood, MA, 2006, 95.
(44) Placidi, M.; Cannistraro, S. *Europhysics Letters* **1998**, *43*, 476-481.
(45) Kelly, R. T.; Woolley, A. T. *Anal. Chem.* **2003**, *75*, 1941-1945.
(46) Tsai, L.-F.; Dahlquist, W. C.; Kim, S.; Nordin, G. P. *J. Micro/Nanolithogr., MEMS, MOEMS* **2011**, *10*, 043009.
(47) Pai, J.-H.; Wang, Y.; Salazar, G. T.; Sims, C. E.; Bachman, M.; Li, G. P.; Allbritton, N. L. *Anal. Chem.* **2007**, *79*, 8774-8780.
(48) Wang, A.-J.; Xu, J.-J.; Chen, H.-Y. *J. Chromatogr. A* **2007**, *1147*, 120-126.

3. MICROFLUIDIC VALVES MADE FROM POLYMERIZED POLYETHYLENE GLYCOL DIACRYLATE*

3.1 INTRODUCTION

Microfluidics is an expanding and vibrant field of research that spans multiple scientific disciplines, including physics, engineering, chemistry, biology, and medicine.[1-3] Areas of emphasis range from materials development[1, 4] and device fabrication[5, 6] to biosensing[7, 8] and point-of-care diagnostics.[9, 10] Some advantages of microfluidics are small sample and reagent volumes, potential for mass production to create low-cost devices, reduced distance for diffusion, high surface-to-volume ratios, and the ability to integrate multiple processes in a single device.[1]

An important facet of microfluidic systems is the need to control the movement of fluid. Many methods have been used to control liquids in microdevices including voltage,[11, 12] valves,[13-15] and channel geometry.[16, 17] Active valves are particularly promising for fluid manipulation due to the ability to rapidly switch between open and closed positions.[10] Microfabricated valves first introduced by Unger et al.[14] were fabricated using two embedded channels in polydimethylsiloxane (PDMS). When pressure was applied to the upper control channel, the flexible PDMS between the channels collapsed into the lower channel and closed it; the valve reopened when the control pressure was released. Later, Grover et al.[15] demonstrated a membrane valve that consisted of a middle PDMS elastomeric layer sandwiched between two rigid glass layers. Flow through the valve was prevented when pressure was applied to the membrane, pushing it against a pedestal within the fluid channel (e.g., blue inset, Fig. 3.1A). The valve was opened with an applied vacuum to lift the membrane off the pedestal. Membrane

valves can also be used in pumps.[18, 19] A key focus of current microfluidics research is integration of multiple processes (e.g., sample preparation, separation, and detection) to provide a complete sample analysis package, requiring minimal user intervention. Microfabricated valves find use in integrated devices ranging from automated systems, such as those where valves are utilized to control and direct fluid for small molecule analysis in the search for life on Mars,[20] to physiological mimicry, such as in a microvasculatory microchip system.[21]

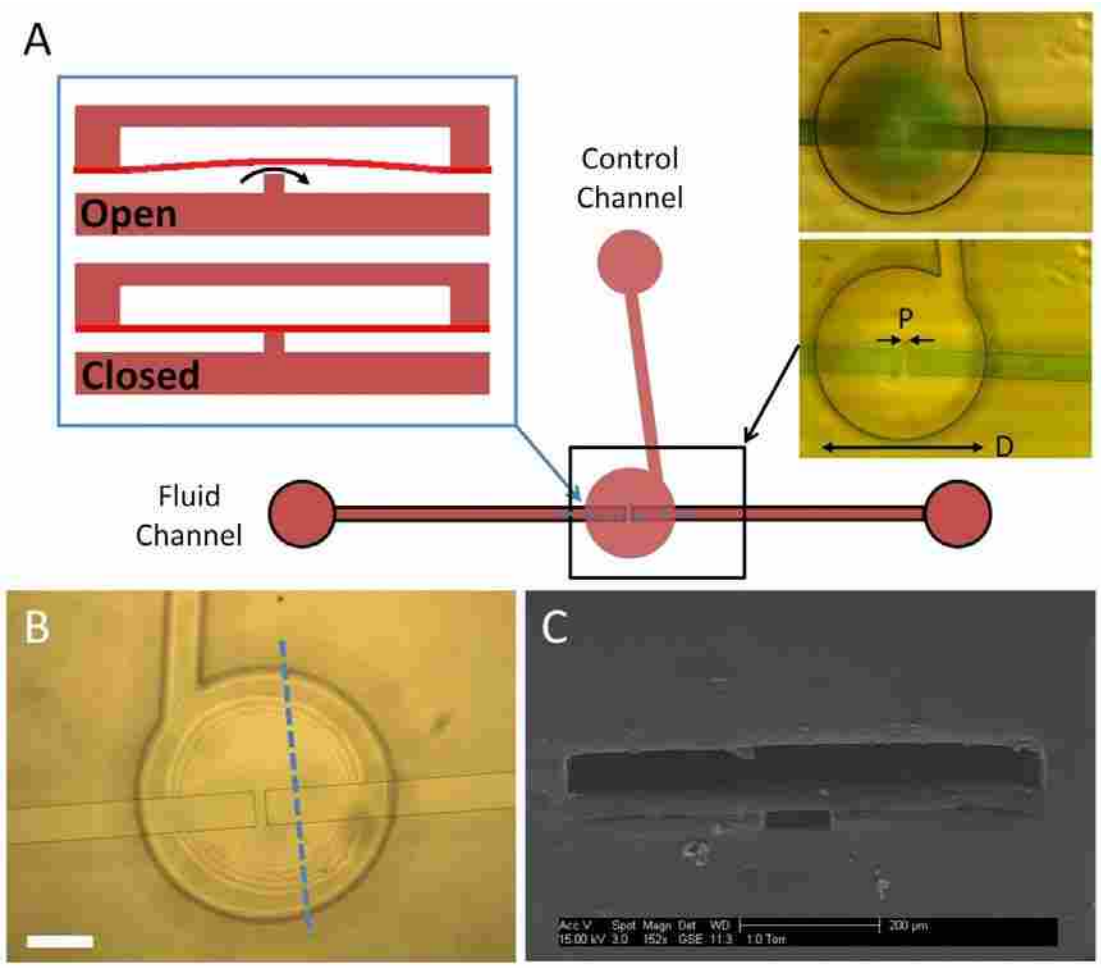

Figure 3.1. Schematic of a three-layer poly-PEGDA valve. (A) The left blue inset is a cross sectional view along the dashed blue line for an open or closed valve. Top-view images on the right show an open (top) and closed (bottom) valve with green dyed fluid added for contrast. Valve diameter (D) is 700 µm, pedestal width (P) is 30 µm, and the fluid channel width is 100 µm. (B) Top-view photomicrograph of a valve before filling with liquid. Interference fringes indicate that the membrane is deflected upward after

the final bonding step. White scale bar is 200 μm. (C) SEM of a three-layer valve device cross-section along the dashed blue line in (B).

Ideally, valves should have a small volume (< 1 nL), be non-adsorptive, resist swelling, and be easily fabricated. PDMS is a common valve material because it is easy to mold; however, it is prone to nonspecific adsorption of proteins and permeation of hydrophobic molecules,[22] which is problematic for bioanalytical applications and nonideal for valves. In response to this disadvantage, other materials (fluoroelastomers[23-25] and a thermoplastic elastomer[26]) have been explored as valve membranes in conjunction with rigid fluidic substrates of cyclic olefin copolymer, poly(methyl methacrylate), or glass. Fluoroelastomers, although resistant to nonspecific adsorption, are normally opaque and difficult to bond. Thermoplastic elastomers, although an improvement over PDMS, are still prone to nonspecific adsorption without chemical modification.[27] Polycarbonate, a non-elastomeric polymer, has been used as a valve membrane in a genetic sensor for tuberculosis; in this setup a solenoid mechanically forced the valve closed.[28] More recently, Chen et al.[29] demonstrated a pneumatically actuated polystyrene valve for oral fluid analysis. However, polycarbonate and polystyrene are both prone to nonspecific adsorption and require large valve areas (>3 mm^2) that lead to greater dead volumes that limit device miniaturization. Polymerized polyethylene glycol diacrylate (poly-PEGDA), another non-elastomeric polymer, is innately resistant to nonspecific adsorption and small molecule permeation.[22] Although this polymer has a higher elastic modulus (>0.1 GPa)[30, 31] than elastomers, its non-adsorptive nature makes it attractive as a material for monolithic membrane valves.

In this chapter, I demonstrate for the first time the construction of all-poly-PEGDA membrane valves for microfluidics. These valves have an 8× smaller area footprint (0.38 mm^2) than

previously demonstrated non-elastomeric (and typically adsorptive) membrane valves. The valves are actuated via standard pressurized control, but do not require an elastomeric membrane material. I have evaluated several different valve designs, including rectangular and circular geometries. Moreover, I have characterized the temporal response and flow performance of these poly-PEGDA valves over a range of pressures and number of actuations.

3.2 MATERIALS AND METHODS

3.2.1 Reagents and Materials

Azobisisobutyronitrile (AIBN), polyethylene glycol diacrylate (PEGDA, M.W. 258), and 2,2'-dimethoxy-2-phenylacetophenone (DMPA) were purchased from Sigma Aldrich (Milwaukee, WI). Phosphate buffered saline (PBS, 10x) was obtained from Fisher Scientific (Pittsburgh, PA) and diluted to 1x by adding deionized (DI) water (18.3 MΩ) from a Barnstead EASYpure UV/UF compact reagent grade water system. Perfluorosilane, (tridecafluoro-1,1,2,2-tetrahydrooctyl)-1-trichlorosilane, was purchased from UCT Specialties (Bristol, PA). SU8 photoresist (2025 and 2050) was obtained from Microchem (Newton, MA).

3.2.2 Device Fabrication

Thermally initiated prepolymer solutions were prepared by mixing 0.01 % w/w AIBN in PEGDA. Photoinitiated prepolymer solutions were prepared by combining 0.015 % w/w DMPA with PEGDA. Solutions were vortexed for 15 s, sonicated for 15 min, and subsequently refrigerated until use.

Poly-PEGDA valves were fabricated in three general processes: thermal polymerization of control and fluidic layers, photoinitiated polymerization of the membrane layer, and final device assembly and bonding (Fig. 3.2). The molds for thermal polymerization were formed using a

clean silicon wafer (Fig. 3.2A) on which SU8 features (~80 μm thick for the control layer and ~30 μm thick for the fluidic layer) had been photolithographically patterned (Fig. 3.2B).[22] The mold was placed inside a glass container containing one drop of perfluorosilane, which began to evaporate when heated to 70°C.[32] The perfluorosilane was vapor deposited onto the surface for 10 min to ease polymer removal from the mold. Poly-PEGDA spacers (~500 μm) were used to define the mold height (Fig. 3.2C), and a 3.5 in glass wafer was used as a cover (Fig. 3.2D). Prepolymer containing AIBN was then introduced into the cavity (Fig. 3.2E), and the entire mold was placed into an oven at 80°C for 1-2 h until polymerization was complete (Fig. 3.2F). The glass cover slide was carefully removed to avoid breaking the wafer (Fig. 3.2G), and the polymerized layers were subsequently removed, diced, and cleaned with acetone and 2-propanol (Fig. 3.2H).

Membrane fabrication was accomplished in a similar fashion, but photopolymerization was used. A clean glass slide was placed on a silicon wafer (Fig. 3.2A), and Mylar spacers (42 μm) were used to define the mold height (Fig. 3.2C). A glass slide was placed on top (Fig. 3.2D), and 70 μL of prepolymer containing DMPA was introduced into the mold cavity (Fig. 3.2E). UV exposure at 365 nm (560 mJ/cm^2) for 110 s was used to polymerize the membrane (Fig. 3.2F). The top surface of the membrane was exposed by removing the glass slide (Fig. 3.2G) immediately before bonding to the control layer (Fig. 3.2I). A clamp was used to hold the layers in contact during two subsequent UV exposures at 365 nm: the first was at 1.84 J/cm^2 for 6 min in a Karl Suss mask aligner and the second was a 12 J/cm^2 exposure for 4 min using a Spectroline SB-100PR UV lamp. Once these layers were bonded, input/output holes were laser cut for the fluid channel, and the bonded control/membrane layer was removed from the glass slide and rinsed with 2-propanol (Fig. 3.2J). The control/membrane layer was then aligned to the

fluid channel layer and clamped together (Fig. 3.2K). Vacuum was applied to the control/membrane layer during alignment and bonding (see Fig. 3.3) to prevent the membrane from being polymerized to the pedestal during the final bonding step. A 42 J/cm^2 UV exposure for 14 min using the Spectroline UV lamp was used to bond the fluid layer and form the completed device (Fig. 3.2L).

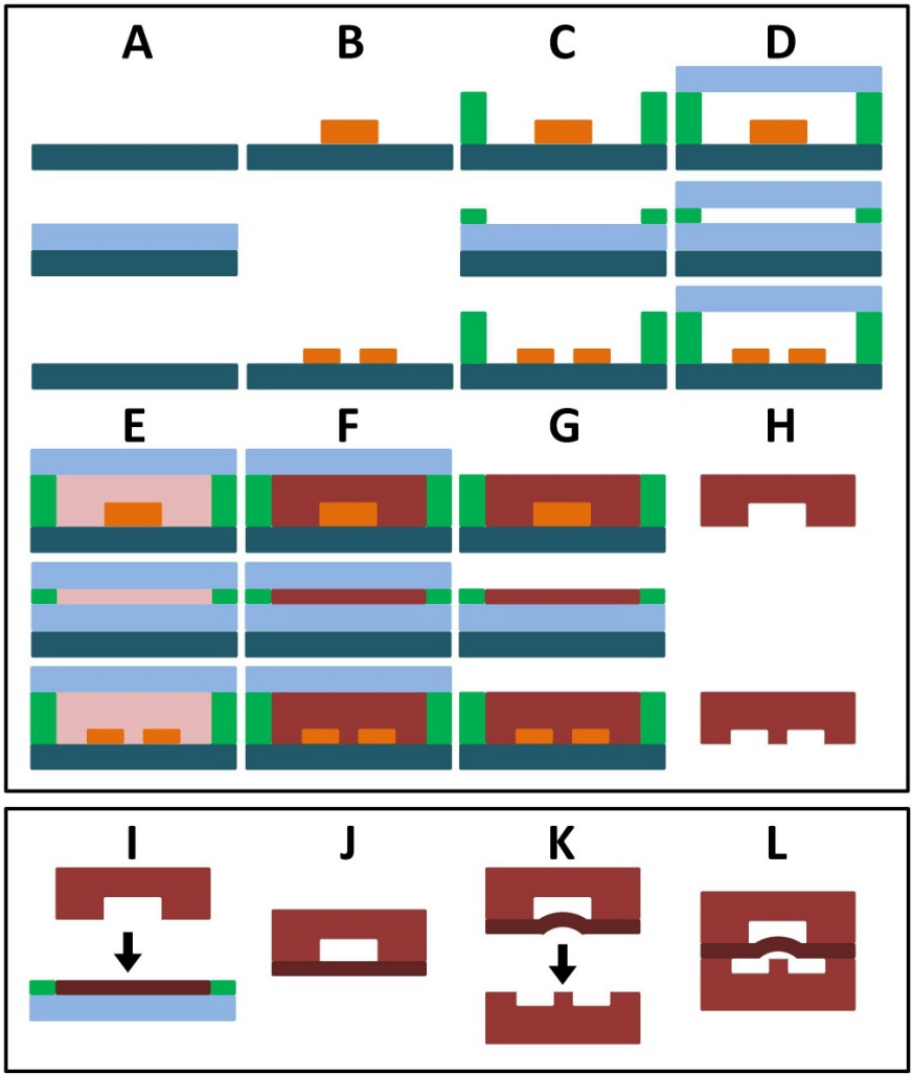

Figure 3.2. Overview of poly-PEGDA valve fabrication. The top box demonstrates fabrication of the polymerized control (top), membrane (middle), and fluidic (bottom) layers. Final assembly is shown in the bottom box. (A) Clean silicon wafers. (B) SU8 patterns define features. (C) Spacers define poly-PEGDA thickness. (D) Glass wafer forms top of mold. (E) Prepolymer is introduced. (F) Polymerization of poly-PEGDA. (G) Glass cover wafer is removed. (H) Finished poly-PEGDA is removed, diced, and

cleaned; an input hole is cut into the control layer. (I) The just-released top surface of the membrane layer (G, middle) is bonded to the control layer (H, top). (J) The bonded control and membrane layers are removed and (K) bonded under vacuum to the fluidic layer using UV light, (L) resulting in a completed valve device.

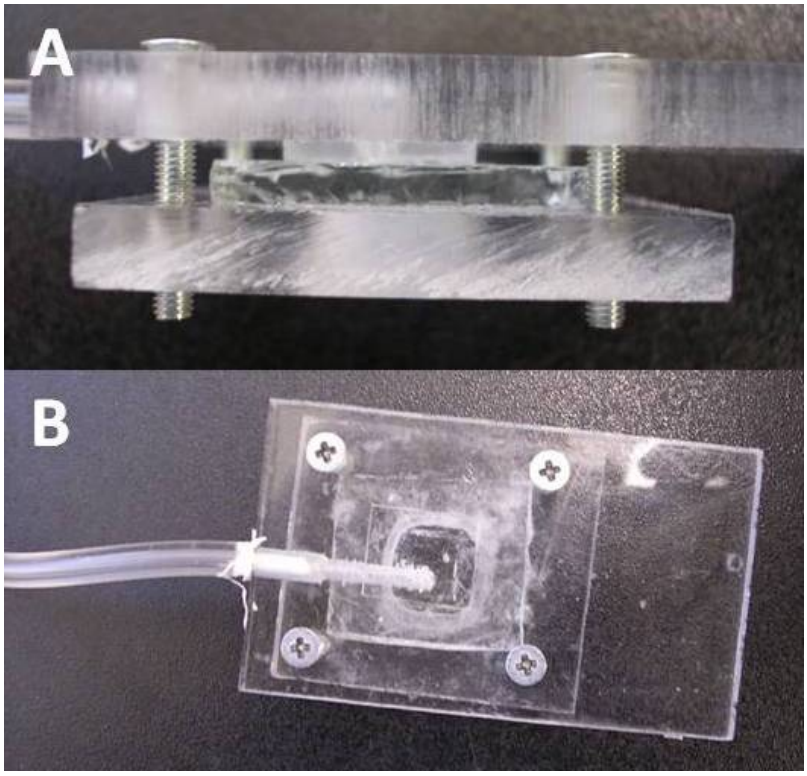

Figure 3.3. Vacuum clamp for bonding. (A) Side-view image of vacuum clamp, which is made up of four layers (PMMA, PDMS, glass, and PMMA). The poly-PEGDA layers to be bonded are placed in between the PDMS and the glass. (B) Top-view photograph of the vacuum clamp. Vacuum from the tubing at the left is routed through a drilled hole in the PMMA and a hole through the PDMS.

Several different valve geometries were explored. Rectangular valves (700 μm x 600 μm) with 5, 15, and 30 μm pedestals were fabricated, as were circular valves with a 350 μm radius and 5, 15, 30, and 125 μm pedestal widths). The width of the fluid channels in the circular valves was 100 μm (see Fig. 3.1); the fluid channel width in the rectangular valves expanded from 100 μm to 600 μm to match the valve dimensions. Channel depths in these devices ranged between 25-35 μm, membranes were ~40 μm thick, and the control channel height was 55-80 μm.

3.2.3 Device Characterization Setup

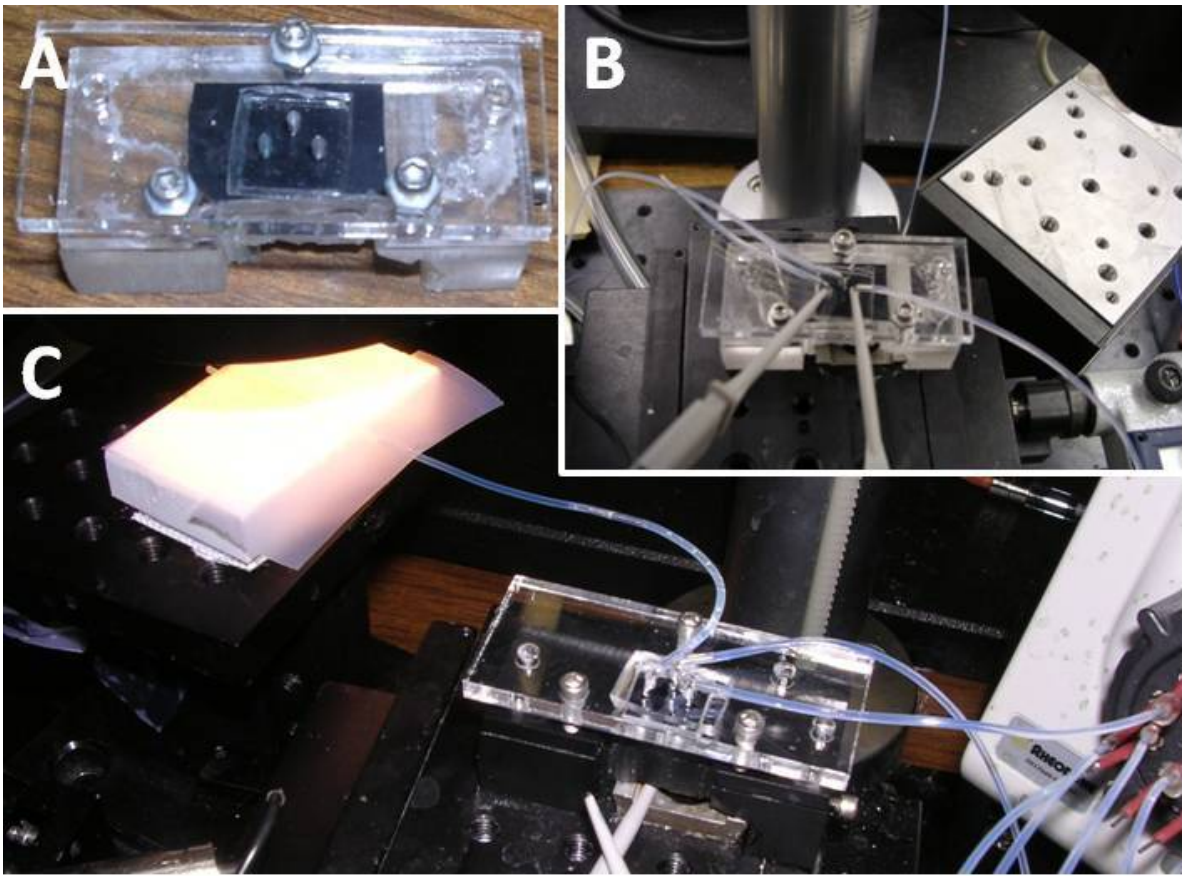

Figure 3.4. Images of the experimental setup. (A) Top-view photograph of device holder. A thin layer of PDMS with metal pins was clamped down by a PMMA cover piece to interface fluid and control lines to the poly-PEGDA device. (B) Top-view photograph of a device in the holder with inserted pins and tubing for pneumatic control and fluid interfacing. The right pin is the fluid input, the center pin is for pneumatic control, and the left pin is the fluid output. (C) Angled-view photograph of the experimental setup. The selector valve on the right was used to release the in-line fluid pressure. The output tubing (to the left) was imaged for meniscus tracking and flow measurement.

Three-layer poly-PEGDA devices were evaluated for functionality, response, and performance. In previous work,[22] I used Nanoports (Upchurch Scientific, Oak Harbor, WA) to connect external fluid lines to poly-PEGDA microfluidics. Herein, a piece of PDMS was clamped on top of a completed device, and hollow metal pins were used to connect the fluid and air lines to the device (see Fig. 3.4), similar to what has been done in some conventional PDMS microfluidic

devices.[33, 34] A syringe pump with an inline pressure sensor (Honeywell 24PCFFA6G) was used to supply fluid to the valve. Regulated, pressurized air with an inline pressure sensor (Honeywell 24PCFFH6G) provided pressure to the control layer. Solenoid valves (Clippard EVO-3M-24) were used to switch control layer pressure for valve actuation. Valves were evaluated by comparing the fluid pressure required for flow to commence at a given control pressure. Video was recorded of meniscus movement in the output tubing and processed using custom LabView code to determine linear flow velocity, which was then converted to volumetric flow rate. When fluid flow through the valve was >0.02 µL/min (0.2% of the syringe pump driven 10 µL/min flow rate), the valve was considered to be open. The Young's modulus for poly-PEGDA was calculated from the pressure required to deflect a circular membrane a known distance using Eq. 3.1 for linear deflection (up to ½ membrane thickness) where P is the applied pressure (Pa), E is the elastic modulus (Pa), r is the membrane radius (m), h is the membrane thickness (m), v is the Poisson's ratio, and y is the deflection (m) at the membrane center.[35]

$$\frac{Pr^4}{Eh^4} = \frac{16y}{3(1-v^2)h} + \frac{7-v}{3(1-v)}\left(\frac{y}{h}\right)^3 \qquad (3.1)$$

Water contact angles were measured using a ramé-hart Goniometer (model 100) with 10 µL water droplets.

The temporal response of valves was measured using a high-speed camera (Photron FASTCAM SA3) and using color change associated with deflection. A valve actuation rate of 1 Hz with a 30% duty cycle and 207 kPa control pressure was used to evaluate the fall (closure) and rise (open) time of valves. The rise time was given by the time required for the valve position to go from 10-90% of its range of motion, and the fall time was determined from the time required for the valve position to drop from 90-10% of its motion range.

Valve performance was evaluated over a range of control pressures (0-207 kPa) and as a function of number of actuations. PBS (~250 μL) was flowed through the fluid layer of each device before evaluating valves. Control and fluid pressures were raised incrementally from lower to higher (0, 70, 148, and 207 kPa). Each valve was actuated at 1 Hz and a 50% duty cycle in increments of 500 for initial testing, and larger increments (up to 100,000) for long-term testing. Each valve was retested over the same range of pressures after each series of actuations. Circular valves with both 15 and 30 μm pedestal widths were used in duty cycle tests.

3.3 RESULTS AND DISCUSSION

3.3.1 Device Characterization Results

Figure 3.1 shows an overview of monolithic membrane valves fabricated entirely from poly-PEGDA. Applied pressure is used to close the valve, preventing fluid from flowing through (Fig. 3.1A), and the valve is opened by releasing the control pressure and allowing fluid pressure to deflect the membrane up, resuming flow. Top-view images of the valve with green colored dye in the fluid channel demonstrate the opening and closure of a valve with a 700 μm diameter and a 30 μm pedestal (Fig. 3.1A - right images). The membrane is deflected up during fabrication to prevent bonding to the valve seat (Fig. 3.1B). An SEM image shows a cross-sectional cut through a poly-PEGDA valve (Fig. 3.1C), illustrating the three-layer fabrication with the deeper control layer channel on top, the poly-PEGDA membrane in the middle, and the shallower fluid channel on the bottom. If a Poisson ratio of 0.35 (similar to that of PMMA[36]) is assumed, the resulting elastic modulus for poly-PEGDA is determined to be ~0.1 GPa based on membrane deflection under applied pressure. Although this Young's modulus is too high to allow poly-PEGDA to form self-collapsible valves similar to PDMS, which has an elastic modulus ranging between 0.05-4 MPa (the number varies by formula),[37] the elastic modulus allows for utilization

of membrane valves. Valves remain functional for fluidic pressures up to 400 kPa and flow up to 150 µL/min. A water contact angle of 55° for poly-PEGDA shows a more hydrophilic surface compared to 68° for PMMA[38] and 100° for PDMS.[39]

I characterized circular valves with 5, 15, 30, and 125 µm pedestals, and ~30 µm deep fluid channels (Table 3.1). With these device dimensions, the 5 µm pedestals became damaged during fabrication such that functional devices were difficult to achieve. However, valves with pedestal widths of 15, 30, and 125 µm all demonstrated similar properties and function. Since valves with larger pedestals (>100 µm) occupy more device space, I focused on characterizing circular valves with 15 µm and 30 µm pedestals. Rectangular valves (see Fig. 3.5) were also characterized but did not maintain a linear relationship between the control pressure and fluid pressure to initiate flow, unlike circular valves (Table 3.1).

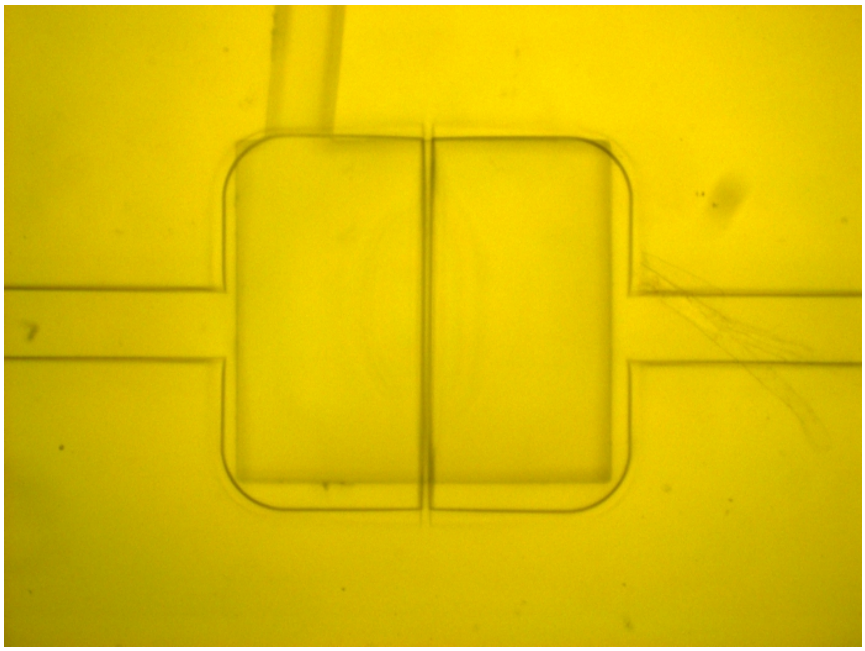

Figure 3.5. Photomicrograph of a rectangular valve with a 15 µm pedestal width, a 600 x 640 μm^2 control layer, a 550 x 600 μm^2 fluid channel in the valve region, and a 100 µm wide fluid channel leading into and out from the valve.

The temporal response of circular valves demonstrated rapid and repeatable actuation (Fig. 3.6). A fall time of 0.019 s to close the valve was determined from the time for the membrane to move from 90% deflected to 10% deflected upon switching on the control pressure. The time required to open the valve after switching off the control pressure (rise time) was 0.105 s. I used smoothed data (11 pt. boxcar moving average) in this calculation to remove minor noise in the position measurement as it approached 90% deflection. These rise and fall times are sufficiently rapid for utilization in microfluidic systems for actuation rates up to 8 Hz. Faster opening times could likely be achieved with either backpressure on the pumped fluid or the application of vacuum to the valve in the opening step.

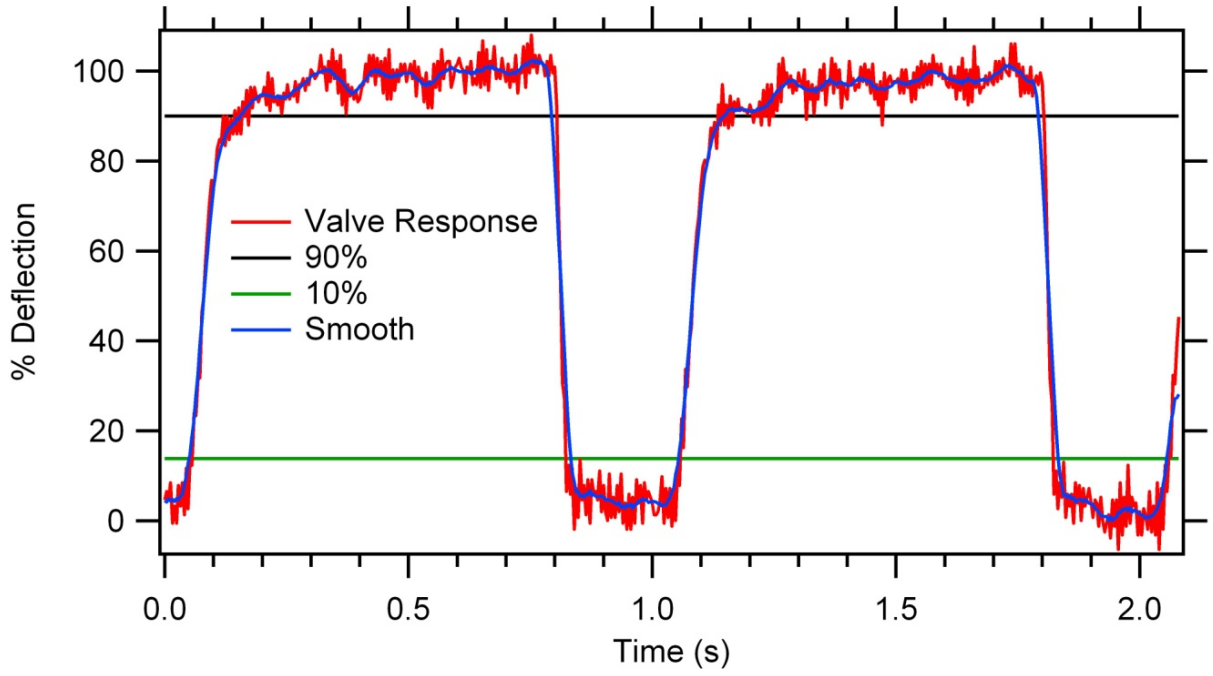

Figure 3.6. Valve temporal response. Valve was actuated at 1 Hz and 30% duty cycle. Fall time (valve closure) was 0.019 s and rise time (valve opening) was 0.105 s. No vacuum was used to open the valve, and the fluid backpressure was negligible in these experiments.

Table 3.1. Summary of Results for Each Valve Geometry.

Pedestal Width	Circular Valve	Rectangular Valve
5 µm	*Pedestals broke*	*Pedestals broke*
15 µm	*Functional valves*	*Valves leaked*
30 µm	*Functional valves*	*Valves leaked*
125 µm	*Functional valves*	*Not tested*

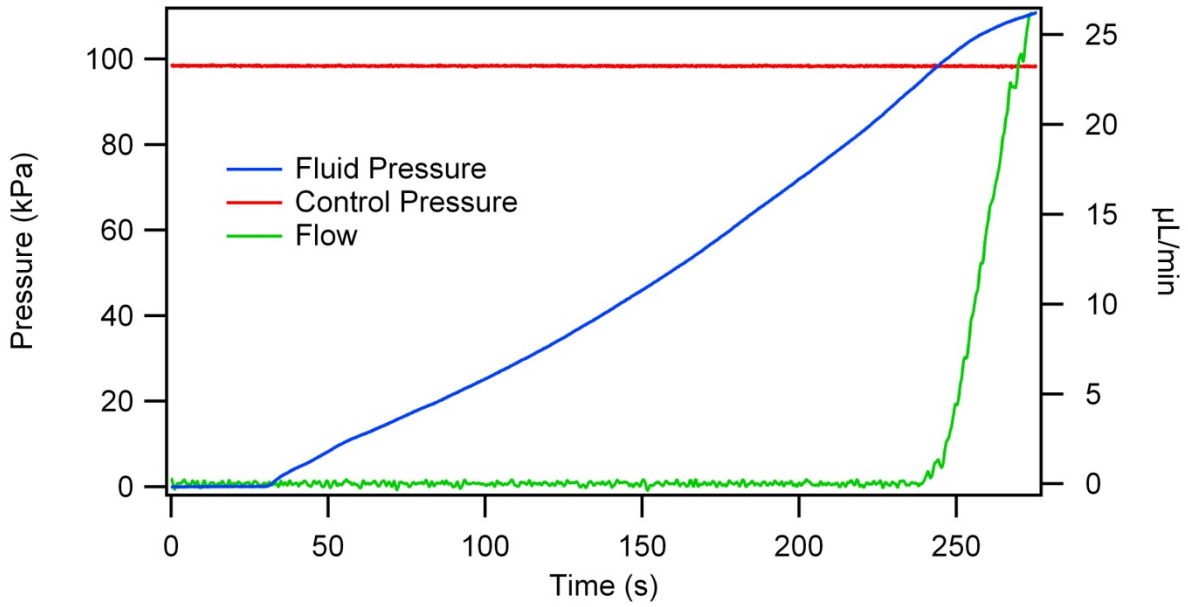

Figure 3.7. Fluid pressure and volumetric flow rate as a function of time for a constant control pressure. Sensors in the fluid and control lines monitor pressures, and meniscus tracking on the fluid output allows for flow measurement. The flow rate increases rapidly once the fluid pressure exceeds the control pressure at ~240 s.

Valves were evaluated by monitoring fluid pressure and flow for a given control pressure. In Figure 3.7, a circular valve with a 30 µm pedestal was tested after the valve had been actuated ~5,000 times. The control pressure was held constant at ~97 kPa, and after 30 s fluid was pressurized into the valve by a syringe pump at 10 µL/min. The 30-s delay in the syringe pump activation provided a baseline for the fluid pressure. Once flow was initiated, the fluid pressure increased until it exceeded the control pressure, at which point the valve opened, providing an

outlet for the pressure and resulting in flow that rapidly increased towards the pump rate. Monitoring of fluid and control pressures as well as meniscus movement, was used in evaluating more than 40 different valves, all of which demonstrated similar behavior. Similar tests were done multiple times for each valve geometry and pedestal width across a range of pressures and a number of valve actuations. The relationship between the control pressure and the fluid pressure at which flow commenced was determined in multiple devices and after various numbers of actuations. Rearranging Eq. 3.1 for *P* gives Eq. 3.2 which provides a relationship between applied pressure and membrane deflection.

$$P = \frac{Ehy\left((\nu^2 - 6\nu - 7)y^2 - 16h^2\right)}{3r^4(\nu^2 - 1)} \tag{3.2}$$

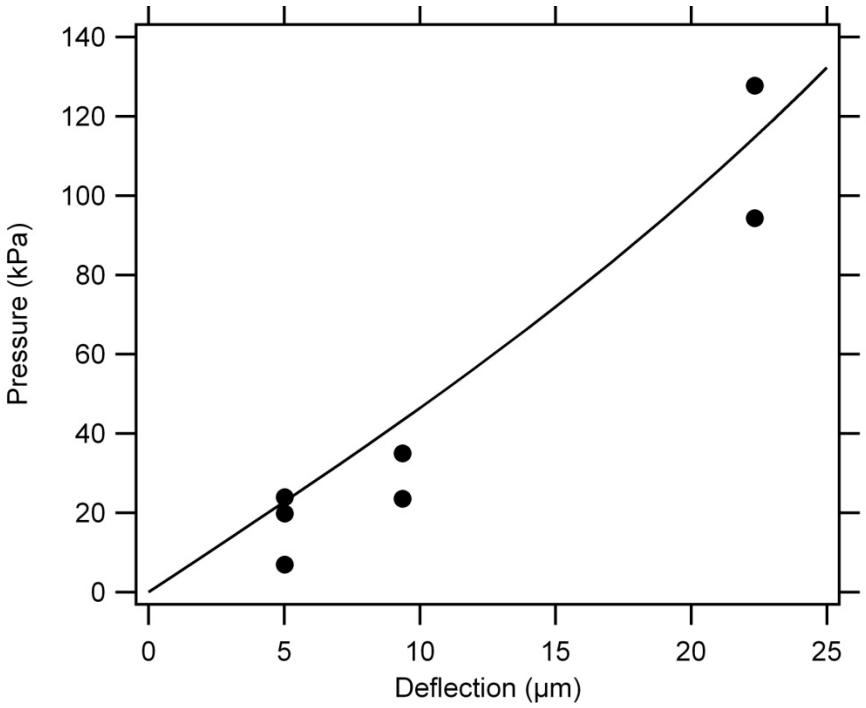

Figure 3.8. Calculated (line) and experimentally measured (circles) deflection via applied pressure, for a 45 μm thick circular membrane with an elastic modulus of 0.13 GPa, a 350 μm radius, and a Poisson's ratio of 0.35. Calculated data are from Eq. 3.2. Very low pressure (~9 kPa) is required for significant membrane deflection (>2 μm).

Figure 3.8 depicts this pressure versus deflection relationship for a 42-μm thick circular membrane with a 350 μm radius, an elastic modulus of 0.13 GPa (see Table 3.2), and a Poisson ratio of 0.35. Less than 8 kPa is required for the membrane to deflect 2 μm, enough to initiate flow. This can be seen in Figure 3.7 as the fluid pressure approaches the closure pressure allowing flow to resume over a small increase in pressure. At 88 kPa (90% of the control pressure) there is no flow, but as the fluid pressure reaches ~95 kPa (97% of control pressure) flow begins (0.02 μL/min) and increases rapidly to >10 μL/min as the fluid pressure exceeds the control pressure by ~6.5 kPa. Valves were expected to open once the fluid pressure exceeded the applied control pressure. However, for newly fabricated devices, a ~47 kPa excess fluid pressure was required to initiate flow through valves (Fig. 3.9A). One possible explanation of this initial pressure offset is stiction between the membrane and the pedestal. However, there was no clear trend in initial pressure offset as pedestal width varied from 15-125 μm. When the valve was actuated 500-1500 times, the fluid pressure required to open the valve decreased toward the control pressure until the plot of fluid vs. control pressure reached a slope of 1 after 1000-1500 actuations.

Table 3.2. Data for Young's Modulus Calculations in Equation 3.1.

***P* (Pa)**	***r* (mm)**	***h* (mm)**	***y* (mm)**	***v***	***E* (Pa)**
1.65E+05	0.87	0.19	0.02	0.35	1.13E+08
1.59E+05	0.87	0.19	0.02	0.35	1.08E+08
1.59E+05	0.87	0.19	0.02	0.35	1.08E+08
2.07E+05	0.87	0.18	0.02	0.35	1.66E+08
1.45E+05	0.87	0.19	0.02	0.35	9.89E+07
2.41E+05	0.87	0.19	0.02	0.35	1.65E+08
			Average *E* (GPa)		**0.13**
				σ (GPa)	**0.03**

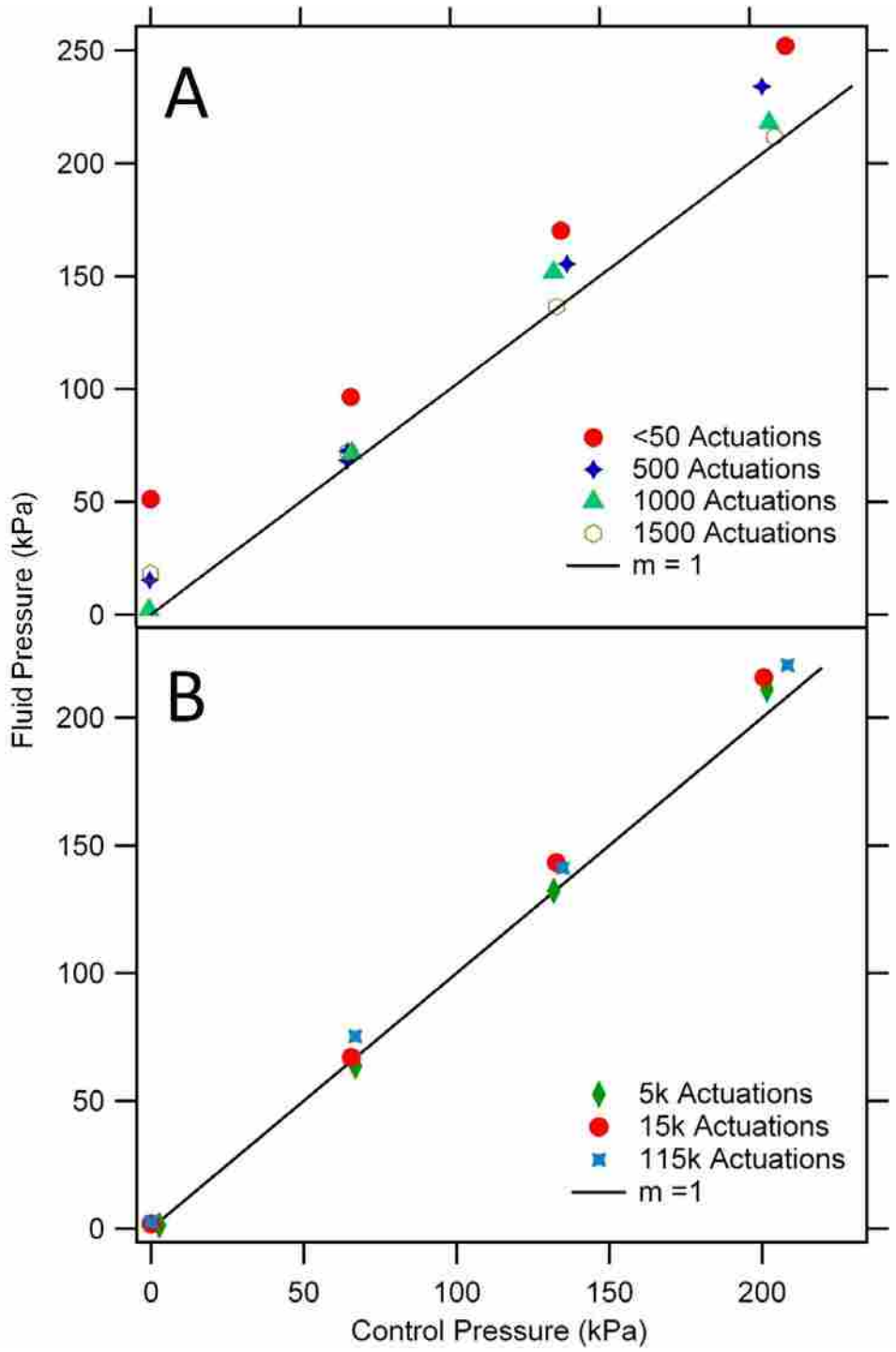

Figure 3.9. Valve performance after a number of actuations as a function of control pressure. (A) Initial valve testing shows a higher fluid pressure is required to open the valve for a given control pressure. After ~1500 actuations, the fluid pressure to open a valve decreases to match the control pressure. A circular valve with a 15 µm pedestal width was used for this test. (B) Valves maintain this linear fluid vs. control pressure relationship to at least 115,000 actuations. A different circular valve with a 30 µm pedestal width was used for this test.

Realignment of polymer chains in the device after multiple valve actuations[40] could increase the elasticity of the membrane, thereby making it easier to close. I further evaluated valves for long-term robustness after very large numbers of actuations (Fig. 3.9B). After 5,000, 15,000, and even 115,000 actuations, the fluid vs. control pressure plot maintained a linear relationship with a slope of 1, thus demonstrating considerable repeatability and potential for long-term use. Since 1000-1500 actuations were needed for valves to show the expected fluid vs. control pressure relationship, the valves were preconditioned by performing 1500 actuations before use. Several different valve designs were evaluated. Rectangular valves with 5, 15, and 30 μm pedestals were tested. As with circular valves, rectangular valves with 5 μm pedestals were easily damaged during fabrication. Unlike in circular valves (Figure 3.1), the fluid channel was widened in rectangular valves to match the control layer design (Fig. 3.5). Rectangular valves did not follow the linear fluid vs. control pressure relationship observed for circular valves in Figure 3.9. In addition, the rectangular valve designs were not as effective as circular ones in valve closure at low control pressures (<70 kPa). The better performance of the circular valves is likely due to the larger surface area of the valve seat in contact with the membrane, which helps the membrane to remain planar in the closed state. In contrast, the valve seat contact area with the membrane is limited to the pedestal only in the rectangular valve design, so the membrane may deflect partially into the fluid layer.

3.3.2 Device Prospects

Three-layer poly-PEGDA valves have reliable fabrication, fast response times, and robustness over a large number of actuations. Valves with pedestal widths down to 15 μm have been successfully made and operated. Possible improvements to these valves include smaller diameters (<200 μm) and fluid channel widths (<50 μm), and thinner membranes (<20 μm), all

of which would further reduce dead volume and improve performance. With combined application of control pressure and vacuum to control lines and appropriate device layouts, arrays of these poly-PEGDA valves have potential for application as peristaltic pumps.[18, 19] Poly-PEGDA valve integration with functional or sensing components in other materials, such as silicon or glass, is also attractive. Finally, the fabrication of embedded electrodes into devices would enable conductivity or impedance detection, as well as valve closure determination.

Poly-PEGDA valves with their intrinsic resistance to nonspecific adsorption are ideally suited for biomolecular and protein assays. One example would be the analysis of Tau protein in cerebrospinal fluid for brain trauma diagnosis[41, 42] via an on-chip microdialysis system[43] that extracts small volumes of cerebrospinal fluid, which could then be fluorescently labeled and purified on-chip[44] for subsequent electrophoretic separation and detection. Similarly, thymidine kinase I in blood serum, which shows promise in diagnosis of hematological cancers,[45] could be captured on-chip using immobilized antibodies,[46] and then reacted with a fluorescently labeled secondary antibody for detection using laser induced fluorescence.[47] A final example is the quantitative analysis of pre-term birth biomarkers in blood serum[48, 49] utilizing poly-PEGDA valves to control sample introduction and pumping for secondary flow required for nanospray mass spectrometry.[50] In these examples, a non-adsorptive device material would enable more of the analyte of interest to be available for detection and provide symmetrical separation peaks.

3.4 CONCLUSIONS

Poly-PEGDA with inherent nonspecific adhesion resistance properties has been used to form microfluidic valves. Multiple device geometries were tested; a circular design had a linear fluid versus control pressure plot over different pedestal widths. A valve opening time of ~100 ms and

a closure time of ~20 ms offer valve operation as fast as 8 Hz with potential for further improvement. A number of replicate measurements after a series of actuations and over a range of pressures demonstrated the functionality and robustness of these poly-PEGDA valves.

The multi-layer fabrication method developed here for valves can be adapted for on-chip pumping, which could aid in the integration of automated on-chip sample preparation with electrophoretic separation. Such pumps could also provide a mechanism for solution mixing, or find use in a closed system where small-volume specimens could be recirculated over a sensor, improving sampling. Finally, attachment of these valve systems to silicon or glass devices could be explored to enable interfacing with micro- and nano-sensors such as microcantilevers, silicon ring resonators, nanowires, etc.

3.5 REFERENCES

(1) Nge, P. N.; Rogers, C. I.; Woolley, A. T. *Chem. Rev.* **2013**, *113*, 2550-2583.
(2) Kovarik, M. L.; Ornoff, D. M.; Melvin, A. T.; Dobes, N. C.; Wang, Y.; Dickinson, A. J.; Gach, P. C.; Shah, P. K.; Allbritton, N. L. *Anal. Chem.* **2013**, *85*, 451-472.
(3) Arora, A.; Simone, G.; Salieb-Beugelaar, G. B.; Kim, J. T.; Manz, A. *Anal. Chem.* **2010**, *82*, 4830-4847.
(4) van Midwoud, P. M.; Janse, A.; Merema, M. T.; Groothuis, G. M. M.; Verpoorte, E. *Anal. Chem.* **2012**, *84*, 3938-3944.
(5) Abgrall, P.; Gué, A.-M. *J. Micromech. Microeng.* **2007**, *17*, R15-R49.
(6) Yang, S.; DeVoe, D. L. *Microfluidic Diagnostics: Methods and Protocols*; Humana Press: New York City, NY, 2013; Vol. 949, 115-123.
(7) Trzebinski, J.; Sharma, S.; Radomska-Botelho Moniz, A.; Michelakis, K.; Zhang, Y.; Cass, A. E. G. *Lab Chip* **2012**, *12*, 348-352.
(8) Rivet, C.; Lee, H.; Hirsch, A.; Hamilton, S.; Lu, H. *Chem. Eng. Sci.* **2011**, *66*, 1490-1507.
(9) Chin, C. D.; Linder, V.; Sia, S. K. *Lab Chip* **2012**, *12*, 2118-2134.
(10) Gervais, L.; de Rooij, N.; Delamarche, E. *Adv. Mater.* **2011**, *23*, H151-176.
(11) Mainz, E. R.; Gunasekara, D. B.; Caruso, G.; Jensen, D. T.; Hulvey, M. K.; Fracassi da Silva, J. A.; Metto, E. C.; Culbertson, A. H.; Culbertson, C. T.; Lunte, S. M. *Anal. Methods* **2012**, *4*, 414-420.
(12) Jin, S.; Anderson, G. J.; Kennedy, R. T. *Anal. Chem.* **2013**, *85*, 6073-6079.
(13) Kim, J.; Kang, M.; Jensen, E. C.; Mathies, R. A. *Anal. Chem.* **2012**, *84*, 2067-2071.
(14) Unger, M. A.; Chou, H.-P.; Thorsen, T.; Scherer, A.; Quake, S. R. *Science* **2000**, *288*, 113-116.

(15) Grover, W. H.; Skelley, A. M.; Liu, C. N.; Lagally, E. T.; Mathies, R. A. *Sens. Actuators, B* **2003**, *89*, 315-323.
(16) Mohammed, M. I.; Desmulliez, M. P. Y. *Microsyst. Technol.* **2013**, *19*, 809-818.
(17) Au, A. K.; Lai, H.; Utela, B. R.; Folch, A. *Micromachines* **2011**, *2*, 179-220.
(18) Grover, W. H.; Mathies, R. A. *Lab Chip* **2005**, *5*, 1033-1040.
(19) Stockton, A. M.; Mora, M. F.; Cable, M. L.; Willis, P. A. *Sens. Actuators, B* **2013**, *177*, 668-675.
(20) Kim, J.; Jensen, E. C.; Stockton, A. M.; Mathies, R. A. *Anal. Chem.* **2013**, *85*, 7682-7688.
(21) Schimek, K.; Busek, M.; Brincker, S.; Groth, B.; Hoffmann, S.; Lauster, R.; Lindner, G.; Lorenz, A.; Menzel, U.; Sonntag, F.; Walles, H.; Marx, U.; Horland, R. *Lab Chip* **2013**, *13*, 3588-3598.
(22) Rogers, C. I.; Pagaduan, J. V.; Nordin, G. P.; Woolley, A. T. *Anal. Chem.* **2011**, *83*, 6418-6425.
(23) Willis, P. A.; Greer, F.; Lee, M. C.; Smith, J. A.; White, V. E.; Grunthaner, F. J.; Sprague, J. J.; Rolland, J. P. *Lab Chip* **2008**, *8*, 1024-1026.
(24) Ogilvie, I. R. G.; Sieben, V. J.; Cortese, B.; Mowlem, M. C.; Morgan, H. *Lab Chip* **2011**, *11*, 2455-2459.
(25) Huang, S.; He, Q.; Chen, H.; Huang, J. *Microfluid. Nanofluid.* **2013**, *14*, 329-335.
(26) Rupp, J.; Schmidt, M.; Münch, S.; Cavalar, M.; Steller, U.; Steigert, J.; Stumber, M.; Dorrer, C.; Rothacher, P.; Zengerle, R.; Daub, M. *Lab Chip* **2012**, *12*, 1384-1388.
(27) Pan, T.; Fiorini, G. S.; Chiu, D. T.; Woolley, A. T. *Electrophoresis* **2007**, *28*, 2904-2911.
(28) Wang, H.; Chen, H.-W.; Hupert, M. L.; Chen, P.-C.; Datta, P.; Pittman, T. L.; Goettert, J.; Murphy, M. C.; Williams, D.; Barany, F.; Soper, S. A. *Angew. Chem.* **2012**, *124*, 4425-4429.
(29) Chen, Z.; Abrams, W. R.; Geva, E.; de Dood, C. J.; González, J. M.; Tanke, H. J.; Niedbala, R. S.; Zhou, P.; Malamud, D.; Corstjens, P. L. A. M. *BioMed. Res. Int.* **2013**, *2013*, 543294.
(30) Kim, P.; Jeong, H. E.; Khademhosseini, A.; Suh, K. Y. *Lab Chip* **2006**, *6*, 1432-1437.
(31) Rogers, C. I.; Pagaduan, J. V.; Nordin, G. P.; Woolley, A. T., Orlando, FL, March 11-15, 2012; Pittcon Conference and Expo.
(32) Lee, J. K.; Kung, M. C.; Kung, H. H.; Mockros, L. F. *ASAIO J.* **2008**, *54*, 390-395.
(33) Balagaddé, F. K.; You, L.; Hansen, C. L.; Arnold, F. H.; Quake, S. R. *Science* **2005**, *309*, 137-140.
(34) Ren, L.; Wang, J.-C.; Liu, W.; Tu, Q.; Liu, R.; Wang, X.; Xu, J.; Wang, Y.; Zhang, Y.; Li, L.; Wang, J. *Biosens. Bioelectron.* **2012**, *35*, 147-154.
(35) Kovacs, G. T. A. *Micromachined Transducers Sourcebook*; McGraw-Hill: New York, 1998, 250.
(36) Goswami, A.; Umarji, A. M.; Madras, G. *Polym. Adv. Technol.* **2012**, *23*, 1604-1611.
(37) Fuard, D.; Tzvetkova-Chevolleau, T.; Decossas, S.; Tracqui, P.; Schiavone, P. *Microelectron. Eng.* **2008**, *85*, 1289-1293.
(38) Ma, Y.; Cao, X.; Feng, X.; Ma, Y.; Zou, H. *Polymer* **2007**, *48*, 7455-7460.
(39) Lawton, R. A.; Price, C. R.; Runge, A. F.; Doherty III, W. J.; Saavedra, S. S. *Colloids Surf., A* **2005**, *253*, 213-215.
(40) McKeen, L. W. *The Effect of Creep and Other Time Related Factors on Plastics and Elastomers*, 2nd ed.; Elsevier Inc.: Burlington, MA, 2009.

(41) Süssmuth, S. D.; Reiber, H.; Tumani, H. *Neurosci. Lett.* **2001**, *300*, 95-98.
(42) Franz, G.; Beer, R.; Kampfl, A.; Engelhardt, K.; Schmutzhard, E.; Ulmer, H.; Deisenhammer, F. *Neurology* **2003**, *60*, 1457-1461.
(43) Huynh, B. H.; Fogarty, B. A.; Nandi, P.; Lunte, S. M. *J. Pharm. Biomed. Anal.* **2006**, *42*, 529-534.
(44) Nge, P. N.; Pagaduan, J. V.; Yu, M.; Woolley, A. T. *J. Chromatogr. A* **2012**, *1261*, 129-135.
(45) Alegre, M. M.; Robison, R. A.; O'Neill, K. L. *Cancer Clin. Oncol.* **2013**, *2*, 159-167.
(46) Yang, W.; Yu, M.; Sun, X.; Woolley, A. T. *Lab Chip* **2010**, *10*, 2527-2533.
(47) Salehi-Reyhani, A.; Kaplinsky, J.; Burgin, E.; Novakova, M.; deMello, A. J.; Templer, R. H.; Parker, P.; Neil, M. A. A.; Ces, O.; French, P.; Willison, K. R.; Klug, D. *Lab Chip* **2011**, *11*, 1256-1261.
(48) Vance, C. J.; Esplin, M. S.; Hamblin, S.; Graves, S. W. *Am. J. Obstet. Gynecol.* **2006**, *195*, 1407-1414.
(49) Esplin, M. S.; Merrell, K.; Goldenberg, R.; Lai, Y.; Iams, J. D.; Mercer, B.; Spong, C. Y.; Miodovnik, M.; Simhan, H. N.; van Dorsten, P.; Dombrowski, M. *Am. J. Obstet. Gynecol.* **2011**, *204*, 391.e391-391.e398.
(50) Chambers, A. G.; Mellors, J. S.; Henley, W. H.; Ramsey, J. M. *Anal. Chem.* **2011**, *83*, 842-849.

4. PATTERNED DUAL-SILANE DEPOSITION ON QUARTZ TO ENABLE HYBRID MATERIAL INTEGRATION AND SITE-SPECIFIC FUNCTIONALIZATION

4.1 INTRODUCTION

Microfluidics consist of microfabricated 1–500 μm features that allow for managing femtoliter to nanoliter fluid movement.[1] As channel size decreases, the surface-to-volume ratio increases and surface chemistry becomes more influential. As microfluidics has focused on biosensing, the ability to change the available surface chemistry inside microfluidic channels and adapt that chemistry for better biocompatibility[2] and probe attachment (e.g., peptides,[3] proteins,[4] and DNA[5]) has become more important.

Site-specific functionalization is desirable in biosensing because it creates areas of differing surface chemistries that allow for various applications. Ness et al.[6] demonstrated inkjet printing as a method to attach biotinylated bovine serum albumin to one side of a microcantilever to generate differential stress when interacting with streptavidin. Sweetman et al.[7] showed that photolithography can be used to pattern areas onto porous silicon with three different silane pairs. Adaptation of this process for use with quartz, which is transparent down to 185 nm[8] and has low autoflourescence,[9] could allow the integration of different materials while providing regions for further chemical modification via well characterized methods.

Polymerized polyethylene glycol diacrylate (poly-PEGDA) is a nonspecific adsorption resistant material desirable for utilization with biological samples.[10] Poly-PEGDA is optically clear, resistant to permeation of small molecules, and suitable for use with electrophoresis (see Chapter 2) and valves (see Chapter 3).[10, 11] Bonding poly-PEGDA microfluidics with different

substrate materials (e.g., glass, silicon, or electrode-patterned materials) provides broader application for biosensing and device integration.

Evaluation of dual-silane patterning and poly-PEGDA device bonding to silicon and quartz is demonstrated in this Chapter. Photolithographic patterning of a silane-functionalized surface enables area-specific silane removal through HF etching of the exposed regions. This also creates a clean surface for subsequent deposition of a different, secondary silane on the etched regions. Dual-silane deposition onto these substrates makes bonding to poly-PEGDA possible through UV exposure, while providing specific locations for crosslinking desired molecules to the surface. An amine-reactive fluorescent molecule is utilized to evaluate the dual silane deposition process on quartz. Preliminary results for site-specific secondary attachment using glutaraldehyde as a crosslinker and a reactive fluorophore are discussed in this Chapter as well.

4.2 MATERIALS AND METHODS

4.2.1 Reagents and Materials

Nanostrip was acquired from Cyanotek (Fremont, CA) and buffered oxide etchant (BOE, hydrofluoric acid) was from Transene Company (Danvers, MA). **Warning: hydrofluoric acid is dangerous! Use the proper protective equipment when using!** The base/acid solutions were created by individually diluting hydrochloric acid (EMD Chemicals, Gibbstown, NJ) and sodium hydroxide (EM Science, Gibbstown, NJ) to 0.1 M in 18.3 MΩ DI water (EASYpure UV/UF). Dimethyl sulfoxide (DMSO), glutaraldehyde (8% solution in water), fluoresceinamine, polyethylene glycol diacrylate (PEGDA, 258 Da), 3-(trimethoxysilyl)propyl methacrylate (TMSPMA), 2,2′-azobis(2-methylpropionitrile) (AIBN), and 2,2'-dimethoxy-2-phenylacetophenone (DMPA) were purchased through Sigma-Aldrich (Milwaukee, WI).

AZ2020 photoresist was obtained from AZ Electronic Materials (Branchburg, NJ). Two silanes, 3-aminopropyl-diisopropylethoxysilane (APDIES) and (3-acryloxypropyl)dimethylmethoxysilane (APDMMS), were purchased through Gelest (Morrisville, PA). Alexa Fluor 488 TFP Ester was acquired from Invitrogen (Carlsbad, CA).

4.2.2 Device Fabrication

Poly-PEGDA device fabrication has been described previously (see Section 3.2.2. and Fig. 3.2 for details).[10, 11] For the burst pressure tests and secondary attachment evaluation, the poly-PEGDA fluidic layer (Fig. 3.2. K and L) was replaced with a silanized silicon or quartz die and bonded under UV light exposure as described in Sections 4.2.3 and 4.2.5 below.

4.2.3 Burst Pressure Evaluation Setup

Bonding of the poly-PEGDA control and membrane layers has been discussed previously in Chapter 3.2.2. A hole was cut into the poly-PEGDA membrane using a CO_2 laser cutter (VersaLASER VLS 2.30, Scottsdale, AZ). Pieces (~1 cm^2) of clean silicon were plasma cleaned for three minutes utilizing a Harrick Plasma Cleaner (~18 W) and then placed in a 2% silane solution (either APDMMS or TMSPMA) in toluene for 2 h to functionalize the surface. When the deposition was complete, the test samples were removed from the liquid, rinsed with clean toluene and blow dried with dry N_2. The combined control and membrane poly-PEGDA layer was bound to the silicon substrate under UV exposure with a Spectroline SB-100PR UV Lamp (Westbury, NY) at a distance of 4 cm for 20 min. Quartz was bonded to poly-PEGDA under the same conditions.

Nanoports (Upchurch Scientific, Oak Harbor, WA) were attached to the completed device as in Chapter 2.2.3. The same setup used to evaluate burst pressure in Chapter 2.2.5 was used to

evaluate the bond strength. In brief, a syringe pump flowing at 100 µL/min (for APDMMS or TMSPMA on silicon) or 50 µL/min (for TMSPMA on quartz) applied pressure to the bound surface through a hole in the membrane while an inline pressure sensor tracked the change in pressure over time.

4.2.4 Primary Attachment Evaluation

Devices for the dual silane deposition tests were fabricated as depicted in Figure 4.1. (A) Quartz dies were rinsed with acetone and 2-propanol and cleaned overnight in Nanostrip at 90°C. The quartz surface was then treated as follows: immersed in 0.1 M NaOH for 10 s, water rinsed for 5 s, and dipped in 0.1 M HCl for 10 s followed by final water rinse for 8 s. The dies were then blown dry with N_2 and (B) immersed in a 5% APDMMS solution in toluene for 2 h to functionalize the surface. After deposition, the dies were rinsed with clean toluene and dried. Photoresist was (C) spun, exposed, and (D) developed to pattern the surface. (E) The exposed silane was removed with dilute hydrofluoric acid (10:1 water/BOE) for 5 s followed by the same base/acid treatment in (A). (F) APDIES was deposited on the exposed area by submerging the dies into 5% APDIES solution in toluene for 2 h. (G) The photoresist was removed by sonicating the dies in DMSO for 15 min or until the photoresist was completely removed. (H) To evaluate primary attachment, 7 µL of 5 mg/mL Alexa Fluor 488 TFP ester in DMSO mixed with 250 µL PBS was reacted with the die surface for 1 h, rinsed with DI water, dried, and then (I) imaged with a 60 s integration time using a CoolSNAPHQ CCD (Photometrics, Tucson, AZ).

Figure 4.1. Dual silane deposition overview. (A) Clean quartz die. (B) Deposit (3-acryloxypropyl)dimethylmethoxysilane onto device surface. (C) Spin, pattern, and (D) develop photoresist to pattern the surface. (E) Remove exposed silane with dilute hydrofluoric acid. (F) ADPIES deposited on exposed area and (G) photoresist removed. To evaluate primary attachment, an amine-reactive fluorescent molecule is reacted with the die surface, rinsed, and then (I) imaged using a CCD. Secondary attachment is tested by (J) reacting the die with glutaraldehyde followed by (K) incubation with fluoresceinamine. The die is then rinsed and (L) imaged using a CCD.

4.2.5 Secondary Attachment Evaluation

Secondary attachment followed the same fabrication process described for primary attachment in Figure 4.1 A-G. Secondary attachment was tested by (J) flowing glutaraldehyde through the die and letting it react for 45 min. After clearing the glutaraldehyde from the channel with air, the channel was rinsed with DI water, followed by (K) filling the channel with fluoresceinamine and

letting it incubate in the channel for 26 h. The poly-PEGDA layers were then removed from the die, which was then rinsed with DI water, dried, and (L) imaged using a CCD (60 s exposure).

4.3 RESULTS AND DISCUSSION

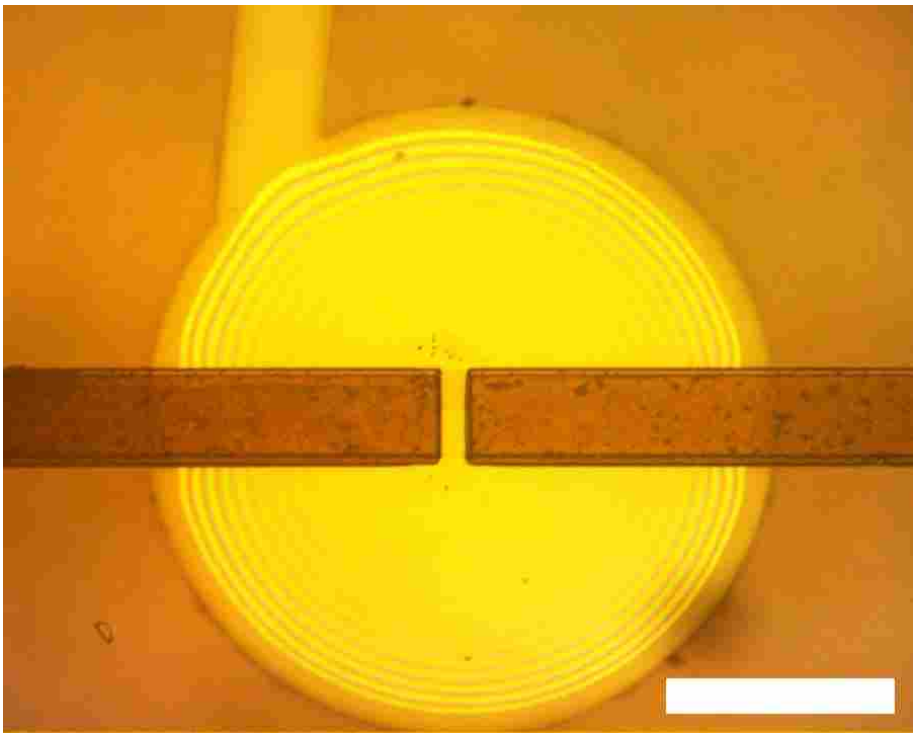

Figure 4.2. Photograph of poly-PEGDA device bonded to quartz. White scale bar is 250 μm.

Figure 4.2 shows an example of poly-PEGDA microfluidic layers bound to a quartz substrate. This is a three-layer valve with a fluidic channel etched into the quartz and bonded to a poly-PEGDA control and membrane layer (See Chapter 3 and Fig. 3.1 for more details).

4.3.1 Burst Pressure Results

The pressure required to separate the bonded layers is proportional to the bond strength between those layers. As seen in Figure 4.3, pressure slowly built up at the interface until a leak caused the pressure to drop at ~60 s. The pressure curves for both the monofunctional and trifunctional

silanes exceeded 230 PSI before leaking, with the pressure >350 PSI for the monofunctional silane curve, well above pressures normally used in microfluidic devices. Neither sample burst at the interface between poly-PEGDA and silicon; the trifunctional silane sample formed a leak at the Nanoport interface and the monofunctional silane sample reached a high enough pressure to cause the syringe pump to shudder and make noise.

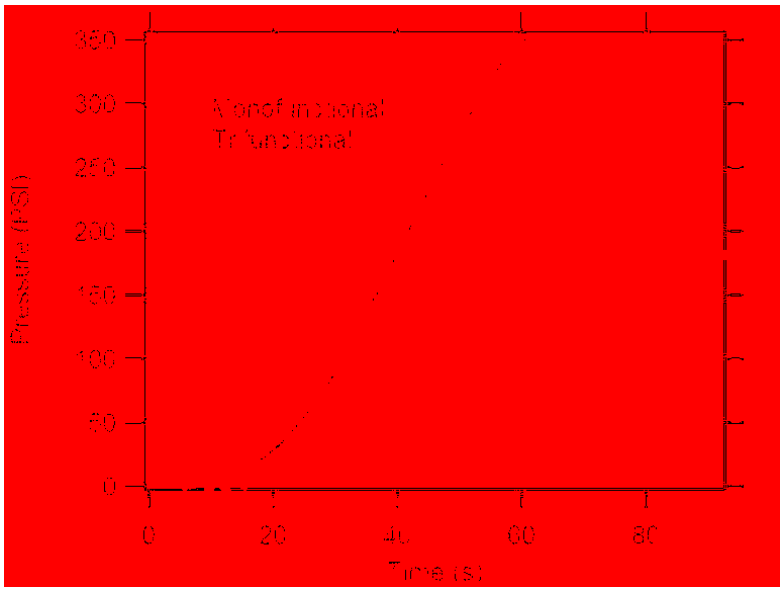

Figure 4.3. Burst pressure results for silane functionalized silicon bound to poly-PEGDA. The green curve is the burst pressure curve for monofunctional APDMMS coated quartz and the curve for a trifunctional TMSPMA deposited surface is in red.

Similar results were obtained when quartz was used instead of silicon (Fig. 4.4), with the pressure reaching ~160 PSI. In this experiment, flow was stopped when 160 PSI was reached even though the bonded layers had not separated, since the pressure achieved was sufficient for most microfluidic applications.

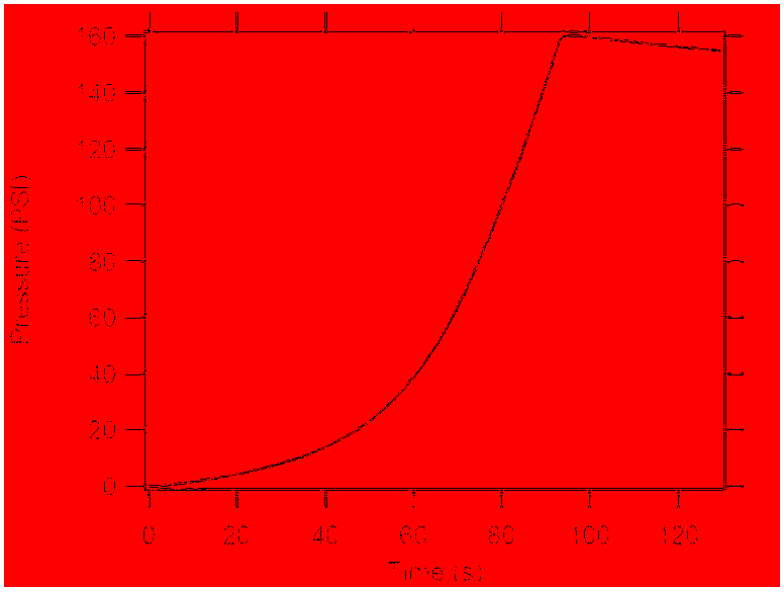

Figure 4.4. Burst pressure result for poly-PEGDA bound to trifunctional TMSPMA functionalized quartz.

4.3.2 Primary Attachment Results

Optimization of the dual-silane deposition process showed that the 10 s base rinse followed by 10 s acid treatment of the quartz surface before silane deposition improved the overall process. This may be due to greater availability of silanols on the treated surface.[12] Dilute buffered oxide etchant (HF) removed the exposed acrylate silane and provided a clean silicon dioxide surface for the ADPIES deposition. It was critical to remove the photoresist after the APDIES deposition (Fig. 4.5), as residual photoresist could prevent a good bond from forming between poly-PEGDA and quartz; residual photoresist also fluoresces which could interfere with device evaluation.

Single-step functionalization of a dual-silane deposited quartz die was demonstrated in Figure 4.6. Comparison to the background image (Fig. 4.6A) demonstrated a marked increase of fluorescence in the amine-functionalized areas (Fig. 4.6B). After the Alexa Fluor 488 TFP ester reaction, both the amine-functionalized and acrylate-functionalized regions increased in fluorescence, with the background-subtracted intensity for the amine-functionalized area being

about twice that for the acrylate-functionalized area. The intensity increase of the acrylate-functionalized areas could be due to nonspecific adsorption of the fluorescent probe that was resistant to being rinsed away or a thin layer of residual photoresist. Either way, the fluorescent probe reacted preferentially with the amine patterned regions of the die.

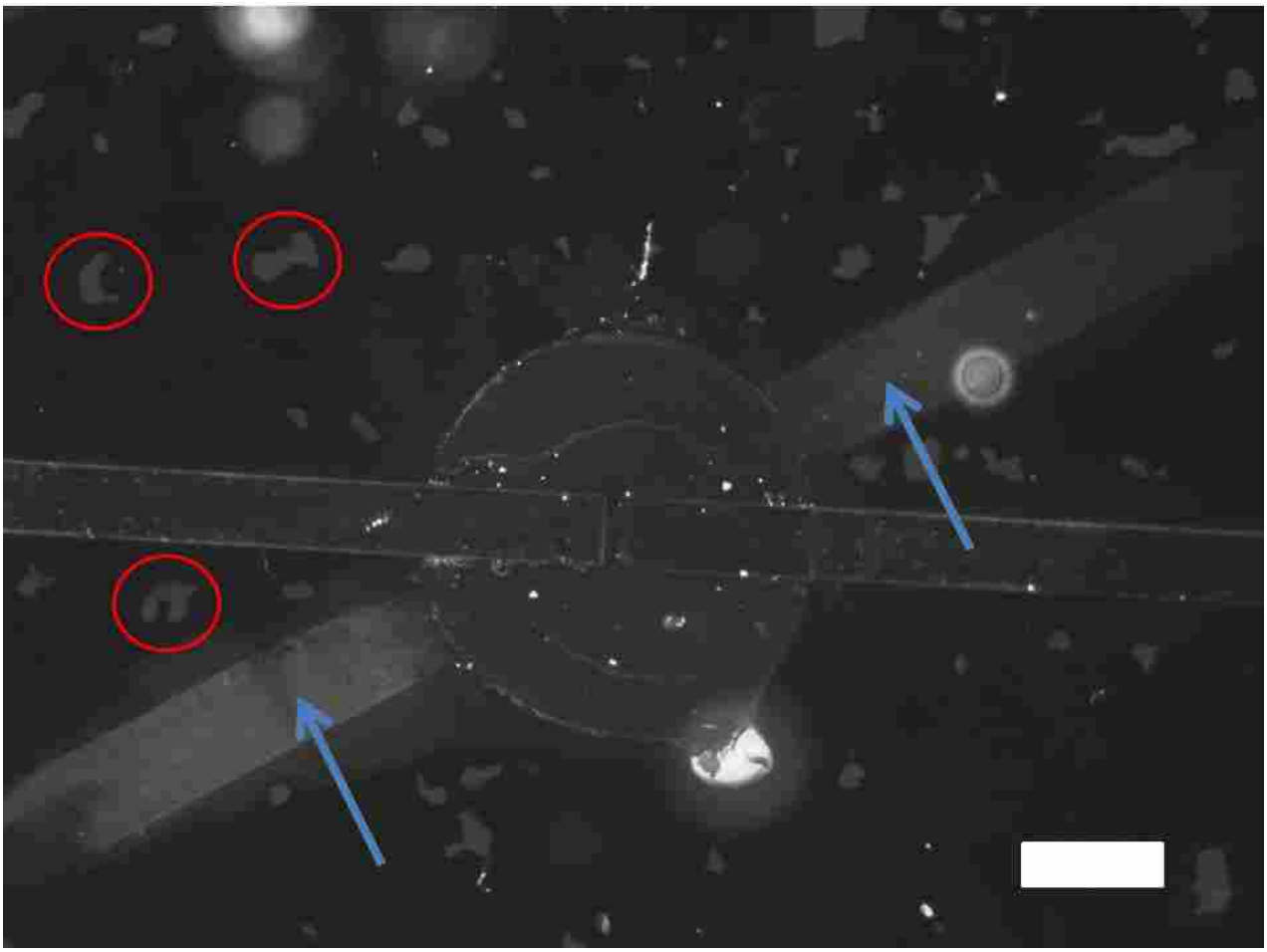

Figure 4.5. Fluorescent image of a device demonstrating the importance of removing all the photoresist after APDIES deposition. Fluorescent functionalized areas are designated by blue arrows while the red circles show photoresist that had not been removed. Scale bar is 250 μm.

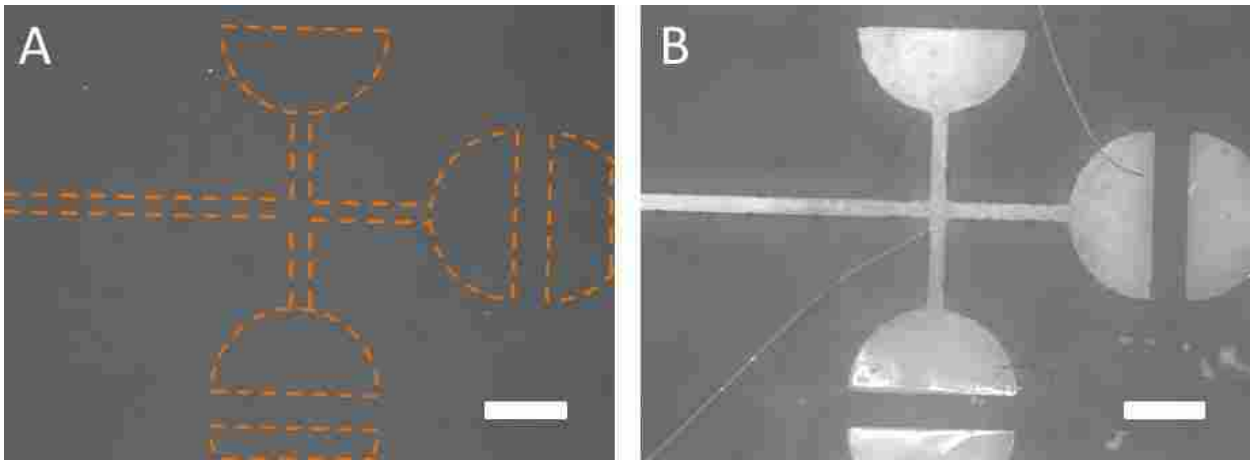

Figure 4.6. Fluorescence comparison (A) before and (B) after Alexa Fluor 488 attachment. White scale bars are 250 µm. The patterned area in (A) before fluorescent attachment is shown by the dashed orange lines. The fluorescently marked amine functionalized areas in (B) are visibly brighter than the background, demonstrating preferential attachment in the patterned areas.

4.3.3 Secondary Attachment Results

Glutaraldehyde is a common crosslinker utilized for attachment of peptides,[13] proteins,[14] and amine-labeled DNA[5] to amine-functionalized surfaces, but reaction conditions vary from paper to paper. Here, I followed a published protocol[5, 13, 14] by reacting the die with glutaraldehyde for a short period (15-60 min), followed by a much longer exposure of an amine-labeled fluorophore (>24 h). The results using a 2.5% glutaraldehyde solution in water are shown in Figure 4.7. The image can be divided into four areas: inside the valve area amine (A) functionalized and (B) unfunctionalized; and (C/D) the same chemistry outside the valve. Unlike the results for the primary attachment, these results were not as clear. The percentage signal difference between regions A and B inside the valve was 2.6% while the difference for C and D outside the valve was 4.9%. These signal differences are significantly lower than those for primary attachment. Clearly optimization is still needed. One noticeable issue was the presence of a visible residue left on the quartz surface everywhere it was exposed to glutaraldehyde. PBS rinsing was unable

to remove this residue so a DI water rinse was used, which was able to remove the bulk of the residue. Due to the reversible nature of the Schiff base formed when glutaraldehyde is reacted with amine,[15] it is possible that glutaraldehyde initially attached covalently to the functionalized surface was partially removed during this water rinse step.

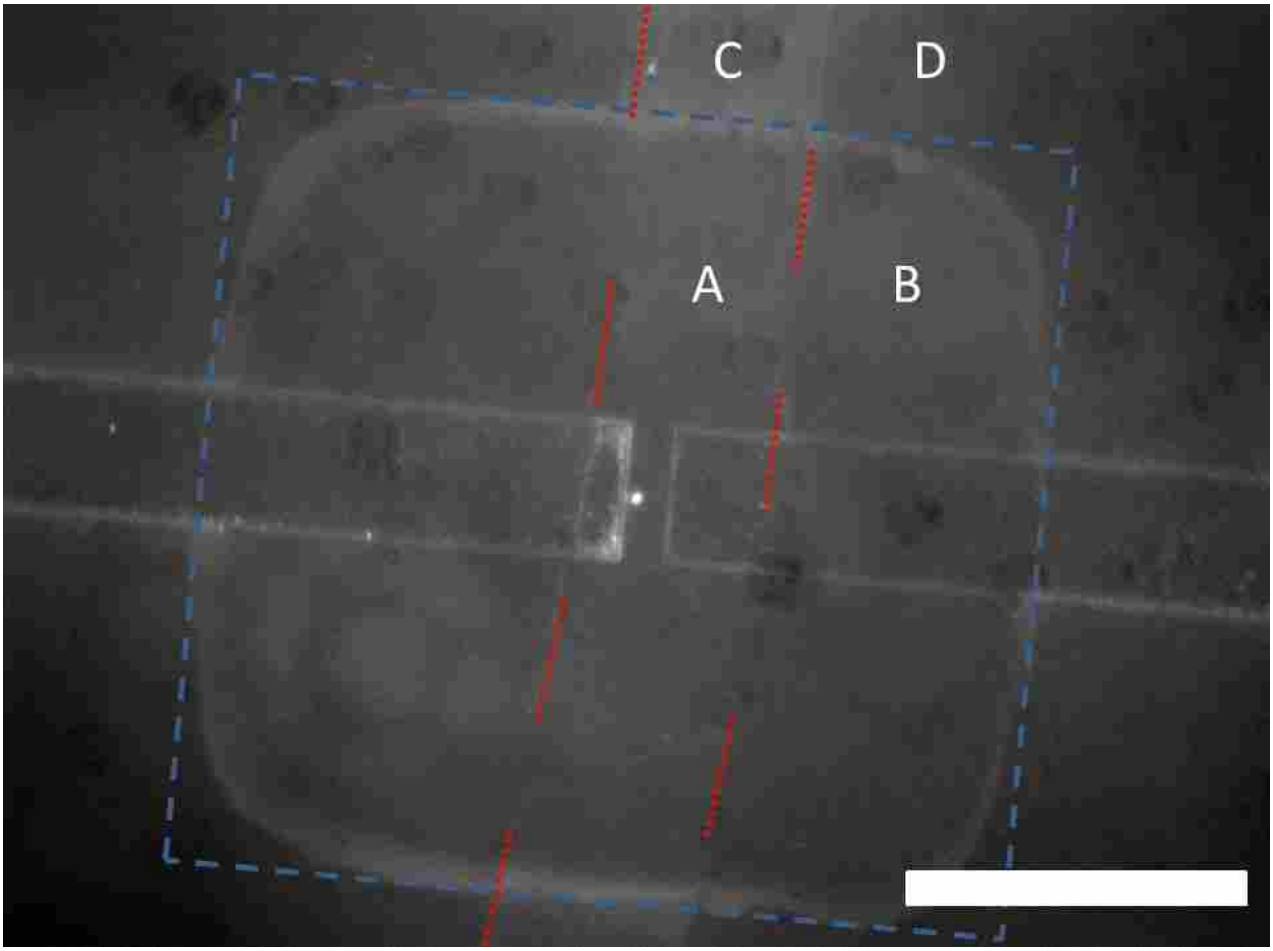

Figure 4.7. Secondary attachment of a fluorescent probe utilizing glutaraldehyde as a cross-linker. The dashed blue line defines the valve area where the valve corners were bonded. The glutaraldehyde and fluoresceinamine functionalized area is shown in between the red dotted lines. The fluorescent image can be split into functionlized and unfunctionalized areas inside (A/B) and outside (C/D) the valve. The scale bar is 250 μm.

4.4 CONCLUSIONS

Integration of poly-PEGDA microfluidics with acrylate-silanized silicon and quartz devices with stability under applied pressures >160 PSI has been demonstrated. Dual silane deposition of TMSPMA and APDIES through photolithographic patterning provided a method, which not only enabled poly-PEGDA bonding to quartz but also created regions on the surface readily available for further chemical modification. Direct reaction of a fluorophore with these amine-functionalized areas showed that site-specific attachment is possible. Exploration and optimization using different surface chemistries, such as epoxy and sulfhydryl, would provide wider application to different surface attachment methods.

Glutaraldehyde, although common in cross-linking, comes with some limitations such as self-polymerization as the cyclic hemiacetal under acidic pH conditions, which gets worse as the solution ages.[15] Thus, there are potential ways to improve the cross-linking reaction. The glutaraldehyde solutions in this experiment were around neutral pH; changing to basic pH (9 or 10) could improve the glutaraldehyde attachment yield.[16] Furthermore, reaction with borohydride[17] or cyanoborohydride[18] to reduce the Schiff base into a secondary amine would improve the bond stability as well. Another alternative would be to switch to a different amine-amine coupler, such as NHS-diazirine[19] which has an NHS ester for the primary amine attachment and utilizes UV light exposure to form the secondary amine attachment.

4.5 REFERENCES

(1) Nge, P. N.; Rogers, C. I.; Woolley, A. T. *Chem. Rev.* **2013**, *113*, 2550-2583.
(2) van Midwoud, P. M.; Janse, A.; Merema, M. T.; Groothuis, G. M. M.; Verpoorte, E. *Anal. Chem.* **2012**, *84*, 3938-3944.
(3) Didar, T. F.; Tabrizian, M. *Lab Chip* **2012**, *12*, 4363-4371.
(4) Chikkaveeraiah, B. V.; Mani, V.; Patel, V.; Gutkind, J. S.; Rusling, J. F. *Biosens. Bioelectron.* **2011**, *26*, 4477-4483.

(5) Chatterjee, D.; Mansfield, D. S.; Woolley, A. T. *Anal. Methods* **2014**, *6*, 8173-8179.
(6) Ness, S. J.; Kim, S.; Woolley, A. T.; Nordin, G. P. *Sens. Actuators, B* **2012**, *161*, 80-87.
(7) Sweetman, M. J.; Shearer, C. J.; Shapter, J. G.; Voelcker, N. H. *Langmuir* **2011**, *27*, 9497-9503.
(8) Duffy, D. C.; McDonald, J. C.; Schueller, O. J. A.; Whitesides, G. M. *Anal. Chem.* **1998**, *70*, 4974-4984.
(9) Pokhriyal, A.; Lu, M.; Chaudhery, V.; Huang, C.-S.; Schulz, S.; Cunningham, B. T. *Opt. Express* **2010**, *18*, 24793-24808.
(10) Rogers, C. I.; Pagaduan, J. V.; Nordin, G. P.; Woolley, A. T. *Anal. Chem.* **2011**, *83*, 6418-6425.
(11) Rogers, C. I.; Oxborrow, J. B.; Anderson, R. R.; Tsai, L. F.; Nordin, G. P.; Woolley, A. T. *Sens. Actuators, B* **2014**, *191*, 438-444.
(12) Cypryk, M.; Apeloig, Y. *Organometallics* **2002**, *21*, 2165-2175.
(13) Xiao, S.-J.; Textor, M.; Spencer, N. D.; Sigrist, H. *Langmuir* **1998**, *14*, 5507-5516.
(14) Zhang, Y.; Zhang, Y.; Jiang, J.; Li, L.; Yu, C.; Hei, T. *Appl. Surf. Sci.* **2011**, *257*, 2712-2716.
(15) Hermanson, G. T. *Bioconjugate Techniques,* 3rd ed.; Academic Press: Boston, MA, 2013, 275-298.
(16) Hermanson, G. T. *Bioconjugate Techniques,* 3rd ed.; Academic Press: Boston, MA, 2013, 589-740.
(17) Ahmed, S. R.; Kelly, A. B.; Barbari, T. A. *J. Membr. Sci.* **2006**, *280*, 553-559.
(18) Park, M. K.; Kee, J. S.; Quah, J. Y.; Netto, V.; Song, J.; Fang, Q.; La Fosse, E. M.; Lo, G.-Q. *Sens. Actuators, B* **2013**, *176*, 552-559.
(19) Gomes, A. F.; Gozzo, F. C. *J. Mass Spectrom.* **2010**, *45*, 892-899.

5. 3D PRINTED MICROFLUIDIC DEVICES WITH INTEGRATED VALVES*

5.1 INTRODUCTION

Microfluidics[1] is a critical technology for an extremely broad range of biomedical applications including tissue engineering,[2, 3] drug discovery,[4] point-of-care diagnostics and pathogen detection in both developed and developing countries,[5-8] and cancer screening using approaches such as cell identification,[9] protein,[10-13] DNA[14] and micro-RNA[15, 16] biomarkers. Microfluidic device prototyping for proof-of-principle demonstration typically utilizes hot embossed or injection molded plastics[1, 17] or polydimethylsiloxane (PDMS).[18, 19] In either case, two or more individually fabricated layers are bonded together to form a completed device. The fabrication process typically involves cleanroom microfabrication of molds using photolithography for one or more of the individual layers, followed by molding and release of each layer and then careful layer alignment and bonding. This sequence of steps can lead to a delay of a week or more between completing the design of a device and actually having one in hand to test; especially taking into account the inevitable problems that crop up for various fabrication steps in a university environment and the turn-around time to design and procure photolithographic masks. To reduce mask acquisition time, mask writers, such as the Heidelberg DWL-66FS laser lithography system,[20] can be used. Fabrication times range from 2 hours for low resolution masks (>5 μm) to ~5 days for high resolution masks (>0.6 μm). Inkjet printing on transparencies is another low cost option for rapid mask printing, taking only a few minutes, but the resolution isn't as good (>50 μm).[21] Moreover, limited material choices for prototyping microfluidic systems also hinders their broad development, as problems such as non-specific adsorption that plague PDMS and other polymers[22, 23] prevent many potential applications from being tested.

Of course, once the masks and processes are in place for a given design, it usually takes only hours to possibly a day or two to produce additional devices of that design. However, initial microfluidic testing often reveals design or performance deficiencies that necessitate modifying the design and starting the process over, thereby incurring yet another significant delay. Numerous cycles around this loop can be required to develop a successful device, which stretches the development time with a concomitantly large increase in personnel costs. Moreover, this lengthy cycle time discourages trying new approaches when faced with tight development deadlines. This is in direct contrast to the "fail fast and often" strategy successfully employed for web and smartphone application software development where early and rapid user feedback is used to guide project development throughout the development cycle. By analogy, 3D printing of microfluidics offers the opportunity to shrink the time from design to first device to an hour or less because the device is created directly in a single step with no need for layer-by-layer fabrication and assembly as with PDMS. This completely changes the development landscape by not only dramatically reducing the opportunity cost of trying new ideas but also permitting a "fail fast and often" strategy in which early and rapid empirical feedback is used to guide and accelerate device development. Moreover, 3D printing does not require a cleanroom environment with its attendant start up investment and ongoing operational costs. In other words, 3D printed microfluidics dramatically lowers the barrier to creating sophisticated microfluidic devices and offers a true rapid-prototyping ability with its attendant benefits to positively disrupt microfluidic development cycles.

Unfortunately, this promise in 3D printed microfluidics has not yet been realized, although there have been a number of efforts in this direction.[24] For example, Kitson et al.[25-27] demonstrated fluidic devices 3D printed by extruding plastic through a heated nozzle. However, this

fabrication method is inherently unable to produce feature sizes and flow channel dimensions needed for microfluidic (as opposed to macrofluidic or millifluidic) device fabrication. For the reported devices, the flow channels had very large cross sections (~4 mm diameter).

A more promising approach for microfluidics is stereolithography in which a vector scanned laser beam or a stationary image pattern from a projector is used to photopolymerize an appropriate photosensitive resin layer-by-layer until a full device is completed. For example, Bhargava et al.[28] report a system in which discrete ~1 cm^3 3D printed cubes, each with internal plumbing to perform a specific passive elementary function (such as an L-joint, mixer, T-junction, XX-junction, etc.), are assembled into more complex fluidic devices in a 3D geometry. Each cube has standardized fluidic interfaces on 2 or more sides according to the elementary function performed within the cube. The cubes snap together to create precise cube-to-cube fluidic connections. While innovative, the overall system size can be comparatively large depending on how many cubes are needed. Furthermore, since the fluid channel minimum cross section dimension ranges from 500-1,000 μm, this is more properly termed a millifluidic system. The cubes themselves are fabricated by a contract manufacturer (FineLine Prototyping, Raleigh, NC) using a proprietary, commercially available resin with a scanned laser stereolithographic 3D printer. This approach is appealing in that it is universally available to any customer, but the large flow channels and system size, and lack of control over resin formulation and, hence, surface and bulk chemistry can be unnecessarily restrictive for many applications.

Interestingly, another group recently published a paper using the same contract manufacturer, except their focus is direct fabrication of entire custom microfluidic devices.[29] They showed that flow channels with cross sectional features down to 400 μm were possible. However, this

approach is still limited to using commercially available resins, and only passive microfluidic components have been demonstrated.

Alternatively, Shallan et al.[30] reported use of an inexpensive commercially available stereolithographic printer (MiiCraft) to fabricate microfluidic devices with flow channel cross sectional dimensions >500 μm. Unfortunately, the two available resin formulations (blue and transparent) are proprietary and supplied by the printer manufacturer. Additionally, the transparent resin exhibits only 60% transmission for a 500 μm thick layer at wavelengths >430 nm and exhibits absorption of small hydrophobic molecules such as rhodamine 6G.

The Fang group and collaborators have built several custom stereolithographic 3D printers that achieve submicron feature sizes for microfluidic devices and use their own resin formulations.[3, 31, 32] The small feature sizes are realized by photoreduction of an image projected by a UV-illuminated dynamic mask (i.e., digital light projector or liquid crystal on silicon microdisplay). However, the required photoreduction reduces the exposed area to only a millimeter or two on a side. To obtain reasonable part sizes (tens of millimeters in each lateral dimension), the image must be stepped many times across each layer using precise translation stages (250 nm positional repeatability). The end result is a complicated and expensive system that does not lend itself to low-cost microfluidic rapid prototyping.

In Chapter 2, I discussed a custom non-absorptive resin that was UV polymerized into a polyethylene glycol diacrylate (poly-PEGDA) microfluidic material. I initially optimized the resin for conventional microfluidic fabrication techniques in which individual layers are molded and subsequently bonded to each other to create a device. The material was also optimized for low non-specific adsorption of proteins, low bulk background fluorescence (i.e., comparable to

PDMS), and high bond strength.[33] In Chapter 3, I demonstrated that despite having a significantly larger bulk modulus than PDMS (>100 MPa compared to ~0.5 MPa), the poly-PEGDA material could be configured in a 3-layer design to create a membrane-type valve with compelling characteristics: 19 ms closure time and 115,000 actuations with no degradation in performance.[34]

Although 3D printed devices have excellent potential for biomedical microfluidic applications, current methods have limitations in terms of resolution, resin versatility, overall device dimensions, and/or prototyping system cost. Moreover, in all cases the reported 3D printed microfluidic devices are composed of only passive elements. In this chapter, I report the first 3D printed active elements in microfluidic systems, showing that both the low-adsorption resin and the basic valve structure can be adapted to successfully create 3D printed valves. I also characterize microfluidic channel fabrication, repeatability, and yield. These results represent the first step toward 3D printed microfluidic devices for integrated analyses of nucleic acids and other molecules in which many active and passive components are incorporated in a single device.[35-40]

5.2 EXPERIMENTAL METHODS

5.2.1 Materials and Methods

PEGDA (M.W. 258), Sudan I, and 3-(trimethoxysilyl) propyl methacrylate were purchased from Sigma Aldrich (Milwaukee, WI). Phenyl-bis-(2,4,6-trimethylbenzoyl) phosphine oxide (Irgacure 819) was acquired from BASF (Vandalia, IL). Prepolymer resin was prepared by mixing 1% (w/w) Irgacure and 0.2% (w/w) Sudan I in PEGDA and sonicated for 35 min. Silanized glass slides were prepared by placing clean slides in a 5% 3-(trimethoxysilyl) propyl methacrylate

solution in toluene for 3 h. After deposition, the slides were scribed (to mark the print face), cleaved, rinsed with clean toluene, blown dry with a nitrogen gun, and stored for later use.

5.2.2 Experimental Setup

I used a B9 Creator 3D printer v1.1 (B9 Creations, Rapid City, SD) to fabricate these devices. To determine feature size fidelity and device yield, I 3D printed 8 samples, each with an identical set of horizontal flow channels with different designed cross sections ranging from 300-500 µm width and 150-250 µm height in 50 µm increments. Vertical flow channels were 3D printed on one die, but with four different vertical holes for each size from 300-450 µm and eight holes for 500-800 µm (each in 50 µm increments). The cross-sectional dimensions were measured using digital photographs processed in ImageJ 1.48v.

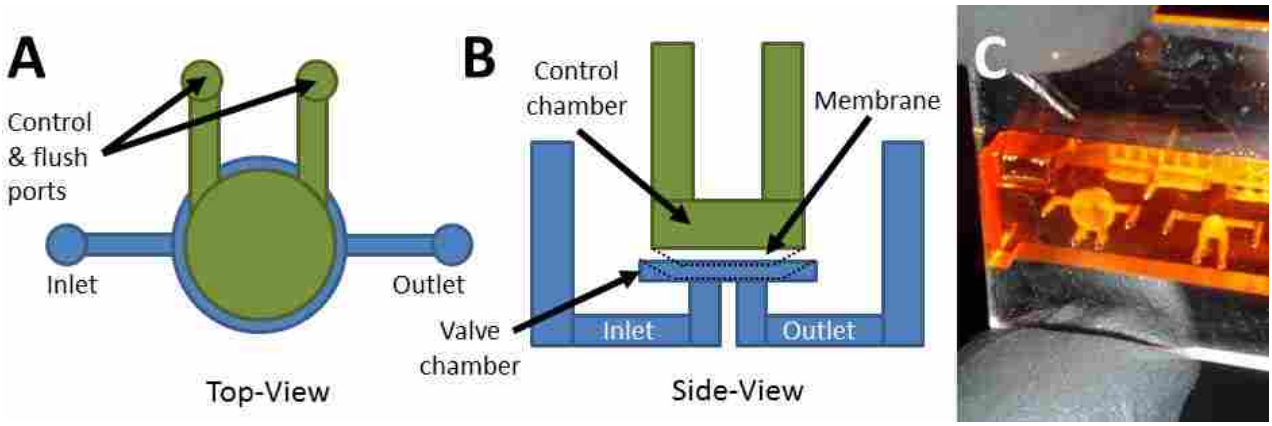

Figure 5.1. Valve schematic and device image. (A) Top view and (B) side view schematics of test valve design. The control chamber (green) and fluidic chamber (blue) regions are voids in the 3D printed device. The control chamber has 2 access ports to enable it to be drained after printing. Pressure can be applied through both ports to actuate the valve, or one channel can be sealed and pressure applied through the other to actuate the valve. Pressurized membrane (black dotted line) shows valve closure. (C) Photograph of a fabricated valve test device looking through the top surface of the device. The left valve has a 3 mm diameter membrane, while the right valve membrane is 1.5 mm diameter. Dead volume of these valves can be approximated as a cone (volume = 1/3 $\pi r^2 h$) where r is radius of the valve and h is the amount of membrane deflection up into the control chamber. For a control chamber height of 500 µm, the maximum dead volume would be ~1.2 µL for the 3 mm valve and ~0.3 µL for the 1.5 mm valve.

Once feasible channel dimensions were determined, these dimensions were then used to create the channels for the valve design. The valve design, shown in Figures 5.1A and 5.1B, consists of a membrane suspended over a valve chamber, on the bottom of which are inlet and outlet openings. When an external pressure source is applied to the control chamber above the membrane, the membrane is deflected downward until it seals the inlet and outlet openings, thereby closing the valve. When pressure is released, the membrane returns to its original position and the valve opens. A photograph of a fabricated test valve device is shown in Figure 5.1C.

The 3D printing process to fabricate a device with a valve is illustrated schematically in Figure 5.2. In brief, double-sided tape was used to affix a methacrylate silane functionalized glass slide to the bottom of the build table before calibrating the build table height for the print. After the resin was introduced into the tray and the projector was focused at the surface of the glass slide, different images were projected for each layer to polymerize each layer and create the desired 3D structure. Once the print was completed, unpolymerized resin was then drained from the structure, resulting in a completed device.

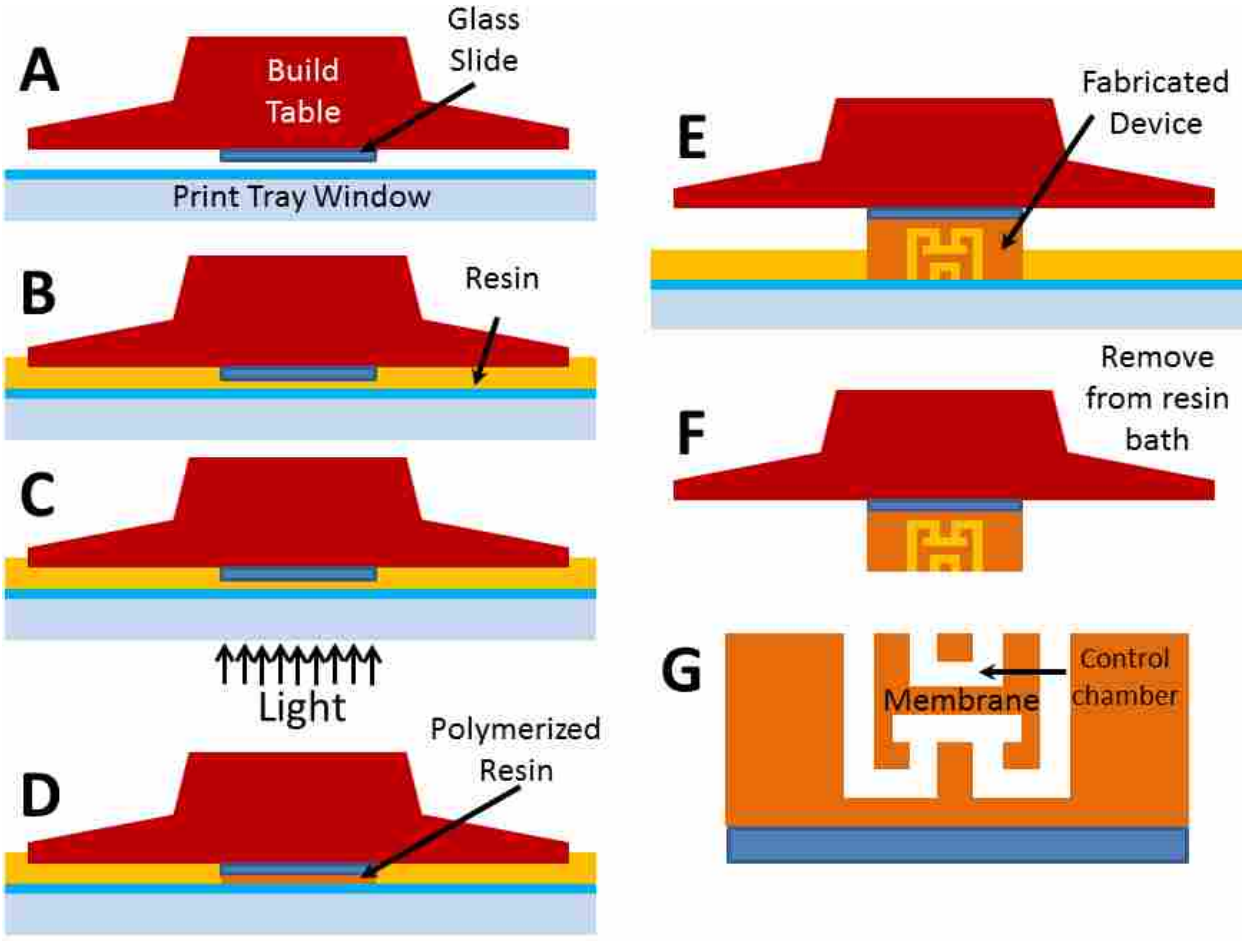

Figure 5.2. Fabrication process. (A) An acrylate silane functionalized glass slide is attached to the bottom of the build table. (B) Resin is added to the print tray and the slide is positioned above the bottom window. (C) The projector image is focused on the bottom surface of the glass slide, which (D) polymerizes resin in the exposed region. (E) The projector image is varied layer-by-layer to create the desired 3D structure. (F) When the device is pulled from the bath after all layers are exposed, the channels contain unpolymerized resin, which must be drained from the structure, resulting in (G) a finished device.

5.2.3 Membrane Thickness

Membrane thickness as a function of exposure time was evaluated by measuring a 2 mm diameter circular single layer membrane (~50 µm) suspended between two 250 µm high chambers. Exposure times between 2 s and 10 s were tested. Membrane thicknesses were measured from digital photographs using ImageJ.

5.2.4 Valve Evaluation and Performance

In Chapter 3, I demonstrated a successful method for valve evaluation.[34] Briefly, two pressure sensors were placed in-line to monitor both the air pressure applied to close a valve and the fluidic pressure applied at the front of the device used to open the valve. A CCD camera was used to track the meniscus at the device outlet which was then converted to volumetric flow rate. The valve was considered open when the flow rate reached 0.2 μL/min. Valves were initially evaluated at air closure pressures of 0, 70, and 140 kPa. Valves were then actuated 400 times at 1 Hz (50% duty cycle) and the pressure tests repeated. This whole process was repeated until a given valve failed.

5.3 RESULTS AND DISCUSSION

5.3.1 Device Characterization Results

My resin formulation in Chapter 3[34] was modified for use in a B9 Creator 3D printer by replacing the original photoinitiator, 2,2-dimethoxy-2-phenylacetophenone (DMPA), with Irgacure 819 and adding an absorber dye, Sudan I. The B9 Creator's light source is a commercial XVGA (1024 x 768 pixels) projector which does not emit UV light. The DMPA UV photoinitiator therefore had to be replaced with a photoinitiator sensitive to the blue end of the visible spectrum emitted by the projector. Likewise, the absorber dye must absorb in the wavelength range covered by the photoinitiator to limit the depth to which the photoinitiator is exposed; otherwise no voids or overhanging features can be fabricated (nearly all microfluidic components involve voids, i.e., locations in which there is no material in the final device; for example, a flow channel). The choice of Sudan I fulfils the absorption requirement, although it has absorbance throughout the visible spectrum, resulting in 3D printed parts with an orange color. Although this is not a problem for this initial proof-of-concept microfluidic valve

development here, many microfluidics applications will require visible optical transparency. Nonetheless, the material reported here is compatible with non-optical sensing methods such as nanowires, microcantilevers, and electrochemical approaches (for example, amperometry, potentiometry, and impedance measurement).[41-46]

At its highest resolution setting, the B9 Creator specifies 50 μm x 50 μm resolution in the X-Y plane (i.e., the plane of each polymerized layer). A typical Z step size (layer-to-layer spacing) is also ~50 μm. Note that the X-Y resolution of the B9 is twice as good as that of the scanning laser 3D printer (100 μm x 100 μm) used by the commercial fabrication service, FineLine Prototyping, mentioned previously, while the Z step size is the same. However, depending on the resin viscosity, actual fabricated flow channel dimensions and yield can be affected more by incomplete draining of uncured resin in the flow channel after 3D printing and prior to final curing of the part than by 3D printer resolution.[29] Hence, taking advantage of improved 3D printer resolution requires development of effective techniques for draining voids.

I found that draining flow channels with either DI water or 2-propanol was effective for this resin formulation. Microscope images of an example channel are shown in Figures 5.3A and 5.3B, while measurement results for horizontal channels are included in Figures 5.3C and 5.3D. Figure 5.3C shows the actual measured size for each designed size for both in-plane (X-Y) and out of plane (Z) dimensions. In most cases the average fabricated size is nearly equal to or somewhat larger than the designed size. Figure 5.3D shows the measured yield as a function of the designed X-Y and Z dimensions, with the smallest design size for 100% yield being 350 μm x 250 μm. Smaller flow channel sizes with high yield are likely feasible with further optimization, such as ensuring that the flow channel Z position and dimensions align with actual fabrication layers as

determined by the software that slices a 3D computer-aided design (CAD) file to prepare it for 3D printing.

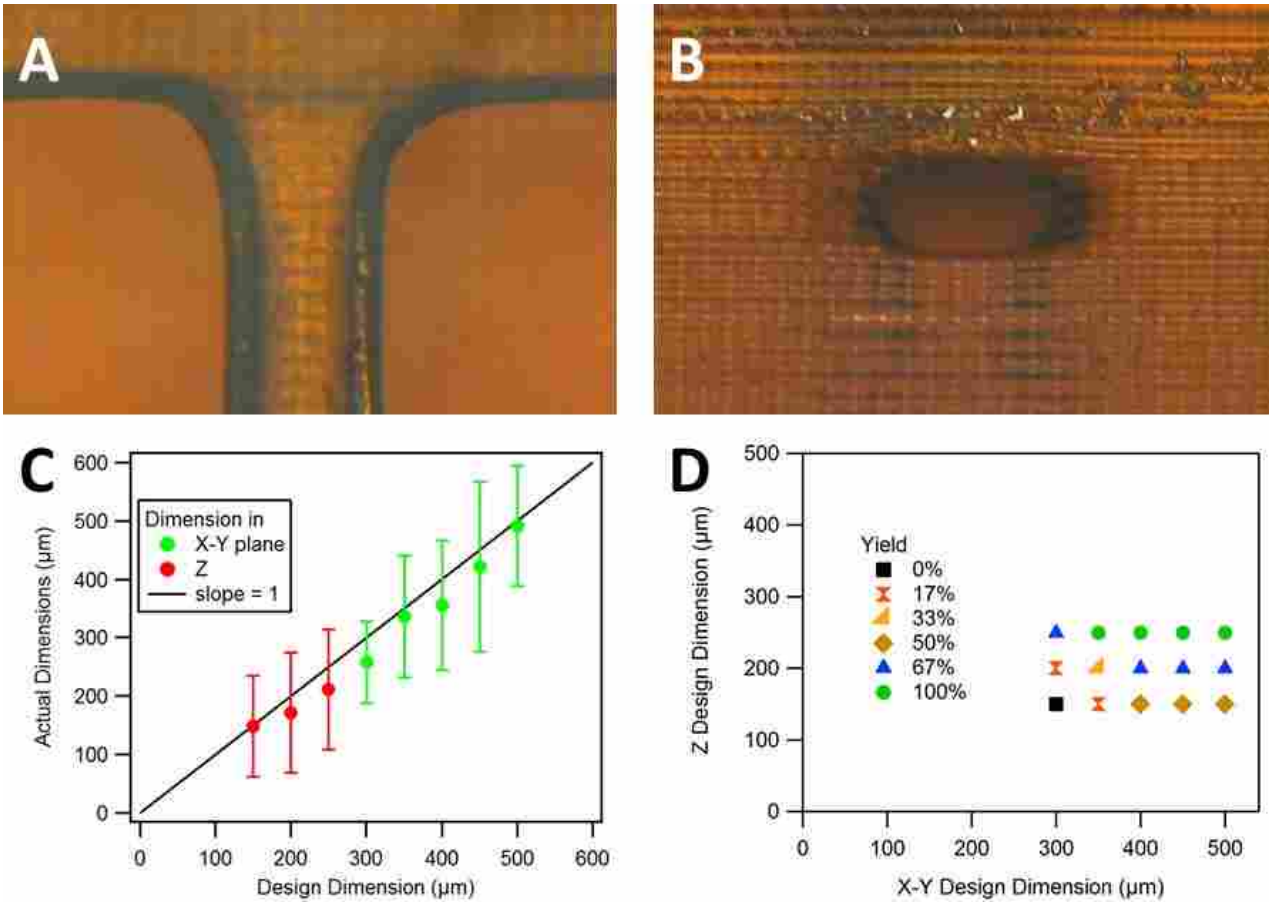

Figure 5.3. Horizontal channel fabrication, repeatability, and yield. (A) Top view and (B) side view of a flow channel with designed cross section size of 350 µm x 250 µm. The measured cross section of the fabricated flow channel is 316 µm x 217 µm. (C) Actual (measured) flow channel size as a function of the designed size (error bars show standard deviation based on measurement of 8 samples). (D) Yield as a function of the designed X-Y and Z dimension sizes for 8 devices where yield represents the frequency of a successfully printed open channel.

The microscope image shown in Figure 5.4A shows a typical example of a vertical cylindrical channel. Measurement results for channels designed with diameters ranging from 300 µm to 800 µm are shown in Figure 5.4B. The smallest vertical channel successfully printed with 100%

yield had a 350 µm designed diameter and 210 µm average measured diameter. As seen in Fig. 5.4B, the as-printed diameters of the holes are smaller than the designed size.

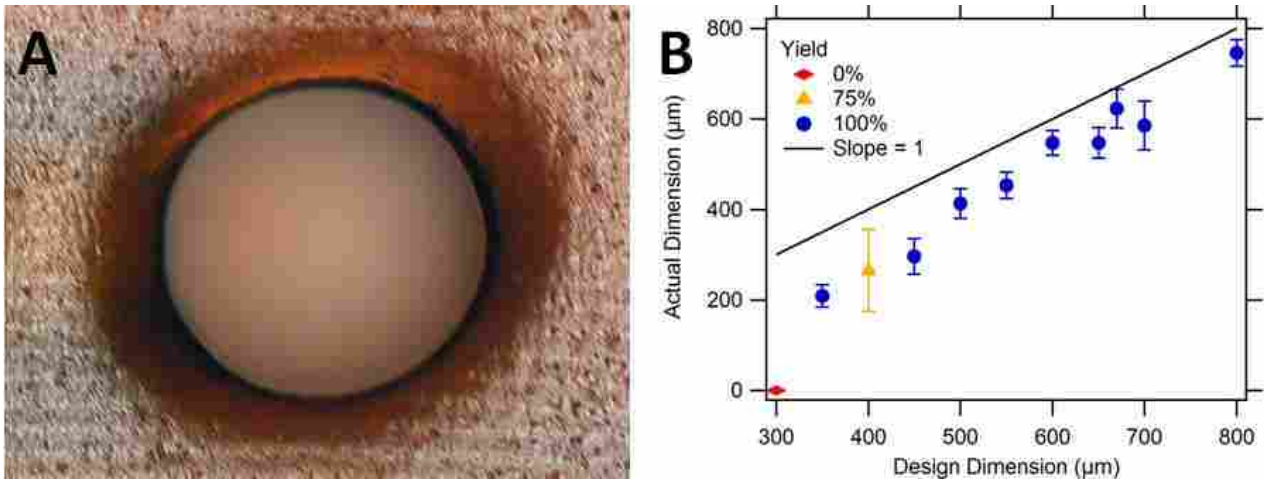

Figure 5.4. Vertical cylindrical channel fabrication, repeatability, and yield. (A) Top view of a designed 650 µm cylindrical channel. The measured diameter of the channel is 606 µm. (B) Actual (measured) cylindrical channel size as a function of the designed size. Successfully printed open channels (yield) as a function of the designed cylinder diameters. Error bars denote standard deviation based on measurement of four channels (300-450 µm holes) or eight channels (500-800 µm holes).

5.3.2 Membrane Thickness

The as-fabricated membrane thickness has a critical effect on valve performance and lifetime. Figure 5.5 shows the measured membrane thickness as a function of layer exposure time. As expected, longer layer exposure time results in greater membrane thickness because the valve chamber behind the membrane is filled with unexposed resin. The longer the exposure, the deeper into this region the polymerization front advances. Note that this not only makes the membrane thicker (and therefore stiffer), but also decreases the distance the membrane must deflect to seal the inlet and outlet openings. My experiments indicate an exposure time in the range of 5.0 to 5.5 s/layer works well. Exposures less than 3 s failed to successfully print due to weak bonding between print layers, and at 3 s the print layers were damaged easily. On the other

hand, exposures greater than 9 s resulted in overpolymerized devices which were prone to cracking under internal stress. With a 5 s exposure time, the total 3D printer build time for a typical 5 mm tall x 8.5 mm x 30 mm device is only 35-40 minutes.

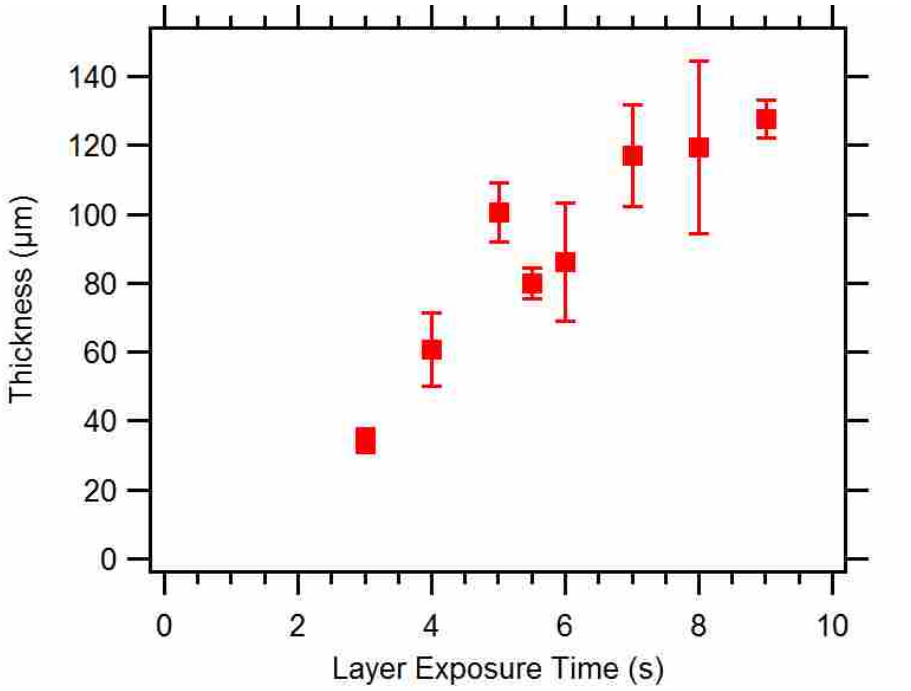

Figure 5.5. Measured membrane thickness as a function of layer exposure time. In the design, the membrane thickness is specified as a single 3D printed layer. Error bars for data points at 3 s or greater exposure time represent standard deviation based on measurement of 4 to 9. There are no error bars for the 3 s data point, which is the average of two samples.

5.3.3 Valve Evaluation and Performance

Figure 5.6A shows the typical performance characteristics of a fabricated valve. The valve is closed by applying ~74 kPa (~20 PSI, red triangle marked curve, left axis) to deflect the membrane down over the valve inlet and outlet channels. Meanwhile, a syringe pump introduces fluid into the valve inlet while the fluid pressure (blue circle marked curve, left axis) and flow rate at the valve outlet (solid green curve, right axis) are monitored (see Chapter 3.2.3 for further details on the measurement method). As expected, the fluid pressure increases within the device

as a function of time until it reaches approximately the control pressure that is used to close the valve membrane. At this point the membrane can no longer remain closed and fluid flows through the valve and out of the device. This performance characteristic is typical of a valve that operates as intended.

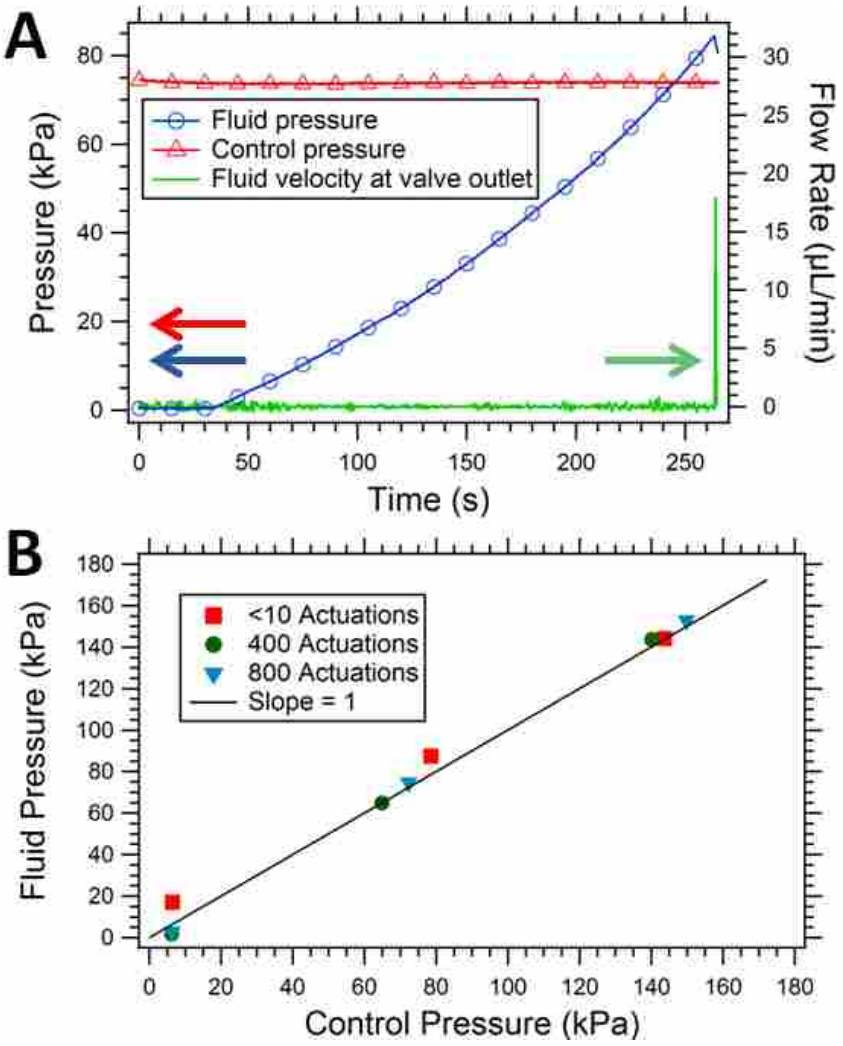

Figure 5.6. Valve operation and evaluation. (A) Operation of a 2 mm diameter valve membrane where the control pressure (red triangles) is the external pressure supplied to deflect the membrane and close the valve, fluid pressure (blue circles) is the pressure that builds up in the inlet channel as the syringe pump pushes fluid into the device, and fluid velocity (green solid line) is the volumetric flow rate at the valve outlet. (B) Fluid pressure at which the valve opens as a function of applied control pressure for a 3 mm valve, before and after 400 actuations and after 800 total valve actuations.

Figure 5.6B shows the fluid pressure at which flow through the device occurs as a function of the control pressure applied to close the membrane for an as-fabricated valve and the same valve after it has undergone 400 and 800 open/close actuation cycles. Each data point represents one measurement similar to what is shown in Figure 6A. The data shown in Figure 6B is representative of what was measured for several devices. The data indicate that when the fluid pressure rises above the control pressure, the valve opens, as expected. Note that there is essentially no difference in valve performance before and after 400 or 800 actuations. I find that the valve membrane typically breaks sometime after 800 actuations. Given my earlier results in Chapter 3.3.1 for poly-PEGDA microfluidic valves where over 100,000 actuations resulted in little change in performance,[34] I am confident that lifetimes of 3D printed microfluidic valves can be dramatically increased.

5.4 CONCLUSIONS

I have successfully demonstrated readily fabricated 3D printed microfluidic channels with valves, within devices that take less than one hour to print. Moreover, the yield for horizontal flow channels with cross sections as small as 350 μm x 250 μm is 100%. Vertical channels were 3D printed successfully as small as 350 μm diameter with 100% yield as well. Undoubtedly, flow channel size can be decreased through further optimization. Valve diameters as small as 2 mm have been shown to be viable and behave as expected with opening fluid pressure approximately equal to the control air pressure applied to close the valve. Switching to a higher resolution printer will likely decrease channel dimensions and valve sizes, while further processing steps such as post-print thermal or UV curing may improve the lifetime of the valves.

Owing to the absorber in my initial resin formulation, the fabricated devices are not fully transparent in the visible wavelength region, and may also have bulk fluorescence. Although these current devices may be incompatible with biosensing based on optical absorbance or fluorescence measurements, ongoing future work to evaluate resin formulations with alternate photoinitiators and absorbers will address these issues. Development of a non-proprietary resin will allow for greater flexibility in modifying polymer properties such as surface chemistry to enable subsequent modification for application in immunoassays or nucleic acid assays, for example. Furthermore, the ability to print these devices directly onto glass surfaces opens up the potential for direct integration with a range of substrates (e.g., glass, silicon, or materials with patterned electrodes) which could dramatically lower the barrier-to-entry to explore lab-on-a-chip biosensors, thereby expanding the lab-on-a-chip research and development community and enabling accelerated biomedical sensor innovation.

5.5 REFERENCES

(1) Nge, P. N.; Rogers, C. I.; Woolley, A. T. *Chem. Rev.* **2013**, *113*, 2550-2583.
(2) Khademhosseini, A.; Langer, R.; Borenstein, J.; Vacanti, J. P. *Proc. Natl. Acad. Sci. U.S.A.* **2006**, *103*, 2480-2487.
(3) Xia, C.; Fang, N. X. *Biomed. Microdevices* **2009**, *11*, 1309-1315.
(4) Neuži, P.; Giselbrecht, S.; Länge, K.; Huang, T. J.; Manz, A. *Nat. Rev. Drug Discovery* **2012**, *11*, 620-632.
(5) Chin, C. D.; Laksanasopin, T.; Cheung, Y. K.; Steinmiller, D.; Linder, V.; Parsa, H.; Wang, J.; Moore, H.; Rouse, R.; Umviligihozo, G.; Karita, E.; Mwambarangwe, L.; Braunstein, S. L.; van de Wijgert, J.; Sahabo, R.; Justman, J. E.; El-Sadr, W.; Sia, S. K. *Nat. Med.* **2011**, *17*, 1015-1019.
(6) Foudeh, A. M.; Fatanat Didar, T.; Veres, T.; Tabrizian, M. *Lab Chip* **2012**, *12*, 3249-3266.
(7) Mulvaney, S. P.; Myers, K. M.; Sheehan, P. E.; Whitman, L. J. *Biosens. Bioelectron.* **2009**, *24*, 1109-1115.
(8) Sin, M. L.; Mach, K. E.; Wong, P. K.; Liao, J. C. *Expert Rev. Mol. Diagn.* **2014**, *14*, 225-244.
(9) Saliba, A.-E.; Saias, L.; Psychari, E.; Minc, N.; Simon, D.; Bidard, F.-C.; Mathiot, C.; Pierga, J.-Y.; Fraisier, V.; Salamero, J.; Saada, V.; Farace, F.; Vielh, P.; Malaquin, L.; Viovy, J.-L. *Proc. Natl. Acad. Sci.* **2010**, *107*, 14524-14529.

(10) Chikkaveeraiah, B. V.; Mani, V.; Patel, V.; Gutkind, J. S.; Rusling, J. F. *Biosens. Bioelectron.* **2011**, *26*, 4477-4483.
(11) Hu, M.; Yan, J.; He, Y.; Lu, H.; Weng, L.; Song, S.; Fan, C.; Wang, L. *ACS Nano* **2010**, *4*, 488-494.
(12) Malhotra, R.; Patel, V.; Chikkaveeraiah, B. V.; Munge, B. S.; Cheong, S. C.; Zain, R. B.; Abraham, M. T.; Dey, D. K.; Gutkind, J. S.; Rusling, J. F. *Anal. Chem.* **2012**, *84*, 6249-6255.
(13) Ziober, B. L.; Mauk, M. G.; Falls, E. M.; Chen, Z.; Ziober, A. F.; Bau, H. H. *Head & Neck* **2007**, *30*, 111-121.
(14) Mulvaney, S. P.; Cole, C. L.; Kniller, M. D.; Malito, M.; Tamanaha, C. R.; Rife, J. C.; Stanton, M. W.; Whitman, L. J. *Biosens. Bioelectron.* **2007**, *23*, 191-200.
(15) Moltzahn, F.; Olshen, A. B.; Baehner, L.; Peek, A.; Fong, L.; Stoppler, H.; Simko, J.; Hilton, J. F.; Carroll, P.; Blelloch, R. *Cancer Res.* **2011**, *71*, 550-560.
(16) Vorwerk, S.; Ganter, K.; Cheng, Y.; Hoheisel, J.; Stähler, P. F.; Beier, M. *New Biotechnol.* **2008**, *25*, 142-149.
(17) Mei, Q.; Xia, Z.; Xu, F.; Soper, S. A.; Fan, Z. H. *Anal. Chem.* **2008**, *80*, 6045-6050.
(18) Friend, J.; Yeo, L. *Biomicrofluidics* **2010**, *4*, 026502.
(19) Sia, S. K.; Whitesides, G. M. *Electrophoresis* **2003**, *24*, 3563-3576.
(20) http://www.himt.de/index.php/dwl-series-overview.html
(21) Duffy, D. C.; McDonald, J. C.; Schueller, O. J. A.; Whitesides, G. M. *Anal. Chem.* **1998**, *70*, 4974-4984.
(22) Huang, B.; Wu, H. K.; Kim, S.; Zare, R. N. *Lab Chip* **2005**, *5*, 1005-1007.
(23) Shah, J. J.; Geist, J.; Locascio, L. E.; Gaitan, M.; Rao, M. V.; Vreeland, W. N. *Electrophoresis* **2006**, *27*, 3788-3796.
(24) Gross, B. C.; Erkal, J. L.; Lockwood, S. Y.; Chen, C.; Spence, D. M. *Anal. Chem.* **2014**, *86*, 3240-3253.
(25) Kitson, P. J.; Rosnes, M. H.; Sans, V.; Dragone, V.; Cronin, L. *Lab Chip* **2012**, *12*, 3267-3271.
(26) Kitson, P. J.; Symes, M. D.; Dragone, V.; Cronin, L. *Chem. Sci.* **2013**, *4*, 3099-3103.
(27) Symes, M. D.; Kitson, P. J.; Yan, J.; Richmond, C. J.; Cooper, G. J. T.; Bowman, R. W.; Vilbrandt, T.; Cronin, L. *Nat. Chem.* **2012**, *4*, 349-354.
(28) Bhargava, K. C.; Thompson, B.; Malmstadt, N. *Proc. Natl. Acad. Sci.* **2014**, *111*, 15013-15018.
(29) Au, A. K.; Lee, W.; Folch, A. *Lab Chip* **2014**, *14*, 1294.
(30) Shallan, A. I.; Smejkal, P.; Corban, M.; Guijt, R. M.; Breadmore, M. C. *Anal. Chem.* **2014**, *86*, 3124-3130.
(31) Sun, C.; Fang, N.; Wu, D. M.; Zhang, X. *Sens. Actuators, A* **2005**, *121*, 113-120.
(32) Zheng, X.; Deotte, J.; Alonso, M. P.; Farquar, G. R.; Weisgraber, T. H.; Gemberling, S.; Lee, H.; Fang, N.; Spadaccini, C. M. *Rev. Sci. Instrum.* **2012**, *83*, 125001.
(33) Rogers, C. I.; Pagaduan, J. V.; Nordin, G. P.; Woolley, A. T. *Anal. Chem.* **2011**, *83*, 6418-6425.
(34) Rogers, C. I.; Oxborrow, J. B.; Anderson, R. R.; Tsai, L. F.; Nordin, G. P.; Woolley, A. T. *Sens. Actuators, B* **2014**, *191*, 438-444.
(35) Crabtree, H. J.; Lauzon, J.; Morrissey, Y.; Taylor, B.; Liang, T.; Johnstone, R.; Stickel, A.; Manage, D.; Atrazhev, A.; Backhouse, C.; Pilarski, L. *Microfluid. Nanofluid.* **2012**, *13*, 383-398.

(36) Kim, J.; Jensen, E. C.; Stockton, A. M.; Mathies, R. A. *Anal. Chem.* **2013**, *85*, 7682-7688.
(37) Collino, R. R.; Reilly-Shapiro, N.; Foresman, B.; Xu, K.; Utz, M.; Landers, J. P.; Begley, M. R. *Lab Chip* **2013**, *13*, 3668-3674.
(38) Godwin, L. A.; Pilkerton, M. E.; Deal, K. S.; Wanders, D.; Judd, R. L.; Easley, C. J. *Anal. Chem.* **2011**, *83*, 7166-7172.
(39) Yu, F.; Horowitz, M. A.; Quake, S. R. *Lab Chip* **2013**, *13*, 1911-1918.
(40) Shackman, J. G.; Reid, K. R.; Dugan, C. E.; Kennedy, R. T. *Anal. Bioanal. Chem.* **2012**, *402*, 2797-2803.
(41) García, M.; García-Carmona, L.; Escarpa, A. Microfluidic system for enzymeless electrochemical determination of inulin using catalytically active metal nanowires. *Microchim Acta* [Online early access]. 10.1007/s00604-014-1384-5 Published Online: http://dx.doi.org/10.1007/s00604-014-1384-5 (accessed 2015/1/19).
(42) McClellan, M. S.; Domier, L. L.; Bailey, R. C. *Biosens. Bioelectron.* **2012**, *31*, 388-392.
(43) Anderson, R. R.; Hu, W.; Noh, J. W.; Dahlquist, W. C.; Ness, S. J.; Gustafson, T. M.; Richards, D. C.; Kim, S.; Mazzeo, B. A.; Woolley, A. T.; Nordin, G. P. *Lab Chip* **2011**, *11*, 2088-2096.
(44) Ness, S. J.; Anderson, R. R.; Hu, W. S.; Richards, D. C.; Oxborrow, J.; Gustafson, T.; Tsai, B.; Kim, S.; Mazzeo, B.; Woolley, A.; Nordin, G. P. *IEEE Sens. J.* **2013**, *13*, 959 - 968
(45) Anderson, K. B.; Lockwood, S. Y.; Martin, R. S.; Spence, D. M. *Anal. Chem.* **2013**, *85*, 5622-5626.
(46) Vázquez, M.; Frankenfeld, C.; Coltro, W. K. T.; Carrilho, E.; Diamond, D.; Lunte, S. M. *Analyst* **2010**, *135*, 96-103.

6. CONCLUSIONS AND FUTURE WORK

6.1 CONCLUSIONS

6.1.1 Single-Monomer Formulation of Polymerized Polyethylene Glycol Diacrylate as a Nonadsorptive Material for Microfluidics

In Chapter 2, I demonstrated that polyethylene glycol diacrylate (PEGDA) can be polymerized via UV exposure and utilized as a microfluidic substrate. Water stability, respectable bond strength, and good optical clarity were shown. Diffusion of small hydrophobic molecules into the bulk material was compared between poly-PEGDA and polydimethylsiloxane (PDMS), with poly-PEGDA showing excellent resistance to permeation compared to PDMS. Nonspecific protein adsorption over a range of protein concentrations was compared for both materials, with poly-PEGDA demonstrating lower nonspecific adsorption than PDMS. Under exposure of a low protein concentration sustained over time, poly-PEGDA demonstrated greater resistance to surface fouling than PDMS. Poly-PEGDA made from purified resin also showed a low intrinsic fluorescent background similar to that of PDMS. Electrophoretic separations of amino acids and proteins utilizing poly-PEGDA as a microchip capillary electrophoresis substrate showed symmetrical, well-resolved peaks with good theoretical plate counts. These separations, along with resistance to nonspecific adsorption and low background fluorescence, demonstrated the potential benefits of using poly-PEGDA over PDMS as a microfluidic substrate for biological sample analysis.

6.1.2 Microfluidic Valves Made from Polymerized Polyethylene Glycol Diacrylate

Three-layer microfluidic membrane valves made with poly-PEGDA were demonstrated in Chapter 3. Valves were bonded with an applied vacuum to prevent the membrane from sticking closed during UV exposure. Multiple valve geometries were evaluated, but the 700-μm-diameter

circular design yielded the best results: a linear, slope of one, fluid versus control pressure curve for pedestal widths of 15-125 μm. Pressure for deflection experiments demonstrated that these valves require very little pressure (~9 kPa) to generate membrane deflections >2 μm. Valve opening and closure response times were evaluated using periodic applied pressure and pressure release, resulting in a rise time for valve opening of ~100 ms and a fall time for valve closure of ~20 ms. Valves could be operated as fast as 8 Hz with potential for faster valve opening times. Valve response measurements with fewer than 1000 actuations showed that the fluid pressure required to open the valve and initiate flow was about 50 kPa higher than the control pressure. As the valve was actuated more, the fluid pressure required to open the valve dropped to be the same as the pressure applied for valve closure. Poly-PEGDA valves were shown to be robust, remaining functional for up to 115,000 actuations.

6.1.3 Patterned Dual-Silane Deposition on Quartz to Enable Hybrid Material Integration and Site-Specific Functionalization

In Chapter 4, I demonstrated heterogeneous device formation by integrating poly-PEGDA microfluidics with different substrates via acrylate-silane deposition. Good bond strengths in these hybrid devices were shown, with burst pressures >160 PSI for both silicon and quartz bound to poly-PEGDA. Photolithographic patterning of the initial silane, followed by HF etching and subsequent deposition of a secondary silane, allowed for device bonding and site-specific chemical modification. Removing photoresist before poly-PEGDA layer attachment was crucial, as the fluorescence from the resist could interfere with fluorescence evaluation of chemical modified surfaces. Site-specific functionalization was evaluated by reacting amine-silanized areas directly with a fluorophore. Initial results with secondary attachment utilizing glutaraldehyde were also shown but needed more optimization to achieve better fluorescent probe attachment.

6.1.4 3D Printed Microfluidic Devices with Integrated Valves

The poly-PEGDA prepolymer formula from Chapters 2-4 was adapted for utilization in 3D printing. Chapter 5 contains the first demonstration of 3D printed valves in microfluidic systems. Devices up to 5-mm-tall, containing 3D printed microfluidic channels with valves ≥2 mm diameter, were printed in under an hour. Horizontal flow channels with cross sections down to 350 μm x 250 μm and vertical channels as small as 350 μm in diameter were printed with a 100% yield. Membrane thickness was studied as a function of polymerization time; the membrane thickness increased as exposure was lengthened due to polymerization of resin in the void underneath the membrane. Under-exposure of the polymer layers resulted in brittle, unbound layers, whereas over-exposure caused the material to crack under internal stress. Valves with diameters as small as 2 mm were evaluated, having a fluid opening pressure approximately the same as the valve closure pressure.

6.2 FUTURE WORK

6.2.1 Evaluation of Pumps and Passive Channel Components Made from Poly-PEGDA

The multi-layer fabrication method for creating poly-PEGDA valves in Chapter 3 can be adapted for on-chip pumping, which could then be integrated with electrophoretic separation for automated, pressure-driven, on-chip sample preparation (see Fig. 6.1). Pumps made from poly-PEGDA would provide decreased analyte adsorption and potentially contribute to lower detection limits. These pump systems could be integrated with a monolithic column, which could be chemically derivatized with antibodies for sample extraction and preconcentration followed by subsequent electrophoretic separation.[1, 2] Such pumps could also find use in sample preconcentration and on-chip labeling where a reverse phase functionalized monolithic column is utilized to retain molecules before subsequent reaction and elution.[3] Other applications of these

pumps are in solution mixing or utilization in a closed recirculation system where small-volume samples could be flowed back and forth across a sensor for improved detection efficiency. Integration of these valve systems with silicon or glass devices including ones with deposited electrodes could enable interfacing with micro- and nano-sensors such as microcantilevers, silicon ring resonators, nanowires, etc.

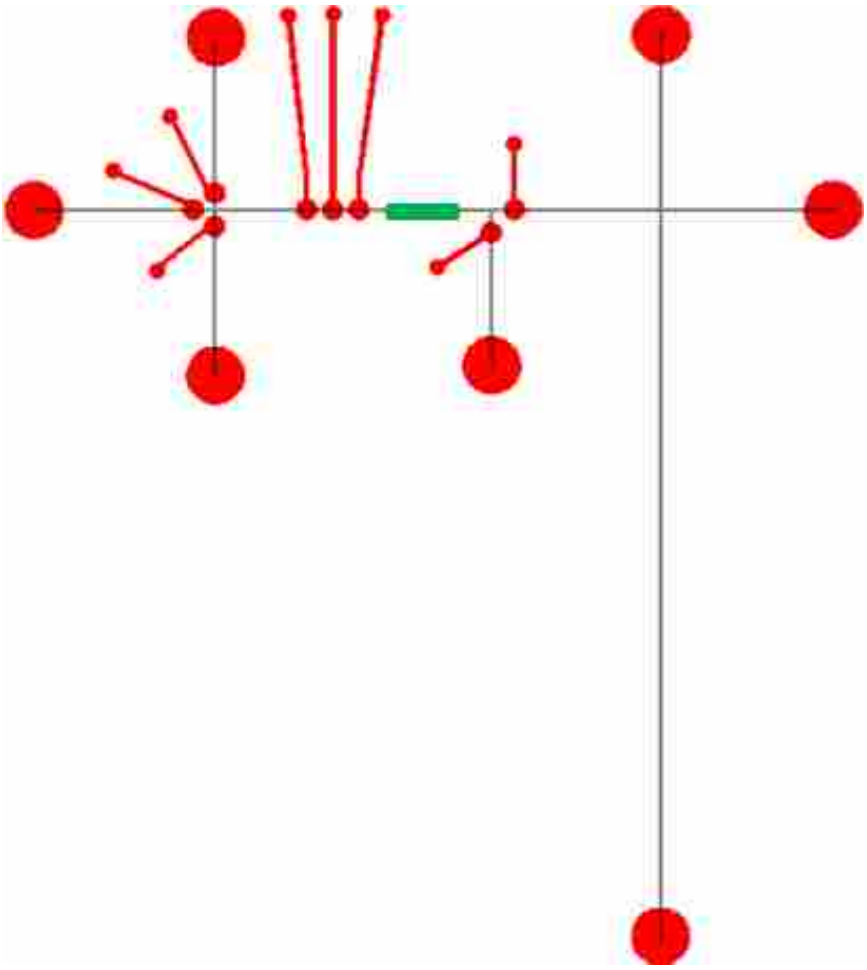

Figure 6.1. Poly-PEGDA device with integrated pumps and valves, for solid-phase extraction and electrophoretic separation. Sample reservoirs are shown as larger diameter red circles, while applied pressure inputs are shown as the smaller red circles attached to the valves. The green channel region shows an area where a monolithic column could be included for solid-phase extraction before electrophoretic separation.

6.2.2 Optimization of Surface Chemistry Attachment

Since only initial attempts for secondary probe attachment are demonstrated in this work, further optimization is needed. In Chapter 4, glutaraldehyde solutions were used around neutral pH, so changing to a basic solution with a pH of 9 or 10 might improve the attachment yield.[4] Subsequent reaction with borohydride[5] or cyanoborohydride[6] has been shown to reduce the Schiff base into a secondary amine and could improve the attachment stability and density. Since glutaraldehyde has some limitations, including self-polymerization under acidic conditions and as solutions age, attachment conditions for different amine-amine couplers should also be investigated. One such alternative, NHS-diazirine,[7] has an NHS ester for primary amine attachment. Secondary amine attachment to the diazirine would be initiated by UV light exposure, which is achievable through a bonded glass substrate. Ultimately, this process will be used for protein and amine-DNA immobilization which will provide site-specific regions for affinity capture or fluorescent probing. Expansion to include different surface chemistries, such as epoxy and sulfhydryl, would provide a wider range of functionalization modalities and more biomolecule crosslinking options.

6.2.3 Reformulation of 3D Printing Poly-PEGDA Resin for Better Resolution, Decreased Coloration, and Reduced Background Fluorescence

Due to the Sudan I absorber chosen for the initial 3D printing resin in Chapter 5, the fabricated devices had an orange color and likely had bulk background fluorescence. Since a different absorber is required when switching from a visible light projector, as used in Chapter 5, to a UV LED-based projection system centered at 385 nm (Asiga Freeform Pico27), the resin formula can be modified to create clear, 3D printed devices with lower background fluorescence. Exploration and optimization of a new resin formula will include investigation of photoinitiators and UV

absorbers <410 nm. Initial experiments should focus on diphenyl(2,4,6-trimethylbenzoyl) phosphine oxide as a potential photoinitiator and BLS 99-2 as a UV absorber.

Creation of a non-proprietary resin would provide the ability to adapt the polymer properties for different applications, such as surface modification for application in immunoassays or nucleic acid assays, for example. The Pico27 3D printer has a higher pixel resolution then the B9 Creator, improving from 50 μm/pixel to 27 μm/pixel. This should improve the printable dimensions for channels and valves. The effect of reduced layer thickness (down to 25 μm) on channel dimensions should also be explored. Furthermore, post-print thermal- and UV-curing should be evaluated to see if valve longevity can be improved.

Since the 3D devices demonstrated in Chapter 5 were printed directly onto a silanized glass substrate, direct integration with a range of substrates (e.g., glass, silicon, etc.) is possible, but will need to be optimized. Directly creating heterogeneous microfluidics through 3D printing could potentially expand lab-on-a-chip research and development and enable faster biosensor innovation.

In Chapter 5, 3D printed valves were successfully demonstrated, but pumps were not tested. Two different initial pump designs have been laid out to be characterized and to determine the expelled volume during valve closure as well as the maximum actuation rate. In Figure 6.2, a larger, centralized valve can be used to pump fluid through the system, while opening the valves on either side to control the direction of the flow. Geometric optimization will be necessary to maximize the expelled valve volume while decreasing the interconnecting channel volumes.

Another design option is shown in Figure 6.3. With an inverted middle valve, all three valves can be located closer together, resulting in a decreased device footprint and smaller dead volumes.

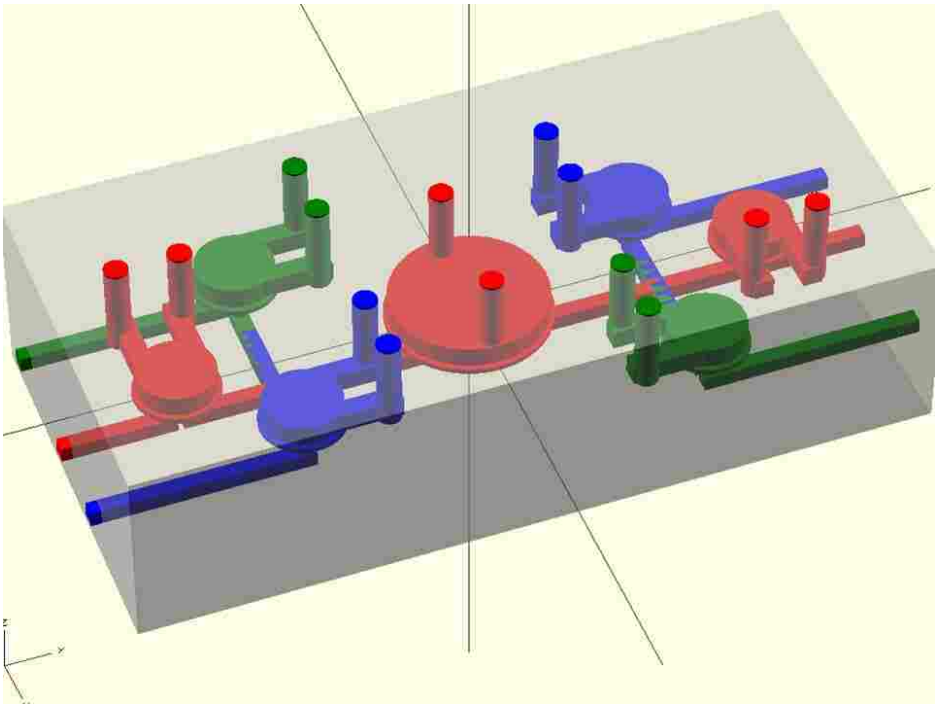

Figure 6.2. Schematic of a pump network utilizing a centralized larger valve to push fluid through the system. The smaller valves on the left direct the flow of three different solutions into a common channel and into the larger displacement valve (red, middle). The three valves on the right direct the displaced fluid into different flow channels.

Figure 6.3. Schematic of a 3-valve peristaltic pump where the middle valve is inverted to decrease the channel volume in between the valves. Side-view of the valves showing an inverted middle valve.

Different passive component designs will also be explored (Fig. 6.4), including Y-branched channels, micromixers, and different tubing connectors. Y-branches will allow determination of the resolution of diagonal patterns using the Pico27 3D printer. Micromixers will provide another mechanism (besides valves) to mix solutions on-chip where in-channel mixing is limited due to low Reynolds numbers. Exploring different chip-to-world interfaces will provide an alternative to metal pins currently used, which can introduce debris into the system.

Figure 6.4. Sample individual passive components in 3D printed microfluidics. Flow channel (yellow, front), L-bend (green, front), T-junction (blue, front), Y-junction (red, front), XT-junction (yellow, middle), XX-junction (green, middle), Moebius mixer (red, middle), and connector for flexible tubing (blue, back).

In summary, the development of poly-PEGDA in this work shows a strong case for poly-PEGDA as a replacement for PDMS in biological applications. Poly-PEGDA is an optically clear polymer with low background fluorescence, resistance to nonspecific adsorption, resistance to small molecule permeation, and moderate flexibility (Young's modulus of ~0.13 GPa).

Demonstrated functionality with electrophoretic separations, valve operation, and hybrid material integration makes poly-PEGDA an excellent candidate for broad use in micro-total analysis systems, microfluidics, and biosensing. Continued development of poly-PEGDA as a microfluidic substrate with pumps, other integrated materials, and patterned surface attachment will provide a more versatile tool for application in this growing field.

6.3 REFERENCES

(1) Yang, W.; Sun, X.; Wang, H.-Y.; Woolley, A. T. *Anal. Chem.* **2009**, *81*, 8230-8235.
(2) Yang, W.; Sun, X.; Pan, T.; Woolley, A. T. *Electrophoresis* **2008**, *29*, 3429-3435.
(3) Nge, P. N.; Pagaduan, J. V.; Yu, M.; Woolley, A. T. *J. Chromatogr. A* **2012**, *1261*, 129-135.
(4) Hermanson, G. T. *Bioconjugate Techniques,* 3rd ed.; Academic Press: Boston, MA, 2013, 589-740.
(5) Ahmed, S. R.; Kelly, A. B.; Barbari, T. A. *J. Membr. Sci.* **2006**, *280*, 553-559.
(6) Park, M. K.; Kee, J. S.; Quah, J. Y.; Netto, V.; Song, J.; Fang, Q.; La Fosse, E. M.; Lo, G.-Q. *Sens. Actuators, B* **2013**, *176*, 552-559.
(7) Gomes, A. F.; Gozzo, F. C. *J. Mass Spectrom.* **2010**, *45*, 892-899.